Thermodynamic and Directed Physical Characterization of Bacteriophage Lambda Capsid Maturation

Shannon Kruse

A dissertation
submitted in partial fulfillment of the
requirements for the degree of

Doctor of Philosophy

University of Washington

2015

Reading Committee:
Carlos Catalano, Chair
Abhinav Nath
Kelly Lee

Program Authorized to Offer Degree:

School of Pharmacy – Medicinal Chemistry

University of Washington

Abstract

Thermodynamic and Directed Physical Characterization of Bacteriophage Lambda Capsid Maturation

Shannon Kruse

Chair of the Supervisory Committee:
Professor Carlos E. Catalano
Department of Medicinal Chemistry

All viruses undergo a multistep developmental process to assemble a mature virus. An essential step in the assembly of complex double-stranded DNA viruses is packaging the viral genome into a pre-formed procapsid shell. In bacteriophage λ, packaging of ~15 kb of DNA triggers a dramatic conformational change that expands the shell and increases the capsid volume two fold; this is a common feature in most dsDNA viruses. It has been recently demonstrated that expansion of the lambda procapsid is reversible and I have characterized the thermodynamic features of the transition. The data indicate that significant hydrophobic surface area is exposed in the expanded shell. It has been further shown that the gpD decoration protein adds to the expanded capsid lattice to stabilize the shell. GpD is a monomer in solution but self-assembles as a trimer spike at the three-fold verticies of the icosahedral capsid. Addition of gpD to the expanded capsid surface stabilizes the capsid from both external as well as internal forces. I propose that the hydrophobic patches exposed in the expanded capsid shell serve to nucleate gpD oligomerization at the capsid surface. I also propose that there are three additional non-covalent interactions that play important roles in stabilizing the expanded capsid from extreme internal pressure as DNA packaging is completed. Here I examine those interactions in detail along with gpD trimerization at the capsid surface using defined *in vitro*

biochemical assay systems. The results of this thesis provide insight into the complex nature and importance of capsid maturation for bacteriophage lambda that are generalizable to all of the complex dsDNA viruses, both prokaryotic and eukaryotic.

Contents

Page

Figure, Tables and Equations

Acknowledgments

I would first like to specifically say thank you to:

- Dr. Matt Honaker for all of the advice, wisdom, and quality guidance you gave me during this process.
- Dr. Jenny Chang for the assistance with learning numerous protocols and the fun discussions.
- Dr. Eri Nakatani-Webster for the example and insight over the years.
- Dr. Ben Andrews for the guidance and wisdom of thinking like a scientist and reaching the next hold.

Additionally I would like to thank Dr. Carlos E. Catalano without whom none of this would be possible.

A special thanks also to my committee for listening, being flexible, and all of the guidance.

To my former lab mates, thank you. I appreciate all the help and guidance I have gotten from various members of the Catalano lab: Dr. Rishi Sanyal, Dr. David Ortiz, and Lucas Monkkonen.

Outside of the research lab I would like to thank my fellow classmates who helped provide a support group while learning the ropes.

To my family and friends: thank you for constantly encouraging me and being understanding about the crazy schedule.

To my husband: Thank you for the support, patience, and help. I was truly blessed to be able to do lab work with you.

Finally, I would like to thank my parents who always held me to a high standard, encouraged me to do my best, and “enjoy the experience”.

Dedication

For their constant support and encouragement, I dedicate this dissertation to my Parents:

Kelly and Pat Kruse

My Husband:

Joseph Lambert

And my Friends:

Mel and Brooks

(Thanks for the companionship and friendship)

Chapter 1: Introduction

Viruses

The word virus comes from the Latin meaning toxin. The first recorded therapeutic use of a virus was during the attempted vaccination by Edward Jenner to prevent small pox in 1798 (Jenner, 1798). Although the presence of viruses in the vaccine was still to be discovered, the long history of virology was just beginning. It was not until 1935 that the components that make up a virus would be discovered (Pennazio & Roggero, 2000).

Viruses require a host cell to replicate and are known to infect prokaryotic, eukaryotic, and archaeal hosts. All viruses are made up of variations on three major components; nucleic acid material, proteins, and sometimes lipids and carbohydrates (Lansing Prescott, 1998). Genomes can consist of RNA or DNA, which can further be separated into single stranded (ss) or double stranded (ds), as well as linear or circular. In the case of ss RNA viruses the polarity of the genome can also be positive or negative, adding additional diversity. Positive RNA viruses have genomes that are similar to mRNA and can therefore start immediate translation upon infection. In contrast, negative sense RNA is *complementary* to mRNA and requires conversion to positive RNA by a viral RNA polymerase. Regardless of the specific type, the nucleic acid is contained in a viral coat composed of protein and sometimes further encapsulated in a lipid shell referred to as an envelope (Lansing Prescott, 1998).

Viruses vary greatly both in their physical dimensions and in the size of their genomes. Typically the size of the viral genome is an indicator of the size of the viruses;

however, the recent discovery of the largest recorded virus suggests the shell can overestimate the genome size on occasion. The discovery of the pithovirus, which has a viral shell of 0.5um in diameter despite the genome only being 1.9 to 2.5 megabases, increased the known size range of viruses from 10nm to 0.5um in diameter (Legendrea, et al., 2014). These vastly different sized viral shells also come in many shapes, which further differentiate viruses.

There are many variations on a few basic nucleocapsid types. First there are helical nucleocapsids that can be rigid or flexible rods. Additionally there are icosahedral shells that can be spherical or near spherical. Prolate capsids are elongated icosahedral shells, which is a capsid shape common among bacteriophages. In addition, these capsids may be enveloped, which possess a lipid membrane around the protein shell. Finally, “complex viruses”, such as poxvirus, are more difficult to define morphologically. The label of complex implies they could be a mix of the previously mentioned shells, contain extra structures such as a tail, or have a multifaceted outer wall that is not just a lipid membrane (Lansing Prescott, 1998).

Common and clinically important viruses exemplify the aforementioned viral diversity. Rhinovirus, which is responsible for the common cold, is a single stranded, positive-sense, RNA virus that has a non-enveloped icosahedral viral shell (Rossmann, et al., 1985). Ebolavirus in contrast is a single stranded, negative-sense, RNA virus with a long filamentous, enveloped nucleocapsid (Feldmann, Klenk, & Sanchez, 1993). Adeno-associated virus, which is used therapeutically in gene-therapy, is a single stranded DNA virus which has a non-enveloped icosahedral capsid (Rayaprolu, et al., 2013). Finally, herpes simplex virus 1 (HSV-1) is a complex dsDNA virus that

possesses a large (150kb) genome, an envelope, and a pleomorphic tegument between the envelope and the viral protein shell encapsulating the genome (Grünewald & Cyrklaff, 2006). Many bacteriophage, including lambda and T4, are also complex dsDNA viruses that possess multiprotein “tail” structures (Casjens, Hohn, & Kaiser, 1970).

Bacteriophage Classification

Bacteriophages are generally defined by type, of which there are many. For example, there are nine types of phages that infect *Escherichia coli* (Casjens S. R., 2005). A type is classified by having a similar lifestyle, transcription pattern, chromosomal gene order, and by their ability to infect related bacterial hosts. It is important to note that phages of the same type do not have to have similar gene sequence, but rather homologous genes and genetic organization. These analogous genes give rise to similar proteins with conserved function. This extends to eukaryotic viruses, such as the herpesviruses, where gene function is conserved, especially in the virus assembly proteins. It is due to this protein similarity that model systems, such as bacteriophages, are of such use in our understanding of eukaryotic virus biology.

Complex dsDNA Viruses

The complex dsDNA viruses included eukaryotic (herpesvirus) and prokaryotic (bacteriophage lambda) members and are characterized by large genomes encoding a high number of proteins. The viral developmental pathway is highly conserved among both prokaryotic and eukaryotic complex dsDNA viruses and is summarized as follows. (Calendar & Abedon, 2006)**;** (Roizman & Palese, 1996),

In general viral development includes the assembly of preformed viral "procapsids" and the synthesis of viral genomes in independent pathways. These pathways converge when a packaging motor, known as terminase, then translocates the genome into the capsid shell, a process known as DNA packaging. Packaging of the genetic material triggers a major re-organization of the capsid proteins in the shell, often yielding an expanded structure that increases the internal volume of the capsid, in some cases two fold (Galisteo & King, 1993) (Duda R. L., Hempel, Shabanowitz, Hunt, & Hendrix, 1995). In most cases, the expanded shell is unstable and a variety of approaches are utilized to stabilize the structure so that DNA packaging can continue to completion. These can include chemical cross-linking and proteolysis (Figure 1-1). Following capsid stabilization packaging of the genetic material continues to completion.

Figure 1-1. General virus assembly pathway for complex dsDNA viruses. The pathway is unidirectional *in vivo* and progresses though each step sequentially. DNA packaging, shell expansion, shell stabilization, and full genome packaging are the major steps in the assembly pathway.

Bacteriophages

Bacteriophages, meaning bacteria eaters in Greek, are dsDNA viruses that infect bacterial hosts. First discovered at the beginning of the 1900's by both Frederick Twort and Félix d'Hérelle, bacteriophages potential use as antimicrobials was immediately considered (Sulakvelidze, Alavidze, & Morris, 2001). They were first used as

antimicrobials to treat dysentery caused by *Shigella* (Brussow, 2013). It was later reported that phages were also used to treat colitis, enteritis, and typhoid fever (Keen, 2012). While bacteriophages showed promise therapeutically, their use declined markedly with the discovery of antibiotics such as the penicillin and the subsequent use of sulfa drugs (Sulakvelidze, Alavidze, & Morris, 2001). Recent issues with multi-drug resistance has resulted in renewed interest in phage therapy.

Phages were additionally used in furthering molecular biology research in the 20th century (Bratkovic, 2010). In the 1950s Hershey and Chase utilized phage T2 as a model system to study viral replication and to affirm that DNA serves as genetic material (Hershey & Chase, 1952). Phage ϕX174 also played a key role in biology being the first organism to have its entire genome sequenced (Sanger, et al., 1977). Bacteriophages lambda and Mu have been used to better understand recombinant DNA technology and Lambda has served to shed light on transcriptional regulation.

More recently, a new field known as physical virology has emerged that seeks to characterize virus development using modern biochemical, biophysical, and structural approaches. In this respect, bacteriophage lambda has been well characterized with *in vitro* assays developed to examine genome replication, procapsid assembly, DNA packaging, shell expansion, and shell stabilization. Further, our lab has developed an assay where a fully infectious virus may be assembled with purified components *in vitro.* Robust purification methods for lambda phage proteins have been developed over the last half century. The extensive characterization of lambda's overall viral development pathway also adds to its utility? as a model system. Our lab is interested in biophysical and thermodynamic characterization of the entire lambda assembly pathway. Within

this overall goal, I propose to use bacteriophage lambda to better understand the developmental pathway of complex dsDNA viruses, specifically the capsid expansion and stabilization steps of the viral assembly pathway.

Bacteriophage Lambda (λ)

Bacteriophage lambda was first isolated by Esther Lederberg in 1950 (Lederberg & Lederberg, 1953). As previously mentioned, the use of lambda as a therapeutic declined with the discovery of antibiotics. Nevertheless, lambda continued to be of great use to the field of transcriptional regulation (Oppenheim, Kobiler, Court, & Adhya, 2005). Additionally an increase in the use of lambda has been seen as a platform for phage display (Bratkovic, 2010). More recently lambda has provided an ideal model system for the study of viral assembly in the complex dsDNA viruses.

Model systems are an important part of scientific research. They play an important role in providing molecular detail to our understanding of biology in cases where the more complex systems are intractable due to problems such as protein expression, purification, or solubility. Bacteriophage lambda is well suited as a model system to characterize eukaryotic dsDNA viral assembly due to its similarity in assembly pathways.

Bacteriophage lambda belongs to the order of *Caudovirales,* family *Siphoviridae*. These are icosahedral, non-enveloped bacterial viruses that possess a linear double-stranded genome and a long non-contractile tail. Lambda is known to infect *Escherichia coli,* which initiates with the binding of the viral tail fibers (gpJ protein) to the maltose receptor (LamB) on the bacterium (Randall-Hazelbauer & Schwartz, 1973) (Thirion &

and Hofnung, 1972)**.** This interaction triggers opening of the tail tube and injection of its genetic material through the cell wall into the cell cytoplasm. This is driven, in part, by the pressure generated by the tightly-packaged genome (discussed further below).

Lysogenic Pathway. Once Lambda has injected its genome into the host cell, development may follow one of two different pathways ~ lysogenic vs. lytic. In the former case, viral genetic material is site-specifically inserted into the host genome (Lederberg J. L., 1951). Lysogeny is most often seen during inoculation in nutrient poor media or when a host cell is infected by numerous copies of the virus (Kourilsky P. , 1973) (Kourilsky & Knapp, 1974). During lysogeny the inserted viral genome remains in a latent state, with only the viral cro and cI repressor proteins being expressed. Indeed, it was in this "lysogen" or "prophage" form that lambda was first discovered (Oppenheim, Kobiler, Court, & Adhya, 2005). The cI repressor protein is responsible for keeping the virus in this latent prophage form by binding to the O_R and O_L, operator sites in the lambda genome, which silences transcription of viral proteins from the P_L and P_R promoters (Dodd, Shearwin, & Egan, 2005).

During cellular stress the lambda genome is excised from the host genome due to autoproteolysis of the cI repressor, stimulated by the *E. coli* RecA protein (Dodd, Shearwin, & Egan, 2005) (Hochschild & Lewis, 2009). Excision of the lambda genome initiates lytic development. The hallmark of the lytic life cycle is replication of viral DNA, the production of viral proteins and the assembly of infectious viruses (Oppenheim, Kobiler, Court, & Adhya, 2005). It does not matter if lambda virus enters the lytic life cycle from prophage, or immediately upon genome injection into the host cell; infectious viral progeny and lysis of the host cell is the result.

Lytic Development ~ Genome Replication. Lytic development is the relevant pathway for viral development and starts with DNA replication. Lambda's genome enters the host as linear dsDNA, but quickly circularizes via the complementary 12 base single-stranded "sticky ends" (Daniels, Schroeder, & Al, 1983). Viral DNA replication utilizes the *Escherichia coli* replication machinery, except that the viral gpO and gpP proteins are used in place of the host dnaA and dnaC proteins to initiate replication. These proteins direct the host replication complex to the *ori* site on the lambda genome instead of the *ori*C site of the host genome (Kaguni, 2006). This initial replication of the circular lambda genome is referred to as theta (θ) replication due to the intermediates of this replication looking like the Greek letter "θ", a result of classical bi-directional DNA synthesis (Figure 1-2) During this initial replication between 50 and 100 copies of circular lambda genome are synthesized (Narajczyk et al. 2007)(Taylor and Wegrzyn,1995). At later times, lambda genome replication switches to a rolling circle or sigma (σ) mechanism. This σ replication produces linear genome concatemers linked in a head to toe fashion. (Figure 1-2) Concurrent with DNA replication, protein expression for procapsids and tails is underway, as described below.

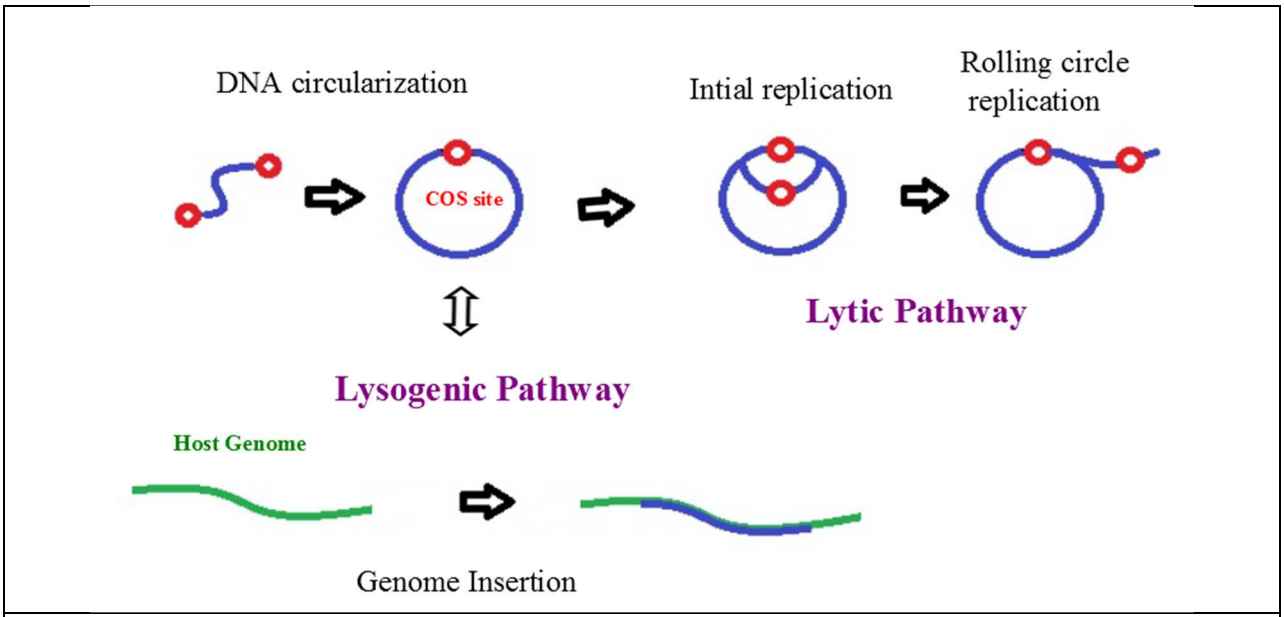

Figure 1-2: Lytic and lysogenic pathways of bacteriophage lambda development. The two possible fates for lambda dsDNA upon entering the host cell. The lysogenic pathway leads to insertion of lambda genome into the host genome and viral latency. In the lytic pathway, the viral genome is first copied into circular daughter genomes. Subsequently, this is followed by rolling circle replication resulting in a linear concatemer of genomes linked head to tail. The lytic pathway can follow the lysogenic pathway once the integrated genome is excised. In all cases, rolling circle replication follows the initial bi-directional replication of the genome.

Lambda Shell Assembly. Assembly of the lambda capsid shell involves multiple viral proteins and the host groELS chaperonin system (Georgopoulos, Tilly, & Casjens, 1983). Shell assembly initiates with the formation of the portal ring, which is made up of twelve copies of viral protein gpB. This step requires both groELS and the lambda scaffolding protein, gpNu3. The portal ring nucleates polymerization of 415 copies of gpE, the major capsid protein into an icosahedral shell, chaperoned by groELS and co-polymerization of ~ 200 copies of gpNu3 that reside within the shell. A limited number of gpC protease proteins (~ 10-20) are also incorporated into the shell interior at this time, which affords the immature procapsid. The viral protease removes 20 N-terminal amino acids from approximately half of the gpB portal proteins, degrades gpNu3 and is auto-proteolytic. The small proteolytic fragments leave the procapsid interior either through

the portal or through small openings in the shell (Medina, Andrews, Nakatani, & Catalano, 2011). The resulting “mature” procapsid shell is composed of 415 copies of gpE arranged as an icosahedron with T = 7 symmetry. There are 12 vertices on the capsid, 11 of which are made up of pentamers of gpE along with 20 faces made of trimers of gpE hexamers. The portal sits at one of the five-fold vertexes and is referred to as the “portal vertex”. This “hole” is where DNA enters the capsid during packaging and exits during infection (Lander, Evilevitch, Jeembaeva, Potter, Carragher, & Johnson, 2008).

Genome Packaging. Approximately 15 minutes after infection, the cell contains 10-20 genome concatemers (immature DNA), ~200 pre-assembled procapsids, and ~200 pre-assembled tail structures containing 11 lambda proteins assembled in the presence of two lambda encoded chaperone proteins (Jun Xu, 2014). The next step in virus development is packaging of individual genome monomers (mature DNA) into the procapsid shells. This involves excision of a single genome from the concatemer and physically translocating the duplex into the procapsid. This is performed by the viral terminase enzyme, which is a hetero-oligomer composed of gpA and gpNu1 subunits (Maluf, Gaussier, Bogner, Feiss, & and Catalano, 2006). The small gpNu1 subunit (20.4 kDa) is responsible for the specific recruitment of terminase to the packaging initiation site (*cos*) in the concatemer (Catalano C. E., 2000). The *cos* site is the junction between the head and tail of a genome in the concatemer; recruitment of terminase to this site is be aided by the *Escherichia coli* Integration Host Factor protein (IHF) which is known to bend the DNA (Rice, Yang, Mizuuchi, & Nash, 1996) (Sanyal, Yang, & Catalano, 2014) (Ortega & Catalano, 2006).

Once recruited to the *cos* site, the large gpA subunit (73.3 kDa) of terminase, which possesses the site-specific endonuclease activity required to excise a genome monomer, nicks the duplex at *cos* to generate the mature left end of the first genome to be packaged (Hang, Tack, & Feiss, 2000) (Hwang, Hang, Neagle, Duffy, & Feiss, 2000) (Rubinchik, Parris, & Gold, 1994). Terminase remains bound to the matured (sticky) end and next binds the portal of a preformed procapsid. This activates the packaging ATPase activity of the enzyme, which translocates DNA into the procapsid. (Figure 1-3) Upon packaging of ~15% of the lambda genome into the procapsid, a remarkable expansion transition occurs (Dokland & Murialdo, 1993) (Fuller, et al., 2007b) (Hohn T. W., 1976). The expansion transition results in shell thinning, increased angularization, and increases the shell diameter by 5-10nm while increasing the volume two fold. The expanded structure is referred to as the capsid. A major reorganization of the procapsid shell, driven by DNA packaging, occurs in most complex dsDNA viruses and the importance of this step can be seen by its conservation throughout a large number of viral assembly pathways (Catalano, Cue, & Feiss, 1995).

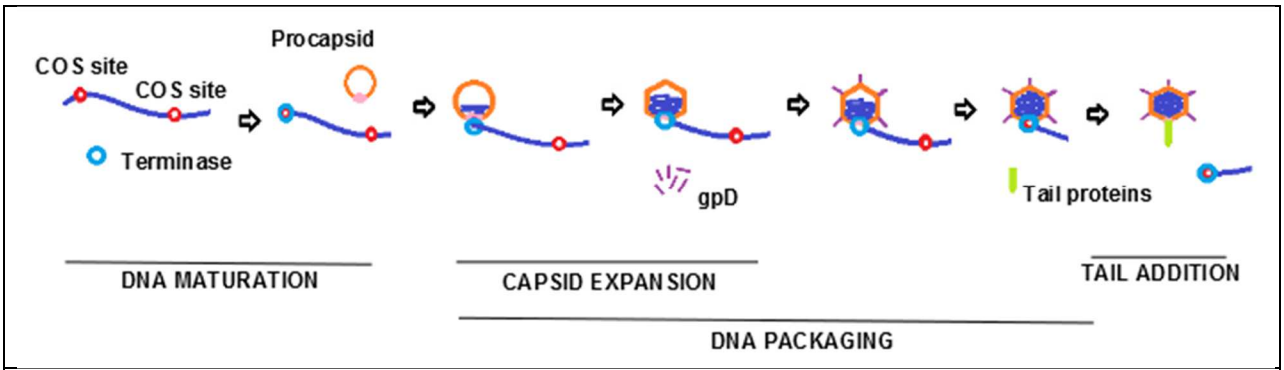

Figure 1-3: Bacteriophage lambda viral assembly pathway. Major stages of the viral assembly pathway are depicted: DNA maturation and packaging, procapsid expansion, capsid stabilization and tail addition. In depth description of the pathway is found in the text.

The expanded lambda capsid is fragile and must be stabilized with the addition of gpD, the viral decoration protein. While dispensable for packaging of sub-genomic DNA, gpD is essential for packaging of the full-length genome. This is discussed further below. Terminase continues to translocate along the duplex until it reaches the next *cos* site in the concatemer (the end of the genome, Figure 1-3). At this point, DNA is packaged to liquid crystalline density and generates over 25 atm internal pressure (Fuller, et al., 2007b). Terminase nicks the duplex at the downstream *cos* site, leaving the complimentary sticky right genome end. The gpW finishing protein replaces terminase at the portal vertex, which releases the terminase-concatemer complex to package another genome into another procapsid. The gpFII adapter protein adds to gpW, followed by a pre-assembled tail complex, which is composed of 11 viral proteins. This affords an infectious virus (Casjens & Hendrix, 1974); (Gaussier, Yang, & Catalano, 2006); (Maxwell, Davidson, Murialdo, & Gold, 2000) which contains a unit-length mature genome that possess complementary 12-base, single stranded "sticky" ends as required for re-circularization upon injection into the host cell in the next infection cycle (Daniels, Schroeder, & Al, 1983).

Procapsid Expansion and Shell Decoration with gpD. As discussed above, genome packaging drives procapsid expansion and the addition of decoration protein stabilizes the expanded procapsid allowing full concatemeric DNA to be packaged to liquid-crystalline density. A thermodynamic analysis of the expansion transition is presented in Chapter 2 of this thesis. In the absence of gpD, the fragile shell breaks due to the tremendous stresses on the capsid shell generated by the densely packaged DNA (Fuller, et al., 2007b) (Tzlil, Kindt, Gelbart, & and Ben-Shaul, 2003). Previous

studies looking at the ability of lambda capsids to package DNA in the absence of gpD show that only sub-genomic lengths can be packaged without loss of capsid integrity (Yang, Maluf, & and Catalano, 2008).

gpD is a monomer in solution but assembles as a trimer upon binding to the expanded capsid surface. The protein does not bind to unexpanded procapsids suggesting that there is exposure of surface area during capsid expansion that is important for the nucleation of gpD to the capsid surface. Additionally it is still unknown what chemical and physical interactions drive binding of gpD to the capsid surface and if these or other interactions are responsible for the stability gpD imparts to the expanded capsid. These questions are directly addressed in Chapter 3 of this thesis.

Viral assembly pathways are unidirectional *in vivo*, and this irreversibility is also seen *in vitro*. This "biological irreversibility" is important for the overall virus developmental pathway to ensure a one way route towards infectious progeny. The irreversibility is highlighted in the viral assembly pathway where proteins specifically add at each step, but not before. There is little to no interaction observed between terminase and the portal until viral DNA maturation is complete. Additionally gpD does not bind to the procapsid but only the expanded capsid shell, which does not expand until DNA packaging has begun. The finishing protein gpW does not interact with terminase or the portal but binds the portal once the genome is fully packaged. This high degree of specificity allows for each step in the assembly pathway to be essentially irreversible and generate stable nucleoprotein intermediates without consequences of off pathway complexes.

Our lab has purified all of the proteins required to assemble an infectious lambda virus under defined conditions *in vitro*. High yield protein purification and *in vitro* assays designed to investigate each step of the viral assembly pathway has made it a decidedly useful model system to study dsDNA virus development. Given the conservation of the developmental pathways in both prokaryotic and eukaryotic dsDNA viruses, lambda is poised to study the general features of viral assembly in the complex dsDNA viruses as well as better understand individual protein function in these pathways.

Current Research

Our lab recently demonstrated that urea can trigger expansion of the lambda procapsid *in vitro* and that unexpectedly, the transion is reversible *in vitro*. This allows thermodynamic investigation of this transition and in Chapter 2 I characterize this important step. I specifically look at the equilibrium between the procapsid state and the expanded capsid state. Additionally, I define the free energy, $\Delta G(H_2O)$, of expansion and my results further provide insight into the nature of the exposed surface area on the expanded capsid that is important in gpD binding.

Structural homology studies performed in our lab have suggested specific molecular interactions that have the potential to be important not only in binding of gpD to the expanded capsid surface, but also necessary for the stability of the expanded capsid imparted by gpD binding. In Chapter 3 of this thesis I directly test the hypothesis that gpD residues Pro17 and His19 specifically interact with gpE residues Trp308 and Asp298, respectively, and that these interactions are necessary for gpD binding and

stabilization of the expanded capsid. Using a combined mutagenesis and biochemical approach I also test the hypothesis presented in Chapter 2 that hydrophobic surface area exposed during procapsid expansion is essential in gpD binding to the casid surface.

Previous studies in our lab have indirectly looked at gpD binding to the capsid and proposed a complex binding model for gpD adding to the expanded caspid surface. I propose that gpD binding to the expanded capsid follows a complex binding model which includes an initial distributive binding event followed by cooperative binding to engender the mature trimer spike. In Chapter 4, I use a gel based gpD addition assay to directly test this hypothesised binding model.

The data described in this thesis details the thermodynamics of the expansion of the lambda procapsid, as well as an in-depth look at the forces responsible for the addition of gpD to the capsid surface. Additionally, the interactions between gpD and the capsid that are responsible for the stabilization of the lambda expanded shell are examined. Both of these steps are imperative for the assembly of not only an infectious lambda virus, but are generalizable to all complex dsDNA viruses, both prokaryotic and eukaryotic. The exact values determined here may not be directly applicable to other dsDNA viruses but the qualitative concepts are. The results of my thesis are important not only for the field of virology, but also have application for the design and development of lambda as a “theragnostic” nanoparticle.

Chapter 2: Thermodynamic Characterization of the Procapsid Expansion Transition

The developmental pathways for the complex dsDNA viruses are remarkably conserved in both eukaryotic and prokaryotic viruses. Major steps of note in virus development are DNA replication, procapsid assembly, and packaging of a single genome into the preformed procapsids. The pathway for assembling an infectious virus from macromolecular precursors follows a specific, typically unidirectional pathway. These steps are highly conserved in the complex dsDNA viruses, especially between the herpesvirus groups and many bacteriophages (Figure 2-1).

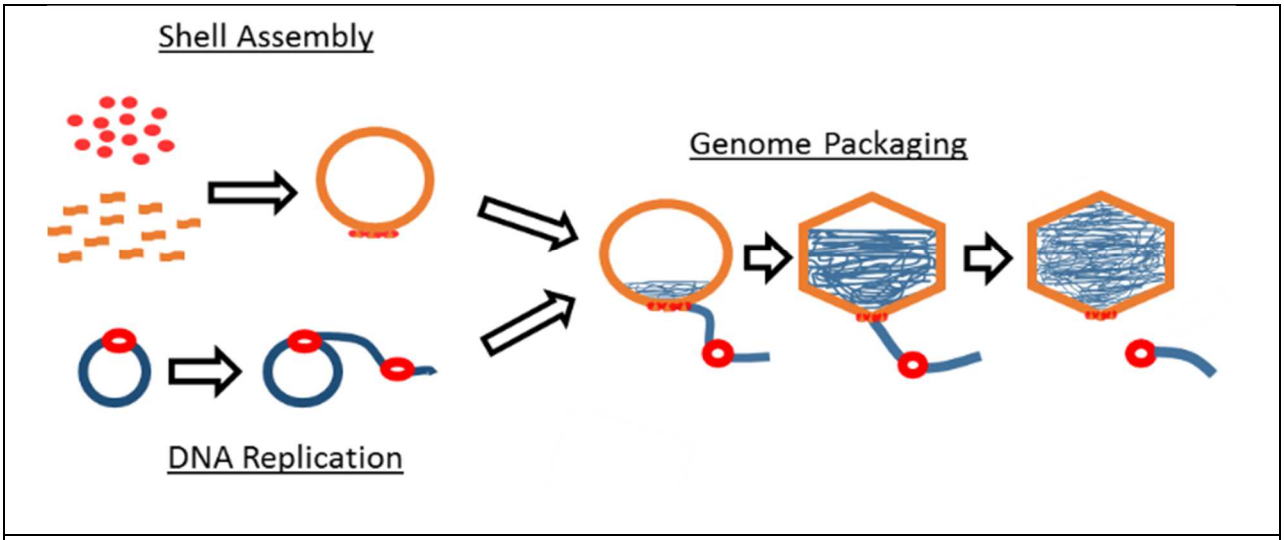

Figure 2-1. General viral assembly scheme. Major steps of a complex dsDNA viral assembly pathway are depicted. The methods of each step vary but the end result is similar as depicted here.

Complex dsDNA Viral Assembly. The general viral assembly pathway starts where the DNA replication and procapsid assembly pathways end, bringing the two products together in the packaging of viral genomes. The major steps of viral assembly

are packaging initiation, shell expansion, shell stabilization, followed by final genome packaging (Figure 2-2). Numerous phages including lambda T4, T7, phi29 along with phage P22, and the eukaryotic herpesviruses are known to use a nanomotor, known as terminase, to package a viral genome into a preformed viral shell (Casjens S. R., 2011).

Figure 2-2. General virus assembly pathway for complex dsDNA viruses. The pathway is unidirectional in vivo and progresses though each step sequentially. DNA packaging, shell expansion, shell stabilization, and full genome packaging are the major step in the assembly pathway.

Shell Expansion. The initiation of packaging into the viral shell causes subsequent shell expansion. Major conformational alteration of the viral shell during genome packaging is a common feature in the developmental pathways of the dsDNA viruses. In many cases, including bacteriophages lambda, HK97 and P22, the shells undergo an expansion transition (Galisteo & King, 1993) (Duda R. L., Hempel, Michel, & Shabanowitz, 1995) (Heymann, Cheng, Newcomb, Trus, & Brown, 2003). In other cases, such as bacteriophage phi29 and herpes simplex virus, the shells do not expand in size but the capsids are still observed to gain a more angular appearance during the packaging process. For a number of these viral systems, the procapsids can be expanded *in vitro* with the use of pH, temperature, and/or denaturants (Galisteo & King, 1993) (Duda R. L., Hempel, Shabanowitz, Hunt, & Hendrix, 1995) (Kunzler & Hohn, 1978). In each of these cases, the expansion transition is essentially irreversible and it is commonly accepted that this ensures a one-way progression through the pathway.

Shell Stabilization. The expanded viral shells are fragile and require stabilization. Methods of stabilization vary between viruses. HK97 for example, employs an autocatalytic chemical cross-linking of its subunits to stabilize the expanded capsid (Lee, Gan, Tsurata, Hendrix, Duda, & Johnson, 2004). Other viruses use "stabilizing" decoration proteins. Examples of these are adenovirus, the herpesviruses, bacteriophages lambda and T4 (Fuller, et al., 2007b) (Tzlil, Kindt, Gelbart, & and Ben-Shaul, 2003) (Wendt & and Feiss, 2004).

Viral assembly pathways are strongly conserved in all the complex dsDNA viruses, and it is commonly believed that the process is highly unidirectional. The large amount of genetic, biochemical, and structural characterization that has been done on bacteriophage lambda makes it an idea model system to study specific steps of the viral assembly pathway. A brief overview of the lambda assembly pathway is described below and depicted in Figure 2-3.

Replication of Lambda DNA. An in depth discussion of bacteriophage lambda DNA replication is presented in Chapter one. Briefly, during the latter stages of infection, lambda DNA is replicated by a σ "rolling circle" mechanism, that yields concatemers of single genomes linked in a head to toe fashion (immature DNA). These concatemers are the preferred packaging substrate and are "matured" by the packaging motor, terminase.

Assembly of the Lambda Procapsid Shell. Concurrent with DNA replication, viral protein synthesis affords structural proteins that self-assemble into procapsid and tail complexes. Lambda procapsid assembly follows an ordered pathway that yields a

procapsid shell that is matured into a larger capsid structure. Assembly begins with the viral protein, gpB, which self assembles into a dodecameric ring structure known as the portal. The portal ring nucleates polymerization of gpE, the major capsid protein, into an icosahedral shell, chaperoned by co-polymerization of the gpNu3 scaffolding protein. The shell is made up of 415 copies of gpE in an isometric T=7 icosahedral lattice composed of gpE hexamers that form the faces of the icosahedron and pentamers that form 11 of the 12 vertices; the portal ring is situated at a unique “portal vertex” (Wurtz, Kistler, & Hohn, 1976) (Imber, Tsugita, Wurtz, & Hohn, 1980). At this stage of capsid maturation the hexamers are asymmetric (Black, 1989) (Dokland & Murialdo, 1993). The viral protease gpC is also included in limited quantities into the nascent procapsid interior (Casjens & Hendrix, 1974). gpC is responsible for proteolysis of the N-terminal 20 residues from approximately half of the gpB proteins making up the portal and for proteolysis of gpNu3 contained within the shell; it is also auto-proteolytic. Digested fragments generated by gpC leave the procapsid either through the portal or through small holes in the viral shell. This yields the mature procapsid composed of an icosahedral gpE shell with a single gpB portal ring situated at a unique vertex, which serves as the opening through which DNA is packaging into the procapsid.(Figure 2-3)

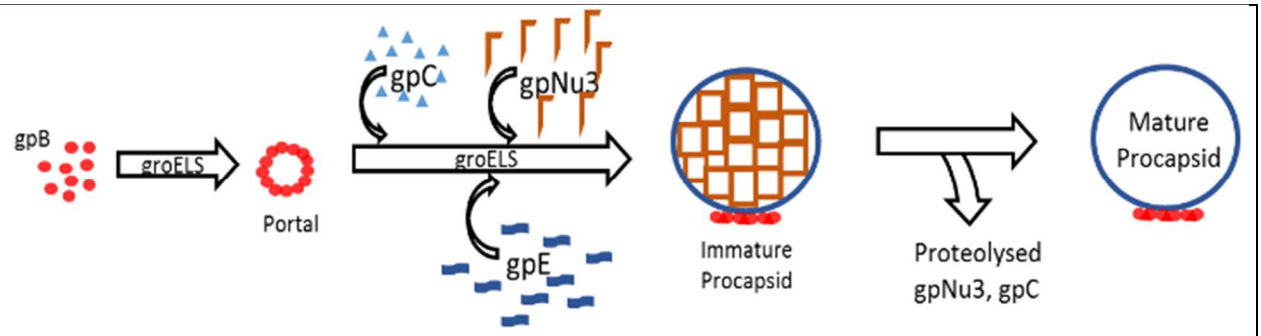

Figure 2-3. Scheme of lambda procapsid assembly in vivo. Twelve copies of gpB chaperoned by groELS form a dodecameric ring called the portal. The portal ring nucleates gpNu3 and gpE copolymerization, along with a limited number of gpC, to form the immature procapsid. GpC is autoproteolytic and also degrades gpNu3 and the 20 N-terminal residues of ~6 of the gpB. Proteolysis products leave through the portal of the mature procapsid.

Genome Packaging The DNA replication and procapsid assembly pathways converge at this point. The enzyme terminase is responsible for maturing concatemeric DNA and simultaneous packaging of DNA into the capsid. As described in detail in Chapter one, terminase and IHF cooperatively assemble at the *cos* site using the small terminase subunit to direct specific binding. Terminase cuts the duplex at *cos* and then binds to the portal of the preformed procapsid. This activates ATP hydrolysis, which drives the motor to package the dsDNA into the viral procapsid (Catalano C. E., 2000).

The Procapsid Expansion Transition. After packaging of ~15 kb of viral DNA, expansion of the procapsid takes place (Figure 2-4) (Fuller, et al., 2007b). During expansion the procapsid undergoes a large reorganization of the capsid proteins assembled into the shell. The asymmetric gpE hexamers rearrange to form a defined six-fold symmetry, the shell increases from a diameter of ~50nm to a diameter of ~60nm and its internal volume increases two fold (Fuller, et al., 2007b) (Dokland & Murialdo,

1993). The result of this expansion is a thinner, more angular capsid that can accommodate the full length, 48.5 kb viral genome.

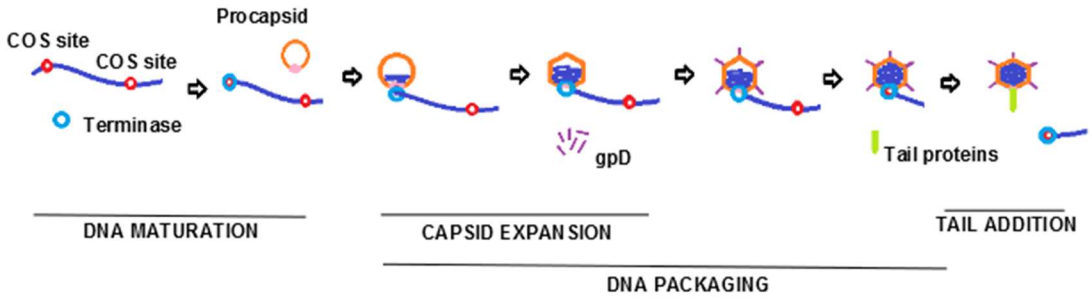

Figure 2-4: Bacteriophage lambda viral assembly pathway. Major stages of the viral assembly pathway are depicted here. DNA maturation and packaging are followed by procapsid expansion. This is followed by capsid stabilization, full genome packaging, and then tail addition. These steps are considered a one directional pathway.

gpD Addition. The expanded shell is fragile and addition of gpD, lambda's decoration protein, is essential for stabilization of the expanded capsid (Yang, Maluf, & and Catalano, 2008) (Imber, Tsugita, Wurtz, & Hohn, 1980). GpD is a monomer in solution and does not bind to the procapsid; however, the protein binds as a trimer spike to the expanded capsid surface at each of the 140 three-fold axes (Lander, Evilevitch, Jeembaeva, Potter, Carragher, & Johnson, 2008). gpD binding stabilizes the expanded capsid against both internal and external forces. In Chapters three and four of this thesis I describe studies that seek to determine the nature of cooperative gpD assembly at the expanded capsid and to identify important molecular interactions that are responsible for capsid stabilization.

The Procapsid Expansion Transition. Previous work by Kunzler and Hohn showed that 4M urea triggers lambda procapsid expansion *in vitro*. The shells are

morphologically identical to those expanded by DNA packaging (Kunzler & Hohn, 1978) (Hohn T. W., 1976) (Figure 2-5). Additionally, analytical ultracentrifugation studies confirmed that the molecular weight of the expanded shells was identical to that of the procapsids (Kunzler & Hohn, 1978). This indicates that expansion is a result of a conformational change of capsid proteins and not due to proteolysis or the addition of supplementary proteins.

Figure 2-5. In vitro and in vivo methods of lambda procapsid expansion. Urea and DNA packaging triggered expansion result in similarly expanded procapsids.

Our lab recently reported the surprising observation that the expansion of lambda procapsids was fully reversible with the addition of magnesium. In this chapter, I further investigate urea-triggered procapsid expansion *in vitro* and examine the biochemical, physical, and structural characteristics of the expansion-contraction transition and equilibrium. I find that the transition from procapsid to expanded capsids is fully reversible and strongly affected by temperature, magnesium concentration, urea concentration, and salt concentration (Figure 2-6). The data indicate that magnesium and urea stabilize the procapsid and expanded capsid conformations, respectively. I define the thermodynamic features of the transition and confirm that urea-expanded capsids are biologically competent, similar to those generated by DNA packaging.

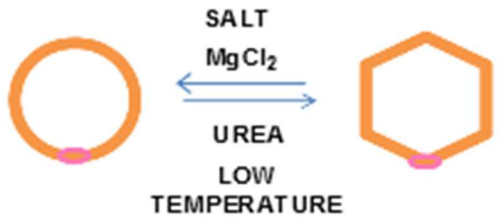

Figure 2-6. Equilibrium between lambda procapsid and expanded procapsid. Urea and low temperature stabilize the expanded procapsid state while salt and $MgCl_2$ stabilize the procapsid state.

Material and Methods

Experimental details for these studies are presented in Chapter 5.

Results

DNA packaging is vital for the assembly of an infectious virus. Packaging triggers procapsid expansion *in vivo*, which is an essential step for packaging the full-length genome. In order to better understand this transition, I here study in detail urea-triggered capsid expansion *in vitro*.

Urea Driven Procapsid Expansion. Hohn and co-workers demonstrated that lambda procapsids could be expanded with urea *in vitro* and I recapitulated this result. As shown in Figure 2-7, 2.5 molar urea effectively expands procapsids *in vitro*. Consistent with published results, the capsids remain expanded when urea is removed by dialysis in the presence of low concentrations of $MgCl_2$ (<1 mM); however increasing the magnesium concentration in the dialysis buffer (~15 mM) resulted in contraction of the capsids back to the procapsid conformation (Figure 2-7). Additionally our lab showed that procapsids could be expanded in urea, buffer exchanged out of urea, and contracted with magnesium for several cycles. This observation demonstrates that the

expansion transition is fully reversible. This result was very surprising because until this time it was believed that procapsid expansion was irreversible, both *in vivo* and *in vitro*.

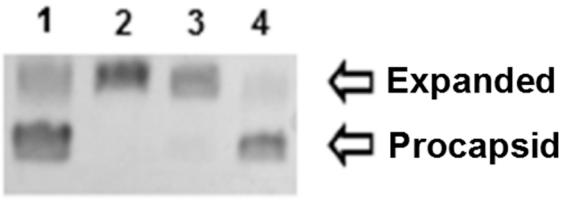

Figure 2-7. Lambda procapsid expansion and contraction is a reversible transition. Native agarose gel depicting the difference in mobility between the procapsid and expanded capsid shells. Lane 1, procapsids. Note there is a small and variable amount of pre-expanded shells in the procapsid preparations; Lane 2, procapsids expanded in 2.5 M urea; Lane 3, urea expanded procapsids buffer exchanged into buffer without urea; Lane 4, expanded capsids exchanged into buffer containing 15mM $MgCl_2$ contract back to the procapsid state.

Our lab further demonstrated that procapsids can be expanded by urea in a concentration dependent manner (Medina 2010) (Figure 2-8). Close inspection of the gel reveals that no bands except procapsids and expanded capsids are present, suggesting that there are no expansion or contraction intermediates. In other words, expansion is an apparent two-state transition. The fraction of procapsids expanded at each urea concentration was quantified by video densitometry as described in Materials and Methods (Chapter 5) and the data analyzed as described below (Figure 2-9).

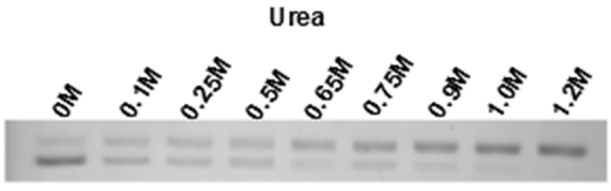

Figure 2-8. Urea concentration dependent procapsid expansion. Procapsid expansion in 0.2 mM $MgCl_2$. Procapsids were incubated with indicated urea concentrations on ice for 10 min and the fraction expanded was analyzed by agarose gel as described in Materials and Method. The expanded shells run slower on the gel, as demonstrated in Figure 2-7.

Thermodynamic Characterization of Procapsid Expansion. The data presented above indicate that the urea-triggered procapsid expansion can be treated as a fully reversible, two-state transition (Figures 2-7 & 2-8). These features allow a rigorous thermodynamic characterization of the process. Towards this end, I analyzed the expansion transition data by adapting the well-established protocols used to characterize chemical denaturation curves common to protein unfolding experiments. Specifically, the approach outlined by Santoro and Bolen was adapted to determine the free energy of the transition, $\Delta G(H_2O)$, for procapsids expanded in the presence of 0.2 mM magnesium (Figure 2-9) (Equation 2-1).

$$F_E = \frac{(m_P*[U]+b_P)+(m_E*[U]+b_E)*exp\left[-\left(\frac{\Delta G_{H_2O}}{RT}+\frac{m_G*[U]}{RT}\right)\right]}{1+exp\left[-\left(\frac{\Delta G_{H_2O}}{RT}+\frac{m_G*[U]}{RT}\right)\right]}$$

Equation 2-1. Linear extrapolation analysis of the expansion transition. F_E is the fraction of expanded capsids as a function of urea concentration [U]. m_p and m_E represent slope while b_P and b_E represent y-intercepts of pre- and post-baselines, respectively. $\Delta G(H_2O)$ (kcal/mol) is the free energy of the transition in the absence of urea and m_G (kcal/mol*M) is the denaturant *m* value. R (the ideal gas constant) and T (temperature in Kelvin) were held constant in the NLLS fit.

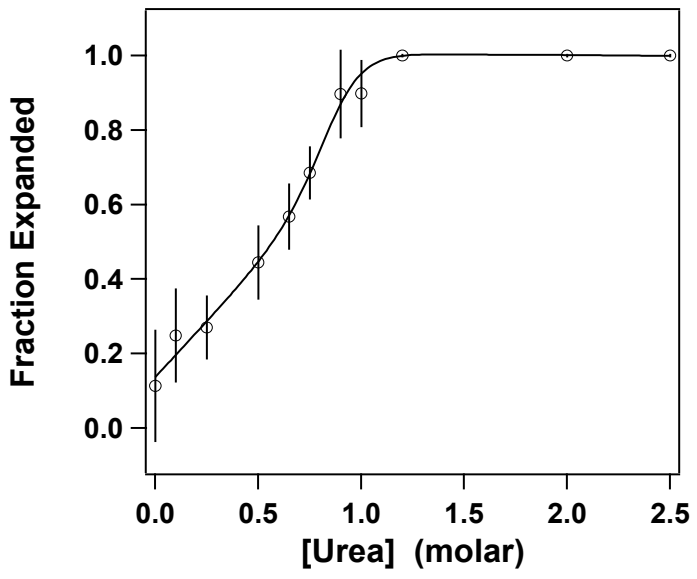

Figure 2-9. Graph of fraction of expanded procapsids verses urea concentration in the presence of 0.2 mM $MgCl_2$. The data presented in Figure 2-8 was quantified to afford the fraction of procapsids expanded (F_E) as a function of urea concentration. Each data point represents the average of three independent experiments. The errors bars represent standard deviation. Note the pre-transition slope, which I attribute to heterogeneity in the procapsid sample (discussed below). The fitting routine allows deconvolution of the pre-transition baseline from the primary transition.

The expansion data were analyzed according to equation 2-1 using non-linear least squares (NLLS) approaches. This allows for the best fit of pre and post transition baselines, which affords a more accurate extrapolation to obtain the $\Delta G(H_2O)$ and *m*. The data presented in Figure 2-8 were fit to equation 2-1 holding R and T constant, and allowing the other variables to float to their best fit values. This affords a $\Delta G(H_2O)$ ~3 kcal/mol. The use of equation 2-1 allows for the "flattening" of the baselines to allow for direct analysis of the major transition under the assumption of two-state behavior.

In addition to $\Delta G(H_2O)$, this analysis provides the concentration of urea required to expanded 50% of the total procapsids ($[urea]_{1/2}$) as well as the denaturant "*m*" value. The latter represents the slope of the Fraction Expanded vs. [urea] plot within the transition region. While this value has been interpreted in various ways, it correlates well with the exposure of hydrophobic surface area during the transition; the larger the value,

the more surface area exposed (Santoro & Bolen, 1988). In the case of procapsid expansion, the denaturant *m* value is relatively large, which suggests that a large amount of hydrophobic surface area is exposed.

Effect of Mg on Urea-Triggered Expansion. Divalent cations are known to play an important role in many viral assembly processes (Brady, 1977) (Yanagi, 1989). Specifically, divalent metals have been shown to play important roles in capsid assembly and stability (Bode & Harrison, 1973) (Salunke, Caspar, & Garceat, 1989). More directly, preliminary data in our lab suggested that magnesium at elevated concentrations drove the expanded lambda shell back to the procapsid conformation (Figure 2-6). Therefore, I next examined the effect of magnesium concentration on urea-triggered expansion.

I repeated the urea-expansion study, however this time in the presence of increased concentrations of magnesium (3 mM or 10 mM). The resulting data appears in Figure 2-10a along with the 0.2mM magnesium data. The figure clearly demonstrates that magnesium has an antagonistic effect on procapsid expansion, and in a concentration dependent manner. Magnesium strongly affects the concentration of urea required to expand half of the procapsids ($[urea]_{1/2}$) (Figure 2-10b). Analysis of each data set affords a $\Delta G(H_2O)$ for procapsid expansion of 10.0±3.0 kcal/mol and 13.4±2.4 kcal/mol in the presence of 3 mM and 10 mM $MgCl_2$, respectively. Importantly, I note that while magnesium strongly affects the $\Delta G(H_2O)$ for the transition, the denaturant *m* value remains large and relatively unaffected. This is discussed further below.

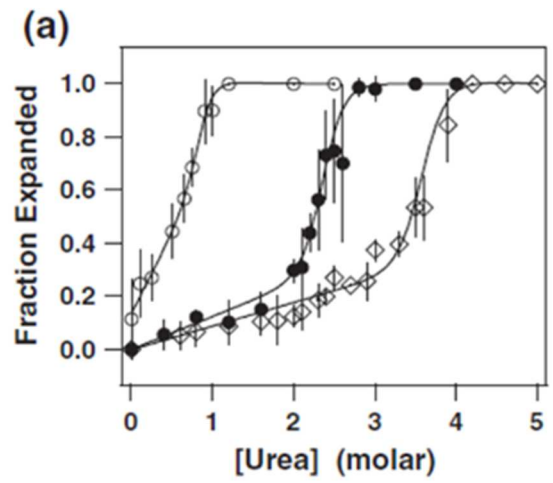

Figure 2-10. Thermodynamic analysis of urea driven procapsid expansion. a. *Fraction of Procapsids expanded in relation as a function of urea and magnesium concentration.* Expansion in the presence of ○ = 0 mM $MgCl_2$, ● = 3 mM $MgCl_2$, ◇ = 10 mM $MgCl_2$. Samples were incubated on ice for 10 min in the presence of the indicated concentrations of urea. Fraction of expanded capsids was quantified by agarose gel assay. Each data point represents n=3 independent experiments, with error bars indicating the standard deviation.

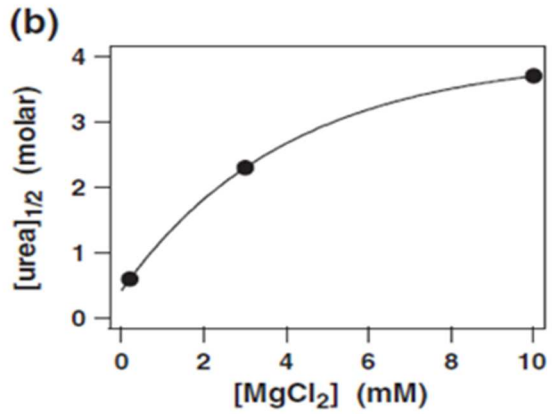

b. *Magnesium antagonism of urea procapsid expansion.* Data presented in **a.** were analyzed to afford the concentration of urea needed to expand 50% of the procapsids at respective concentration of magnesium. Increased magnesium concentrations impede urea driven procapsid expansion in a concentration dependent manner.

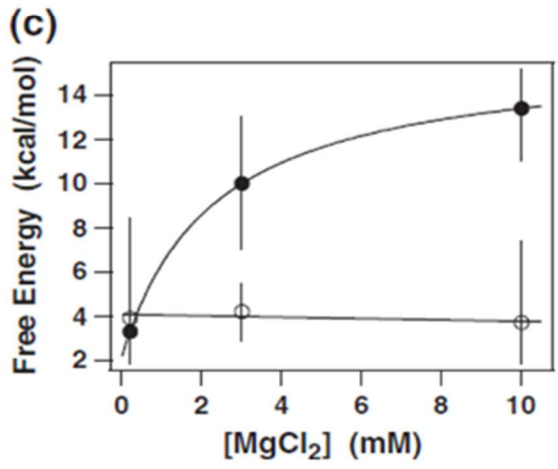

c. *ΔG(H20) of procapsid expansion.* The data presented in Panel a were analyzed according to Equation 2-1 to yield the free energy of expansion (●) and denaturant "m" value (○) as a function of magnesium concentration. Increased magnesium stabilizes the procapsid conformation but has little effect on the denaturant "m" value.

Temperature and Salt Effects on the Lambda Procapsid and Urea Expanded Capsid. Though a matter of some debate, the denaturant *m* value is often associated

with the amount of hydrophobic surface area exposed in the transition (Pace & Shaw, 2000). In the case of urea-triggered procapsid expansion, the large denaturant *m* value suggests that expansion is accompanied with the exposure of significant hydrophobic surface area. Temperature and salt are known to affect such transitions and I therefore examined the effects of each of these variables on procapsid expansion to test this hypothesis. Our lab previously observed that urea triggers procapsid expansion at 4°C degrees but not at 25°C. This afforded me a range to start my investigation. The procapsid expansion reaction was performed using 2.5 M urea in 3 mM $MgCl_2$ as described above except that the mixture was maintained at 4°C, 10°C, 15°C, 25°C, or 37°C. The results presented in Figure 2-11 demonstrate a strong temperature dependence on the transition.

I considered the possibility that the transition *rate*, not equilibrium was affected by temperature. Control studies showed that while expansion is complete within three minutes at 4°C, no evidence of expansion is observed at 37˚C even after 30 minutes (data not shown).

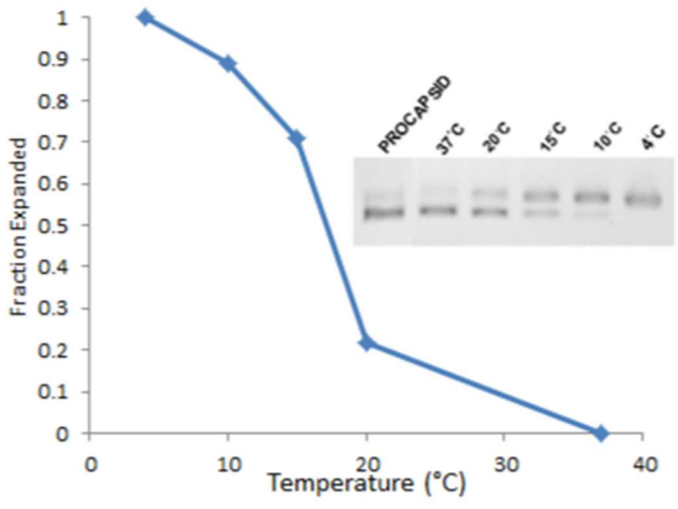

Figure 2-11. Effect of temperature on urea driven procapsid expansion. Graph of fraction of expanded procapsids as a function of temperature. Samples were incubated at the indicated temperature for 30 minutes in 2.5 M urea. ***(Inset)*** Native agarose gel of urea driven procapsid expansion at indicated temperatures.

I next examined the effect of salt on the expansion transition. Procapsid expansion in the presence of 2.5 M urea and 3 mM $MgCl_2$ was performed at 4°C, for 10 min, in the presence of the indicated concentrations of NaCl. The reaction mixtures were then loaded on to an agarose gel and the fraction of procapsids that had expanded quantified by video densitometry. As shown in Figure 2-12, NaCl strongly inhibits the expansion transition, with no expansion observed at concentrations ≥ 500 mM NaCl.

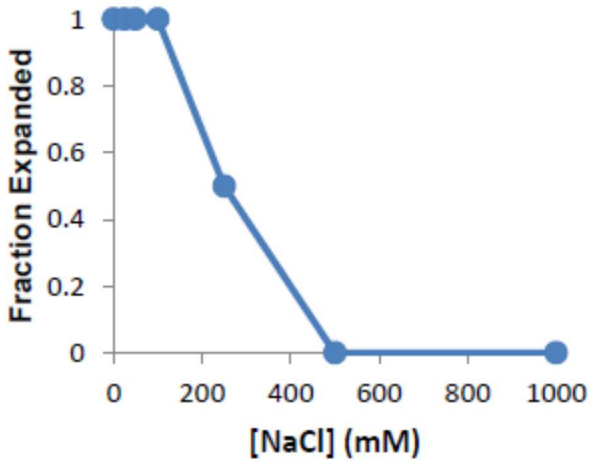

Figure 2-12. Effect of salt on urea-triggered procapsid expansion. Graph showing the fraction of expanded procapsids as a function of salt concentration. Samples were incubated at each salt concentration for 10 minutes in 2.5M urea. Data was obtained from gel densitometry of native agarose gel. Salt concentrations above 100mM impair expansion and no expansion is observed at [NaCl] ≥ 500mM.

Magnesium Drives Capsid Contraction to the Procapsid State?. To gain a better understanding of the effect of magnesium on the procapsid-capsid equilibrium, I examined the effect of magnesium on expanded capsid shells. Expanded capsids were prepared by incubation with 2.5M urea followed by removal of the urea by buffer exchange as described in Materials and Methods. The expanded capsids were then incubated with increasing concentration of $MgCl_2$ for 30 minutes at room temperature. The fraction of expanded capsids that contacted back to the procapsid state was quantified using the agarose gel assay. The data presented in Figure 2-13

demonstrates that magnesium drives contraction of the expanded capsid back to the procapsid state in a cooperative and concentration dependent manner. Analysis of the data as described in Materials and Methods affords a $[Mg^{2+}]_{1/2}$ = 1.1±0.1 mM. The experiment was repeated in the same manner except that 2.5 M urea was included in the in the reaction buffer. As expected, Mg^{2+} drove contraction of the expanded capsid in a concentration dependent manner; however a significantly higher concentration of Mg^{2+} is required to achieve 50% contraction; $[Mg^{2+}]_{1/2}$ = 6.5±0.4 mM.

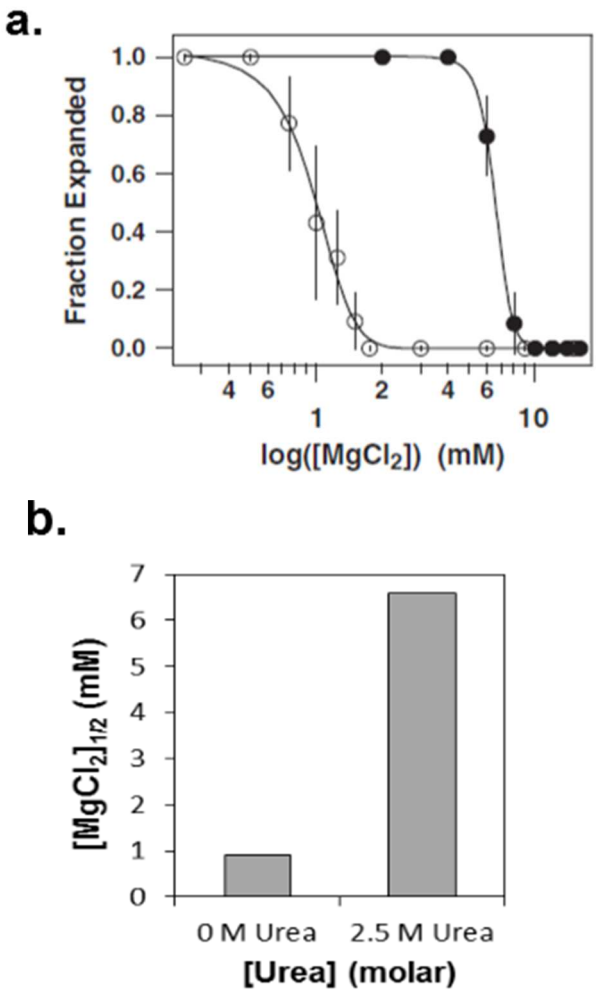

Figure 2-13. a. Magnesium driven capsid contraction. Expanded capsids in the presence of 2.5 M (●) and 0M urea (○) exhibit magnesium driven contraction to procapsid. Each data point represents n=3 independent experiments. Error bars represent standard deviation. Line was fit using simple sigmoid analysis.

b. Urea antagonism of Magnesium driven expanded capsid contraction. The data presented in Panel a were analyzed to obtain the concentration of magnesium needed to contract 50% of the expanded capsids. Increased urea concentrations impede magnesium contraction in a concentration dependent manner.

Biological Competence of the In Vitro Expanded Capsids. To ensure that urea expanded procapsids were biologically relevant, gpD the lambda decoration protein, was incubated with procapsids that had been expanded in 2.5M urea and then exchanged into buffer containing no magnesium as described in Materials and Methods (Chapter 5). Figure 2-14 shows that gpD efficiently adds to the urea expanded capsid surface but not to procapsids indicating that the expanded shells possess a structure conducive to decoration.

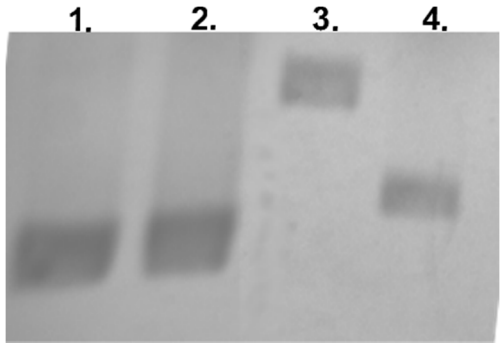

Figure 2-14. Agarose gel showing addition of gpD to urea expanded capsids. Lane 1. Procapsids. Lane 2. Procapsids + gpD. Lane 3. Urea expanded capsids. Lane 4. Urea expanded capsids + gpD. Both procapsids and urea expanded capsid samples that contain gpD were incubated on the benchtop for 30 minutes prior to being loaded on the gel. Note that gpD does not interact with the procapsid shell.

Discussion

Viral genome packaging into preformed procapsids is a vital step in complex dsDNA viral assembly pathways. Commonly, packaging of the genome triggers a procapsid expansion step that results in a larger, thinner, more angularized shell. This expansion step has previously been thought to be irreversible, ensuring that unidirectional packaging is accomplished.

It has been suggested that rearrangement of the proteins assembled into the viral shell is necessary to balance the need for strong subunit interactions among major capsid monomers in the mature capsid, while avoiding off-pathway and aberrant structures during shell assembly. The prevailing thought is stability, and thus fidelity, can be imparted to the capsid if stable interactions are established only upon rearrangement during expansion. Therefore, optimal contacts lost during viral shell assembly, due to quasi-symmetry, are not as detrimental in the mature viral capsid (Gertsman, Guttman, Lee, Speir, Duda, & Johnson, 2009). This concept is consistent

with the high degree of conservation of the shell expansion step in complex dsDNA viral assembly pathways.

In addition to expansion *in vivo,* previous *in vitro* studies showed preformed viral shells from a number of phages can be expanded using heat, denaturants, or pH, which resulted in irreversible expansion (Duda R. L., Hempel, Michel, Shabanowitz, Hunt, & Hendrix, 1995) (Galisteo & King, 1993) (Kunzler & Hohn, 1978) (Newcomb, et al., 1996) (Jardine & Coombs, 1998). These *in vitro* studies are consistent with the biological irreversibility observed *in vivo.* Therefore, the observation that urea-triggered expansion of the lambda procapsid is fully reversible was unexpected and is significant.

Capsid Expansion. I have demonstrated that urea and magnesium stabilize the expanded and contracted conformation of the lambda procapsid, respectively (Figures 2-7 and 2-13). I have also shown that this can be modeled as a highly cooperative, fully reversible, two state transition. This allowed me to perform a rigorous thermodynamic characterization of procapsid expansion that has not been possible in other systems to date. The results from my studies indicate an apparent $\Delta G(H_2O)$, for procapsid expansion, of ~13 kcal/mol in the presence of 10mM $MgCl_2$, which is close to that found *in vivo* (Medina, Nakatani, Kruse, & Catalano, 2012).

How does this free energy of expansion relate to the natural expansion process triggered by DNA packaging? The free energy required to expand *one* procapsid in the presence of 10 mM $MgCl_2$ is ~ 2.2×10^{-23} kcal, or ~90 (pN·nm) per capsid (see Medina 2012) (Medina, Nakatani, Kruse, & Catalano, 2012). The biological significance of this can be seen by considering single molecule studies performed in the Smith lab looking

at the work required to package DNA into the procapsid. These studies suggest that at the time of expansion, ~15 kb of duplex DNA is packaged and the motor is generating ~4 pN of force (Fuller, Raymer, Kottadiel, Rao, & Smith, 2007) (Tsay, Sippy, Feiss, & Smith, 2009). Genome packaging is presumed to create the force that ultimately provides the energy to expand the procapsid. Therefore, using this force and considering that work=PΔV the pressure generated by the packaged DNA can be calculated as equal to the force generated by the motor per unit area of the shell. The procapsid surface area is $7.9x10^{-11}$ cm^2 and the approximate pressure generated by the packaged DNA is ~0.05 N/cm^2. The volume of the procapsid is $6.5x10^{-20}$L and the volume of the expanded capsid is $1.1x10^{-19}$L thus giving ΔV as $4.5x10^{-20}$L. This means terminase packaging of DNA results in mechanical work of ~30 pN·nm per capsid, which is on the order of that calculated from the free energy of expansion *in vitro* above.

Magnesium Capsid Interactions. The importance of divalent metals in virus assembly and infectivity has been show for many viruses. Herpes virus and polyoma viruses rely on calcium for capsid assembly and stabilization. Magnesium has also been shown to be important for the assembly and stability of an infectious lambda virus (Sternberg & Weisberg, 1977) (Sternberg & Hoess, 1995). It has been proposed that Mg^{2+} is responsible for maintaining DNA in a condensed state, acting as a counter ion to help keep the packaged DNA condensed in the viral capsid (Bode & Harrison, 1973). The studies performed here are further consistent with a *metal-capsid* interaction that stabilizes the lambda procapsid conformation, as follows. Recent structural studies that found putative metal-binding sites at the 3-fold axes on the inside of the HK97 capsid surface (Gertsman, Guttman, Lee, Speir, Duda, & Johnson, 2009). I propose that this is

repeated in lambda procapsid, and that this is responsible for the observed stabilization by divalent metals. This hypothesis leads to some interesting predictions. It would suggest that in addition to the force generated by the packaging motor, the packaged DNA strips Mg^{2+} from the inner surface of the procapsid. This would lower the free energy requirement for expansion, as shown by my data. Further, the DNA-bound metal would provide charge neutralization of the DNA, ensuring proper condensation and packaging of the viral genome.

Hydrophobic Forces Stabilize the Procapsid Conformation. I propose that magnesium is only part of the stabilizing force of the procapsid conformation, and that hydrophobic interactions between the capsid proteins in the contracted shell also play a large role. Expansion of the procapsid exposes these hydrophobic surfaces on the exterior of the capsid shell, which is consistent with the observation that urea stabilizes the expanded shell conformation. While the mechanism is controversial, it is generally accepted that urea lowers the free energy required to expose hydrophobic surfaces to water. The general concept is that urea “solvates” hydrophobic residues in water (Santoro & Bolen, 1992) (Baldwin, 1986) (Makhatadze & Privalov, 1992). This is in concert with the results seen in this chapter showing that urea stabilizes the expanded conformation and shifts the equilibrium to the expanded state. In addition, stabilization of the procapsid conformation by salt and temperature are consistent with the hypothesis that hydrophobic interactions stabilize the procapsid state. Both salt, in this concentration range, and temperatures up to ~20°C, increase the strength of hydrophobic interactions (Baldwin, 1986).

Further support for this hypothesis is provided by the large denaturant *m* value associated with urea-triggered expansion of the lambda procapsid. The denaturant *m* value is a reflection of the dependence of the ΔG on the denaturant concentration. This also relates to the change in heat capacity of the transition, which correlates to the exposure of hydrophobic surface area. Therefore, the larger the *m*, the greater the amount of hydrophobic surface area that is exposed in the transition.

For comparison, a typical denaturant *m* value obtained in a protein denaturation study is 1–3 kcal/mol·M. The denaturant *m* values obtained from the work described here was ~4 kcal/mol·M. This suggests that a large amount of hydrophobic surface area is exposed, per mole of capsid, during the expansion transition. In addition the *m* value does not change with increased concentration of magnesium, even though the free energy of expansion is seen to increase significantly. This supports the hypothesis that urea procapsid expansion is a cooperative, two state transition, with the expanded state being the same no matter the concentration of magnesium.

The importance of the exposed hydrophobic surface area can be related to the next step in capsid maturation, addition of the gpD decoration protein. While a monomer in solution, gpD binds as a trimer to the expanded capsid surface, stabilizing the expanded shell (Yang, Maluf, & and Catalano, 2008). Structural studies reveal that the base of the gpD trimer is hydrophobic and I suggest that this interacts with the exposed hydrophobic surface area on the expanded capsid (Lander, Evilevitch, Jeembaeva, Potter, Carragher, & Johnson, 2008) (Yang, Forrer, Dauter, Conway, Cheng, & Cerritelli, 2000) (Iwai, Forrer, Pluckthun, & Guntert, 2005). This interaction stabilizes the

expanded shell and essentially irreversibly locks the capsid into the expanded conformation.

Biological Significance of Exposed Hydrophobic Surface Area in the Expanded Lambda Shell. The data presented above clearly demonstrate that urea can trigger the procapsid expansion transition. While the expanded shells have a morphology indistinguishable from wild-type, it was important to verify that the resulting shells are biologically relevant. The ability of urea expanded procapsids to add the lambda decoration protein gpD demonstrates structural integrity and biological relevance but further evidence supporting this fact was obtained using an *in vitro* packaging assay, as follows.

The *in vitro* packaging assay is a DNase protection assay that reports on DNA that has been packaged into capsids and therefore protected from DNase digestion (Yang, Maluf, & and Catalano, 2008) (Medina E. , 2010). Dr. Elizabeth Medina of our lab demonstrated that the gpD-decorated capsids are fully competent for genome packaging *in vitro* (Medina, Nakatani, Kruse, & Catalano, 2012). Thus, the gpD decoration and *in vitro* DNA packaging studies indicate that the urea expanded capsids are functionally competent and therefore biologically relevant.

Summary. The data presented in this chapter has demonstrated stabilization of the procapsid and expanded capsid state by magnesium and urea, respectively. A thermodynamic characterization of the transition between these two states was also conducted which was made possible by the observation that the transition can be approximated as a reversible, two-state process. Lastly, the proposed association

between hydrophobic surface area exposed upon procapsid expansion and gpD binding to this exposed hydrophobic surface has raised an interesting new avenue for investigation as to the nature of gpD interaction with the expanded capsid surface. These studies are presented in Chapters 3 and 4 of this thesis.

Chapter 3: Interrogation of the Molecular Interactions Responsible for gpD Binding to and Stabilization of the Lambda Capsid Shell

Introduction

The bacteriophage lambda viral assembly pathway contains many distinctive steps that are recapitulated in multiple complex dsDNA viral assembly pathways, both prokaryotic and eukaryotic. Virus assembly is essentially unidirectional *in vivo,* and has irreversible steps throughout the pathway. The packaging of viral genomes into preformed viral shells is a highly conserved process in many viral developmental pathways, including phages lambda, T7, P22, and the herpesviruses to name a few examples (Casjens S. R., 2011). In general, this conduit to an infectious virus starts with assembly of the packaging motor on viral DNA, followed by the motor•DNA complex binding to the preformed procapsid. After packaging of the genome starts, the shell undergoes an expansion step, which is described in detail in Chapter 2 of this thesis.

Figure 3-1. General viral assembly scheme. Major steps of a complex dsDNA viral assembly pathway are depicted. Specific aspects of each step vary but the end result is similar as depicted here. The present chapter focuses on capsid stabilization steps.

Expansion of the preformed viral shell has been reported to take place in nearly all complex dsDNA viruses (Duda R. L., Hempel, Michel, & Shabanowitz, Structural transitions during bacteriophage HK97 head assembly, 1995) (Galisteo & King,

Conformational transformations in the protein lattice of phage P22 procapsids., 1993) (Heymann, Cheng, Newcomb, Trus, & Brown, 2003). DNA packaging triggers this expansion step *in vivo*, which can involve conformational rearrangement and/or proteolytic cleavage of the major capsid subunits. The prevalence of this step, in a multitude of viral assembly pathways, advocates its importance. Procapsid expansion affords a larger capsid volume and a thinner more angularized capsid shell (Dokland & Murialdo, 1993) (Duda R. L., Hempel, Shabanowitz, Hunt, & Hendrix, 1995). However, in most cases this capsid shell is less stable than the procapsid and requires stabilization.

Expanded Shell Stabilization. Viruses use different methods to stabilize the expanded shell. HK97 for example, uses auto-catalytic chemical cross-linking of its major capsid protein to stabilize the shell. The HK97 procapsid expands after proteolytic cleavage of the "scaffolding domain" from the major capsid protein, gp5. Concomitant cross-linking of the expanded capsid stabilizes the expanded shell (Lee, Gan, Tsurata, Hendrix, Duda, & Johnson, 2004). Viruses such as adenovirus, the herpesviruses, and bacteriophage T4 utilize decoration proteins to stabilize the shells (Fuller, et al., 2007b) (Tzlil, Kindt, Gelbart, & and Ben-Shaul, 2003) (Wendt & and Feiss, 2004). Expansion is presumed to be necessary for increasing the volume of the viral shell to allow packaging of the full genome. Additionally, stabilization of the mature viral capsids allows for them to withstand extreme internal and external forces in the wild.

Capsid expansion is seen in many viral assembly pathways. It is proposed that this is due to the necessity of viral shell subunits to initially form contacts that are stable, yet dynamic; these pseudo-stable, reversible contacts promote fidelity in shell assembly

because improperly incorporated subunits can dissociate from the lattice (Lee K. , Tsuruta, Hendrix, Duda, & Johnson, 2005). The balance between forming correct subunit-subunit interactions vs. producing a robust capsid shell that is able to withstand extreme internal and external forces is experienced by all dsDNA viruses. It proposed that this is overcome by preforming viral shells with a higher degree of dynamic subunit-subunit interaction followed by an expansion-rearrangement and stabilizing steps that impart the final stability to the capsid (Lee, Tsuruta, Hendrix, Duda, & Johnson, 2005).

In the case of bacteriophage lambda, packaging of ~15 kb DNA triggers procapsid expansion. This expansion results in a larger (60 nm) capsid that is also two-fold larger in internal volume (Dokland & Murialdo, 1993) (Murialdo H. , 1991). Additionally expansion is proposed to exposure binding sites for the decoration protein, gpD, on the expanded capsid surface (Figure 3-1) (Medina, Nakatani, Kruse, & Catalano, 2012). This addition of gpD to the expanded capsid surface serves to stabilize the shell.

Binding of gpD to the Expanded Lambda Capsid. Published studies have reported that while packaging DNA does not require gpD, stabilization of the expanded shell is necessary for packaging of a full length genome. Further investigation indicates that gpD is responsible for stabilizing the capsid to ensure the last 8-10 kb of DNA can be packaged (Yang, Maluf, & Catalano, 2008). Thus, while sub-genomic fragments (up to 38 kb) are efficiently packaged in the absence of gpD, no DNA packaging is seen with the genome length substrates, most likely due to loss of capsid integrity (Yang, Maluf, & Catalano, 2008).

Studies looking at essential structural features of gpD noted the importance of the N-terminal residues for binding to the capsid (Yang, Forrer, Dauter, Conway, Cheng, & Cerritelli, 2000). Deleting the N-terminal 14 residues disrupted gpD binding to the lambda capsid surface. This study used an *in vitro* complementation assay, which reports on the amount of gpD necessary to make infectious virus that is resistant to EDTA challenge. EDTA chelates Mg^{2+}, which is important in condensation of DNA within the viral shell. In its absence, the packaged DNA expands, increasing the internal pressure caused by the packaged DNA, which ultimately destroys the virus particle. Thus, the complementation assay indirectly examines gpD binding to the lambda capsid surface and structural stabilization of the nucleocapsid. The authors concluded that deleting the N-terminal 14 residues decreases gpD binding to the capsid surface by 1000 fold (Yang, Forrer, Dauter, Conway, Cheng, & Cerritelli, 2000).

Later studies followed up on this observation by using the lambda-like phage 21 decoration protein, shp. Phage 21 shp has 49% sequence identity with gpD and provides the same capsid stabilizing function in phage 21's assembly pathway (Wendt & and Feiss, 2004). These studies found that in four fold excess, *shp* could stabilize the expanded lambda capsid *in vivo* relative to gpD. This result suggested that a homologous protein can suffice in stabilizing an infectious lambda virus. Wendt and Feiss investigated this further by examining EDTA sensitivity of the chimeric particles, which reports on the stability of *in vivo* packaged capsids. These studies utilized a lambda-*shp* chimeric virus that is deleted in gpD but expresses the phage 21 shp protein. These studies demonstrated that the chimeric virus is sensitive to ETDA, while the wild-type virus is not. The study further demonstrated that when the N-terminal

residues of *shp* (1-19) were replaced with the N-terminal residues of gpD (1-14), the lambda-D/*shp* chimeric virus became more stable to EDTA challenge. This affirms the hypothesis that the N-terminus of gpD is important in the binding to the shell surface and/or stabilizing of the DNA-filled lambda capsid (Wendt & and Feiss, 2004).

The Lambda Decoration Protein. gpD is an 11.4 kDa protein expressed as a viral "late" gene from the lambda pR' promoter. The mature gpD protein is made up of 109 amino acids not including the terminal methionine, which is cleaved *in vivo* (Georgopoulos, Tilly, & Casjens, Lambdoid phage head assembly. In Lambda II (Hendrix, R. W., Roberts, J. W., Stahl, F. W. &Weisberg, R. A., eds), 1983) (Hendrix & Casjens, 2006). In solution, gpD is found as a monomer as shown by NMR studies but binds as a trimer to the expanded capsid surface, specifically at the 140 three-fold axes of the icosahedral shell (Imber, Tsugita, Wurtz, & Hohn, 1980) (Yang, Forrer, Dauter, Conway, Cheng, & Cerritelli, 2000) (Iwai, Forrer, Plückthun, & & Güntert, 2005). This results in a 1:1 ratio of gpD to gpE in the mature virus, or 420 copies of gpD assembled into the infectious virus (Casjens S. , 1974) (Imber, Tsugita, Wurtz, & Hohn, 1980) (Yang, Forrer, Dauter, Conway, Cheng, & Cerritelli, 2000).

High resolution NMR structures of the gpD monomer have been solved and in addition a crystal structure of the gpD trimer to 1.1 Å resolution (Iwai, Forrer, Plückthun, & Güntert, 2005) (Yang, Forrer, Dauter, Conway, Cheng, & Cerritelli, 2000). The structures shows a remarkably low amount of "typical" secondary structure, but rather a high amount of random structure (~65% coils and loops) and only one short α helix. (Yang, Forrer, Dauter, Conway, Cheng, & Cerritelli, 2000) The N-terminal 14 residues of gpD are disordered and both the C- and N-termini reside at the base of the trimer where

it binds to the expanded capsid. Interestingly, despite this proximity both termini have been modified with a variety of fusion partners as an extremely useful platform for phage display (Figure 3-2) (Mikawa, Maruyama, & and Brenner, 1996) (Sternberg & Hoess, 1995).

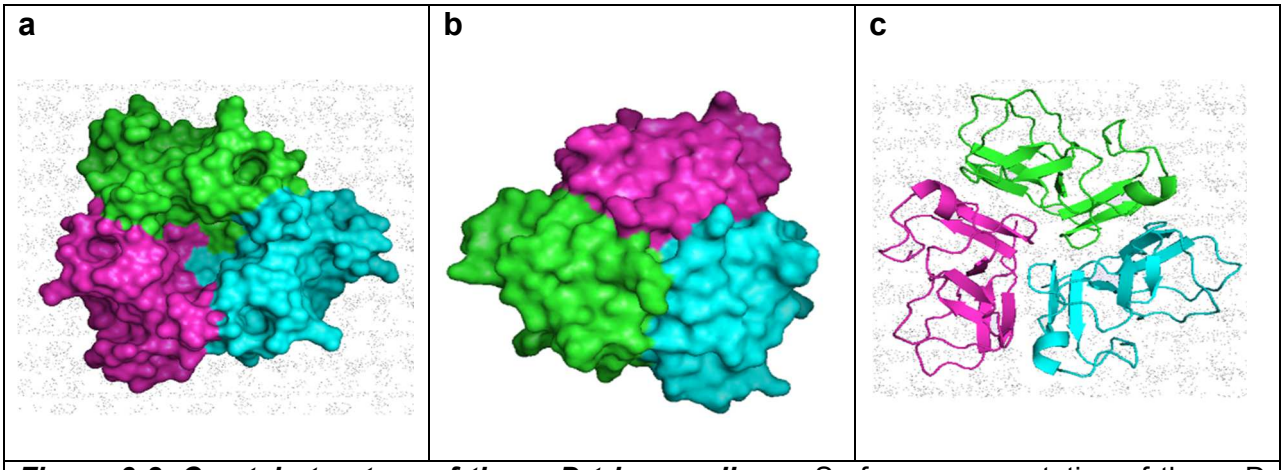

Figure 3-2. Crystal structure of the gpD trimer spike. **a.** Surface representation of the gpD trimer shown in a top (not bound to the capsid) view. Note the presence of a "dimple" at the center of the trimer, as describe in the text. **b.** Surface representation of the bottom view (side bound to capsid) of gpD trimer (surface bound to the capsid). **c.** Ribbon representation of top view of gpD trimer depicting secondary structure. Note the large amount of random secondary structure.

Molecular Interactions Mediating gpD Binding to the Expanded Lambda Capsid: the N-Terminus of gpD. The genetic studies described above demonstrate that N-terminal residues of gpD are important for stabilizing the expanded capsid shell. Johnson and co-workers provided additional insight into the binding of gpD to the expanded capsid surface. Using cryoEM reconstructions of the procapsids and expanded decorated capsids at 13.9Å and 6.8Å, respectively, they were able to better distinguish interactions between gpD and the capsid surface (Lander, Evilevitch,

Jeembaeva, Potter, Carragher, & Johnson, 2008). Using the expanded decorated capsid reconstruction and subtracting the difference of the procapsid cryoEM density, they generated a model for gpD trimer spikes bound to the capsid surface. The crystal structure of gpD was then modeled into the resulting density map, which fit very well, except for a "tube" of density emanating from the spike along the 3-fold axes into the groove on the capsid surface. The investigators suggested that this density corresponds to the N-terminal residues of gpD (which were disordered in the crystal structure) that lay in this groove and donate a fourth strand to a three strand beta sheet formed on the capsid surface by two subunits of gpE. Additionally they found that the beta sheet formed by adjacent gpE subunits is disordered in the procapsid state and that these residues are located on the interior of the procapsid shell (Lander, Evilevitch, Jeembaeva, Potter, Carragher, & Johnson, 2008). A similar observation was made for regions of the capsid that interact with the base of gpD in the expanded shell. The authors proposed that these regions become exposed in the expanded shell conformation for interaction with gpD, and that these interactions "cement" gpD to the expanded capsid surface. Thus, the structural data are consistent with the genetic data discussed above, which indicate that the N-terminus of gpD is important for binding to and stabilizing of the expanded shell.

Molecular Interactions Mediating gpD Binding to the Expanded Lambda Capsid: Pro-His Trimer Rings. Close inspection of the crystal structure of the gpD trimer spike reveals alternating rings of His19 and Pro17 at the base of the gpD trimer (see Figure 3-4). These residues are highly conserved between gpD and the lambda like decoration protein from phage 21, (*shp*, see above). Indeed, significant sequence homology is

seen in the base of both proteins where binding to the capsid occurs (Yang, et al., 2000). The authors speculated that His19 and Pro17 must play a role in gpD binding to the capsid. Unfortunately the lack of a high-resolution structure of gpE, the lambda major capsid protein, precluded the identification of specific interactions with the gpE major capsid protein assembled into the shell.

The molecular details by which the expansion step allows for the capsid cementing protein to bind is not completely understood in any system. However, in lambda, exposure of important binding sites has been shown to be essential, as discussed above. It was not until a pseudo atomic model of the major capsid protein gpE was obtained that an in-depth look at of the binding and stabilization of gpD to the expanded capsid could be proposed.

Molecular Interactions Mediating gpD Binding to the Expanded Lambda Capsid: A Structural Model for the Lambda Capsid Shell. Studies aimed at gaining insight into the possible interactions between gpD and the capsid surface required a high resolution structure of gpE. A pseudo atomic model for the major capsid protein was developed in our lab and modeled into the cryoEM density obtained by Johnson and co-workers (Lander, Evilevitch, Jeembaeva, Potter, Carragher, & Johnson, 2008) to construct a pseudo-atomic structure of a gpE trimer positioned at the icosahedral three-fold axis of the capsid shell (Singh, Nakatani, Goodlett, & Catalano, 2013) (Figure 3-3).

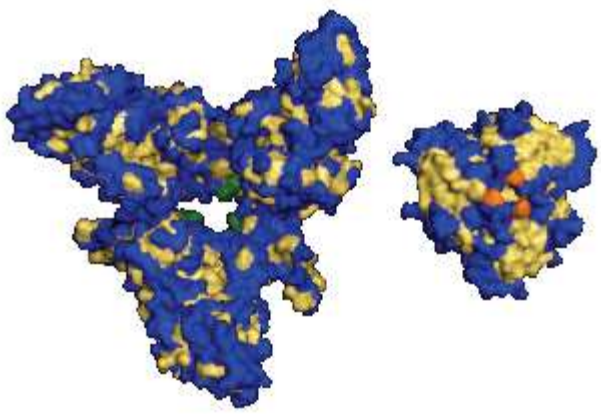

Figure 3-3. Surface representation of a gpE trimer found at the icosahedral three-fold axis of the capsid shell. **Left** View from exterior of the capsid. Pseudo atomic model of gpE trimer at procapsid three-fold axis. Hydrophobic residues are colored yellow. **Right. *Surface representation of a gpD trimer – bottom view.*** Hydrophobic residues are colored yellow.

Out of this model came an interesting observation: a ring of three aspartic acids were observed that lined up with the previously reported ring of three histidines found on the base of the gpD trimer spike (Figure 3-4). Furthermore, an alternating ring of three tryptophan's was also observed and these lined up with the previously reported ring of three prolines found on the base of the gpD trimer spike. Importantly, Pro-Trp interactions have been proposed to be important in a number of protein structures, providing 5 – 7 kcal/mol bonding energy. Based on this pseudo-atomic model, I propose that Asp-His and Trp-Pro bonding interactions play a central role in cooperative gpD assembly at the capsid surface and subsequently stabilizing the expanded shell (Biedermannova, Riley, Berka, Hobza, & Vondrasek, 2008) (Figure 3-4).

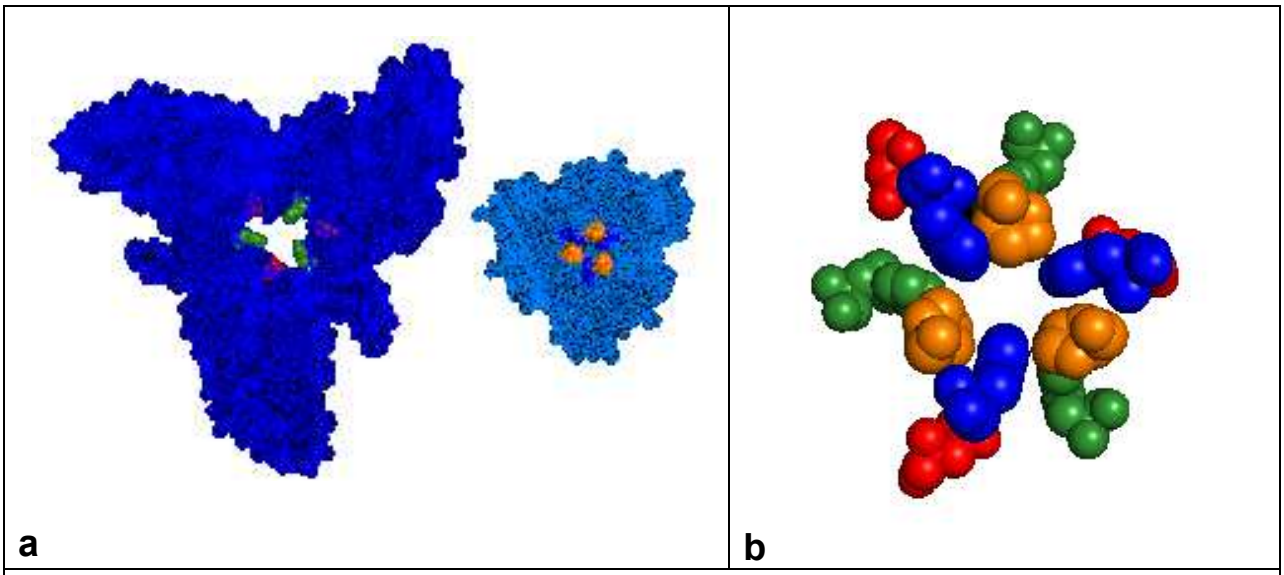

Figure 3-4 Proposed residue interactions between gpD and gpE. **a. Left.** Surface mesh representation depicting gpE residues Trp308 and Asp292 at the capsid three-fold axis in green and red, respectively. **Right.** gpD residues Pro17 and His19 in the trimer spike depicted in orange and dark blue, respectively. **b.** Residues from gpE and gpD superimposed in same colors. This structural model was constructed by Drs. Sing and Nakatani of our lab concurrent with my research.

Based on the pseudo atomic model, I propose multiple binding interactions for gpD binding to the expanded capsid surface. The first is the previously discussed concept that the hydrophobic base of gpD binds to the exposed surface area on the capsid surface as seen in Figure 3-3. This follows closely with the data presented in Chapter two of this thesis. A second interaction is the ordering of the N-terminus of gpD to donate a fourth strand to a three-strand beta-sheet resident at the shell surface, as discussed above. Thirdly, the structural model led to the prediction that the rings of tryptophans and aspartic acids that are formed by trimers of gpE at the three fold axis of the capsid, are important in gpD binding to the expanded capsid as well as stabilizing the expanded shell as I hypothesized above. This array of prolines, histidines, tryptophans, and aspartic acids could potentially provide nearly 40 kcal/mol binding energy for trimerization of gpD at each of the 140 three-fold axis on the capsid surface.

The studies described in this chapter aim to examine the role hydrophobic interactions play in driving gpD addition to the capsid surface. Additionally I directly test my hypothesis that the array of proline, histidines, tryptophans, and aspartic acids are important for gpD binding and stabilizing the expanded capsid and characterize the relative contributions of the putative His-Asp and Pro-Trp interactions to gpD trimer spike assembly and shell stabilization. Specifically, I utilize a mutagenesis approach to determine the roles that these residues have on gpD binding to the capsid surface and the subsequent stabilization of the shell. These mutations are introduced individually, and where possible in combination, to define the role of independent residue in binding and stabilizing the expanded capsid. It is important to remember that though only mutating one residue, the effect will be recapitulated around the capsid close to 420 times. This allows even small changes made to the capsid subunit able to result in large effects.

Material and methods

Reference Chapter 5

Results

The Role of Hydrophobic Interactions in gpD Binding. In Chapter 2 of this thesis, I demonstrated that expansion of the procapsid shell exposes significant hydrophobic surface area and I proposed that this provides a nucleation site for gpD addition. Consistent with this hypothesis, structural studies show that the base of the gpD trimer is largely hydrophobic. Here I directly test my hypothesis that hydrophobic interactions are important for gpD binding to the expanded capsid surface.

Temperature Effects on gpD Binding. Increasing the temperature from 4°C to 20°C has been shown to increase the strength of hydrophobic interactions of folded proteins (Baldwin, 1986). This has been attributed to an increase in the entropic component in this temperature range. This observation provides an experimental approach to directly test my hypothesis that gpD binding to the expanded capsid shell is mediated, at least in part, by hydrophobic interactions. Expanded capsids (40 nM) were prepared as described in Materials and Methods and then incubated with gpD (20 μM) at the indicated temperature for 30 minutes. GpD addition was then quantified using an agarose gel assay and the results are shown in Figure 3-5 (Medina, Nakatani, Kruse, & Catalano, 2012). The data demonstrate that gpD addition is strongly affected by temperature, increasing with increasing temperature. This is consistent with my hypothesis that hydrophobic interactions mediate, at least in part, gpD binding to the capsid surface.

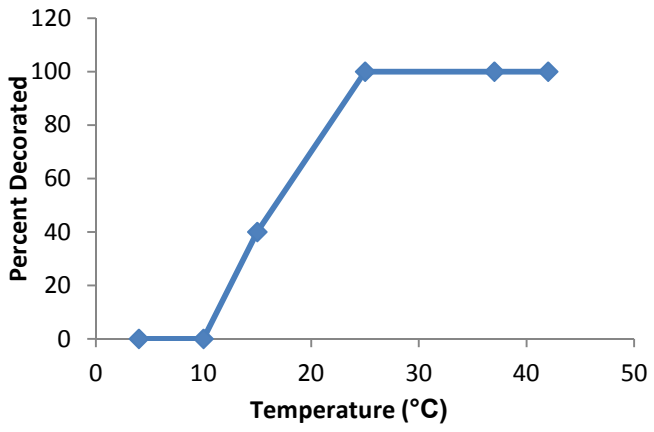

Figure 3-5. Temperature effects on gpD decoration of urea expanded procapsids. Each data point represents amount of gpD addition to expanded capsids when incubated at respective temperature. Percent of expanded capsids decorated with gpD was determined by agarose gel.

Salt Effects on gpD Binding. Sodium chloride in the range of 0.1 to 1 molar increases the surface tension of water; this decreases the "solubility" of nonpolar

residues in water and thus increases the hydrophobic effect (Hofmeister, 1888). According to my hypothesis, this predicts that gpD binding to the expanded capsid will increase with increasing salt concentration. Therefore, I next investigate the effect of salt concentration on gpD binding to the lambda capsid. Expanded capsids (40 nM) and gpD (20 μM) were incubated at room temperature for 30 minutes in the presence of the indicated concentration of NaCl and gpD addition quantified by agarose gel assay. The data presented in Figure 3-6 shows that NaCl in the concentration range between 0 and 1 M had little effect on gpD binding under these conditions. Unfortunately, this study was performed at saturating concentrations of gpD and it is possible that NaCl effects would be observed at a lower (sub-saturating) concentration of gpD. That said, I note that studies presented in Chapter 2 of this thesis showed that concentrations of NaCl $\geq$ 500 mM completely inhibited procapsid expansion. The data presented in Figure 3-6 show that the gpD-decorated shell is resistant to NaCl in this concentration range, indicating that gpD stabilizes the expanded capsid from environmental insults such as elevated ionic strength.

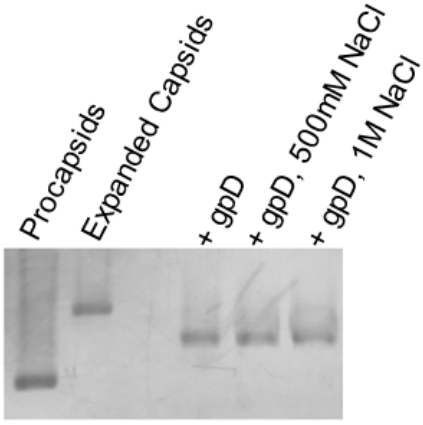

Figure 3-6. Salt effects on gpD addition to the expanded capsid. gpD and expanded capsids were incubated with noted salt concentrations. No stimulation of addition is observed in the presence of salt up to 1M NaCl. Decorated capsids are observed to run faster than expanded capsids likely due to the negative overall charge of gpD at neutral pH.

The Role of Specific gpD and Major Capsid Protein (gpE) Residues in gpD Binding to the Lambda Capsid. Our lab constructed a pseudo atomic model of the major capsid protein assembled into the lambda capsid shell (see above). Close inspection of this model in relation to the crystal structure of gpD exposed potential interactions between gpD and gpE that could play an important role in gpD binding to the capsid. Specifically, an alternating ring of prolines and histidines formed by trimeric gpD have been proposed to play an important role in binding the expanded capsid (Yang, et al., 2000). I noted corresponding rings of tryptophans and aspartic acids presented by gpE trimers at the icosahedral three-fold axes of the shell and that are positioned to directly interact with the proline and histidine, respectively. The studies presented below directly test the hypothesis that gpD residues Pro17 and His19 directly interact with residues gpE Trp308 and Asp292, respectively, and that these interactions are important in binding and/or stabilizing the lambda expanded capsid.

Construction of Mutant Vectors, Expression and Characterization of the Mutant gpD Proteins. I introduced single point alanine mutations to both gpD Pro17 and His19 as described in Materials and Methods. The resulting constructs were *pP17A* and *pH19A*. These vectors were then transfected into *E. coli* BL21 cells and 1 L cultures were grown, the cells harvested, and the proteins purified as described in Materials and Methods. The yield for the two mutant proteins was approximately equal to that of the gpD wild type protein that was grown in concert (Table 3-1), indicating that the mutations did not result in any gross structural aberrations. The purity of the purified preparations was at least 95% (Figure 3-7).

gpD-WT	146.3	mg protein/L of cell growth
gpD-P17A	138.6	mg protein/L of cell growth
gpD-H19A	169.4	mg protein/L of cell growth

Table 3-1. Yield of purified wild-type and mutant gpD proteins. Concentrations were determined by UV and then verified by agarose gel as seen below.

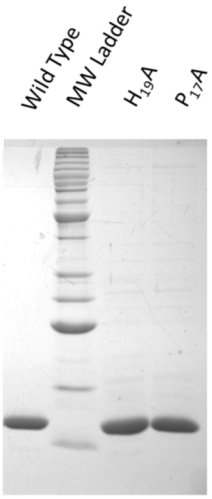

Figure 3-7. SDS PAGE gel of purified gpD-WT, gpD-H19A, and gpD-P17A. 15% SDS PAGE gel of wild type gpD, gpD-H19A, gpD-P17A, and molecular weight ladder. The SDS PAGE gel demonstrates the purity of each preparation.

Folding and Stability of the Mutant Decoration Proteins. I next confirmed that the mutant gpD proteins are properly folded and that the mutations did not affect the stability of the proteins. Circular dichroism (CD) was used to examine the secondary structure of the mutant gpDs in relation to gpD-WT. Figure 3-8a shows the far-UV CD spectra of gpD-WT, gpD-P17A and gpD-H19A. All three proteins possess virtually identical spectra and are consistent with NMR structural data indicating that gpD is composed of primarily random structures (see Figure 3-2C; Table 3-2). However, the spectra of the mutant proteins differ slightly from wild-type in the 230 region. This band is likely associated with a Trp49-Trp87 exciton interaction and suggests that the

mutations may have slightly affected the geometry of this interaction in the folded proteins (Louis-Jeune, Andrade-Navarro, & Perez-Iratxeta, 2012).

6%	α-Helix
19%	β-Sheet
58%	Random Coil
17%	Disordered

Table 3-2. Secondary of gpD-WT predicted from NMR structural data. Secondary structure percentages were calculated from the NMR structure. Calculated values are consistent with the CD spectra and the previously reported crystal structure.

The thermal stability of the proteins was next examined, monitored by CD spectroscopy. Upon heating, all three proteins show a similar loss of secondary structure and exhibit random coil-like spectra at 95˚C (Figure 3-8b). Both mutant gpDs appear to refold while wild type unfolding appears to more irreversible. Notwithstanding, the thermal denaturation curves for the three proteins are virtually identical (Figure 3-8c) and have similar melting temperatures (T_m). (Table 3-3)

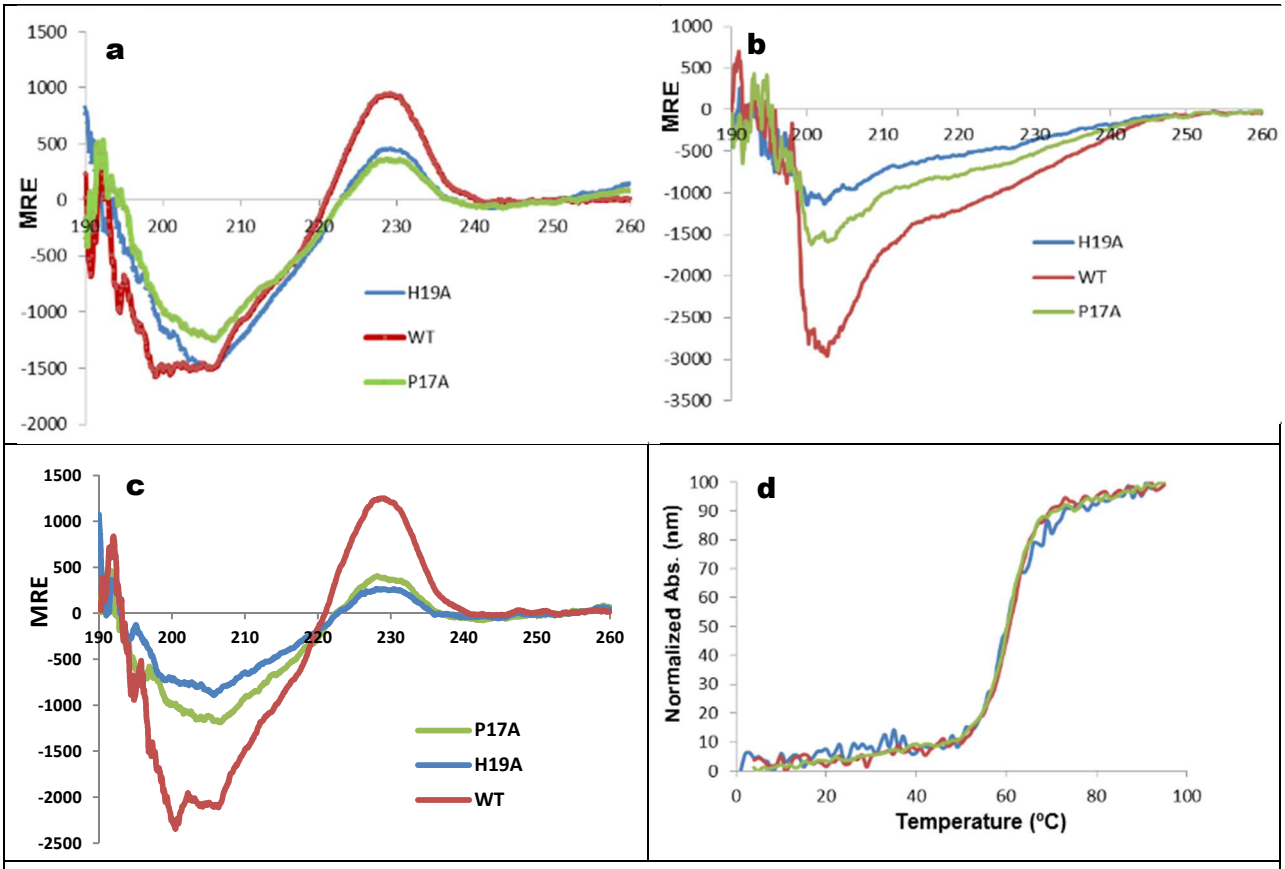

Figure 3-8. Circular dichroism spectra of gpD-WT, gpD-P17A, and gpD-H19A. **a.** Far-UV spectra recorded at 4°C. **b.** Spectra recorded at 95°C. **c.** Spectra recorded after heating to 95°C and then cooling back to 4°C. **d.** Normalized melting curves of gpDs monitored at 230nm.

	T_m
Wild Type	60.5 ± 0.6
gpD P17A	60.5 ± 0.5
gpD H19A	62.5 ± 0.5

Table 3-3. The data presented in Figure 3-8d was analyzed as described in Materials and Methods to obtain the Tm.

The overall assessment from these data is that the mutant gpD proteins are, in general, properly folded and stable, and that the mutations cause little to no changes in secondary or tertiary structure.

Functional Characterization of the Mutant gpD Proteins. I next assessed if the mutant gpD-P17A and gpD-H19A proteins added to the expanded lambda capsid in a similar manner as wild type. Decoration experiments were carried out as described in Materials and Methods using urea expanded procapsids. The reaction mixtures were incubated for 30 minutes on the bench top to be sure complete addition was achieved. The data presented in Figure 3-9 demonstrate that in all cases, the shell is completely decorated at a 1:1 gpD:gpE stoichiometric ratio. This suggests that both gpD-P17A and gpD-H19A add to expanded capsids in a similar fashion as wild type gpD.

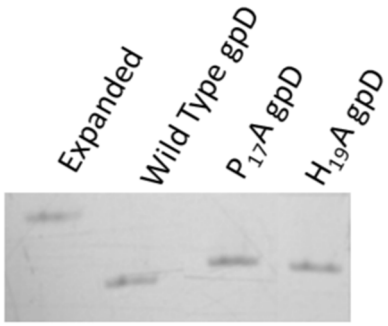

Figure 3-9. Agarose gel of gpD addition to expanded lambda capsids. Each lane contains urea expanded capsids and the specific gpD denoted. Addition of gpD to the capsid surface is apparent by the shifting of the band on the gel. Further addition of gpD did not result in additional shift of the bands indicating that they have been fully decorated.

The stability imparted by gpD to the expanded capsid was next investigated. Packaging a full-length lambda genome is strictly dependent on efficient decoration *and stabilization* of the expanded shell with gpD (Yang, Maluf, & Catalano, 2008). I utilized a DNase protection assay (described in Chapter 2) which directly measures genome packaging into lambda procapsids; in the absence of gpD, no packaging is observed, presumably due to rupture of the shell at high filling densities (Yang, Maluf, & Catalano,

2008). Procapsids purified from *E. coli* NS428 (λ *A*am11 *b*2*red*3 *cI*ts857*S*am7) cells were used in conjunction with gpD-WT, gpD-P17A and gpD-H19A proteins in the genome packaging assay as described in Materials and Methods and shown pictorially in Figure 3-10. In this assay DNase protection correlates directly with packaged DNA, and thus to the stability imparted by gpD to the expanded capsid.

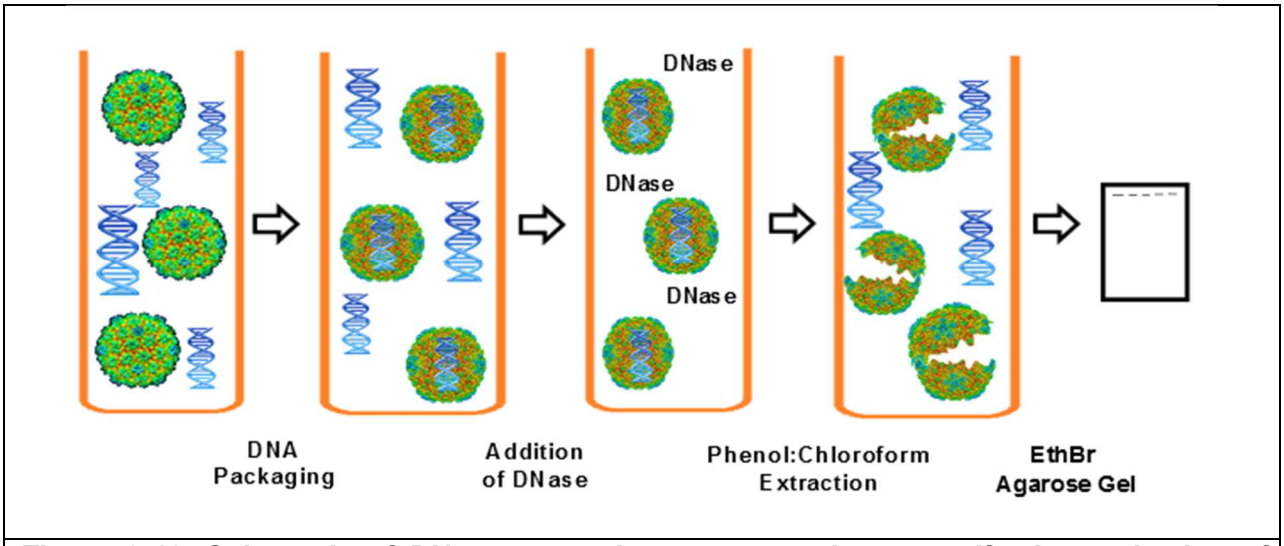

Figure 3-10. Schematic of DNase protection assay used to quantify the packaging of lambda genomes in to lambda viral shells. Lambda DNA and viral shells are incubated in packaging reaction mixture. DNA is packaged into lambda capsids where it is protected from DNase digestion. After DNase addition, any unprotected DNA is digested. DNase activity is stopped with a phenol:chloroform extraction which also denatures capsids and releases packaged DNA, which is imaged on an ethidium bromide-stained agarose gel.

The data presented in Figure 3-11 shows that both the gpD-P17A and gpD-H19A mutant proteins support genome packaging to a similar extent, though roughly 50% lower than that of the wild-type protein. This suggests that though binding to the capsid by gpD-P17A and gpD-H19A was not significantly affected (Figure 3-9), stabilization of the expanded shell as required to package a unit-length genome is significantly impaired by both mutations.

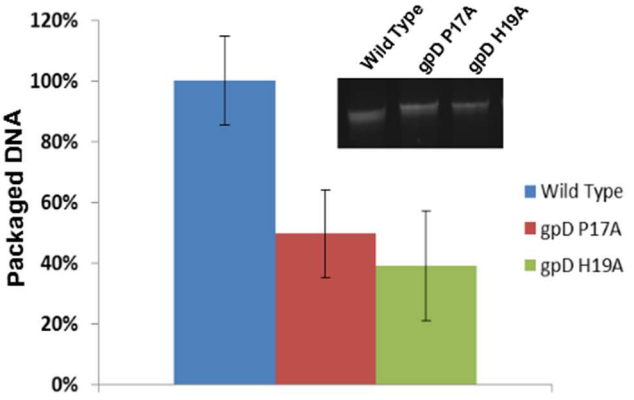

Figure 3-11. Packaging of a full length lambda genome in the presence of gpD-WT, gpD-P17A, and gpD-H19A decorated capsids. Capsids were decorated for packaging using the indicated gpDs. Each bar represents results from three separate experiments and the error bars represent standard deviation. **Inset:** 0.8% agarose gel stained with ethidium bromide displaying packaged DNA protected from DNase.

Role of Major Capsid Protein Residues gpE-Trp308 and gpE-Asp292 in Capsid Decoration and Stabilization. As discussed above, the pseudo-atomic model of the lambda capsid revealed potential interactions between residues Trp308 and Asp292 in gpE with residues Pro17 and His19 in gpD, respectively. Here I describe a mutational analysis of these gpE residues to directly test my hypothesis and to examine the interactions from both capsid and gpD perspective.

Construction of Mutant Procapsid Vectors, Expression and Characterization of the Purified Lambda Procapsids. Plasmids containing the gpE-D292A, gpE-W308A, and gpE-W308F mutations were constructed using pT7cap vector, sequenced, and then transfected into *E. coli* BL21 cells as described in Materials and Methods. Protein expression was induced with IPTG and procapsids were isolated as previously described (Yang, Maluf, & Catalano, 2008). Analysis of wild-type and mutant procapsids at various stages of purification is shown Figure 3-12. The clarified cell lysates possess similar amounts of gpE protein, indicating that expression of the major capsid protein is not affected by the introduced mutations. I next harvested assembled procapsids by

ultracentrifugation (87.2K x g). Lambda procapsids are pelleted during the high-speed spin and the majority of gpE-WT is thus found in the pellet. While gpE-WT, gpE-D292A, and gpE-W308F mutant procapsids pellet as anticipated, the gpE-W308A protein remains largely suspended during the high-speed spin and only a small fraction of the protein was found in the pellet. This observation suggests that the mutation impairs the capacity of the mutant protein to assemble into higher-order structures (i.e., capsid shells). This is further examined below.

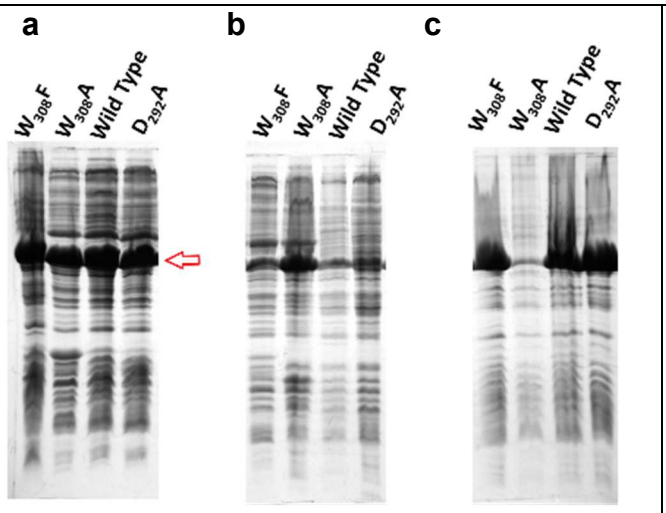

Figure 3-12. SDS PAGE analysis of procapsid purification intermediates. The sample is indicated at the top of each gel, which is stained with Coomassie blue. **a.** Clarified lysis supernatant. **b.** High speed centrifugation supernatant. **c**. High speed centrifugation pellet. Red arrow indicates migration of gpE.

Characterization of gpE-W308A. Assembly of gpE into procapsid shells affords particles that pellet during high-speed centrifugation. The observation that gpE-W308A remains in the supernatant during high-speed centrifugation is thus unexpected. To further characterize this protein, the high-speed supernatant was analyzed by size exclusion gel filtration chromatography (SEC) to determine the oligomeric state of gpE-W308A. Figure 3-13 shows the resulting chromatogram, which indicates the majority of gpE W308A is in a monomeric or low oligomeric state at this concentration.

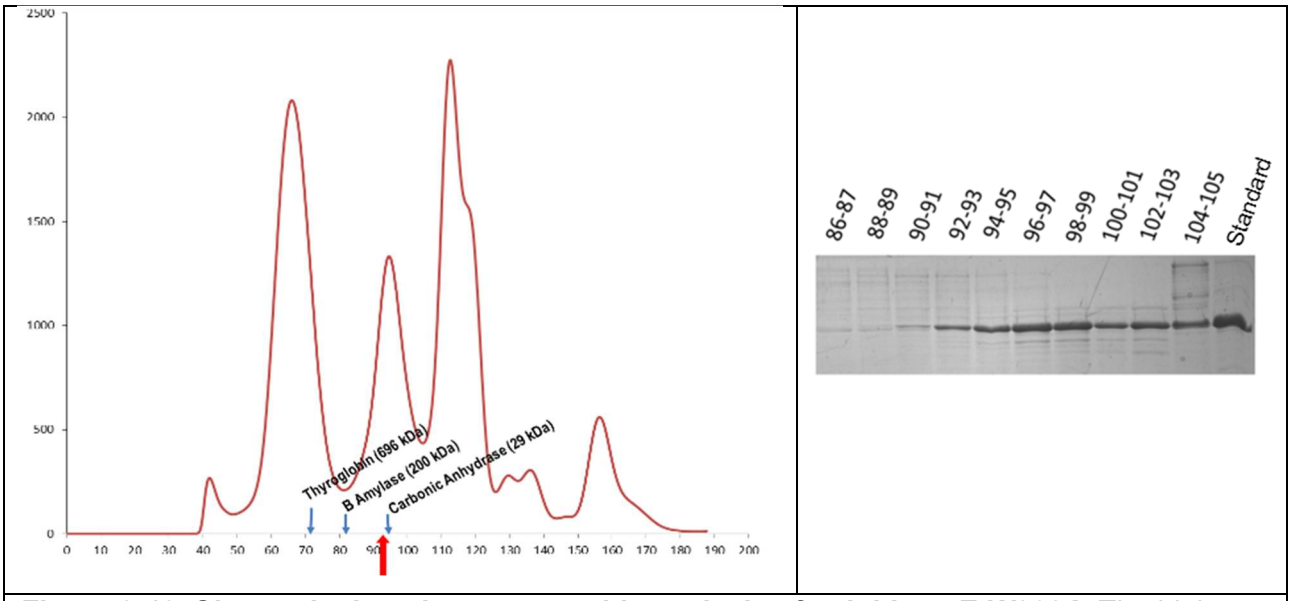

Figure 3-13. Size exclusion chromatographic analysis of soluble gpE-W308A. The high-speed ultracentrifugation supernatant was applied to a S400 SEC column and the column was developed as described in Materials and Methods. **Left Panel.** Chromatogram of the gpE-W308A supernatant. The elution positions of the calibration standards and their respective molecular weights are indicated. GpE-W308A elutes as an apparent monomer (38kDa) as indicated by red arrow. **Right Panel.** SDS-PAGE analysis of fractions (2mL) eluting from the SEC column. The elution volumes are indicated at the top of the gel.

I next asked if the gpE-W308A mutation affects folding of the protein using CD spectroscopy. Figure 3-14 shows the far-UV CD spectra of the protein, which indicates that it possesses significant secondary structure. Comparison of the CD spectra of gpE-W308A in solution to that of wild type gpE assembled into procapsids shows no major differences (data not shown); both possess predominantly alpha helical structures as anticipated. This similarity in the secondary structure of the mutant gpE W308A protein to that of wild type gpE suggests no major impacts on the secondary structure of the mutant protein.

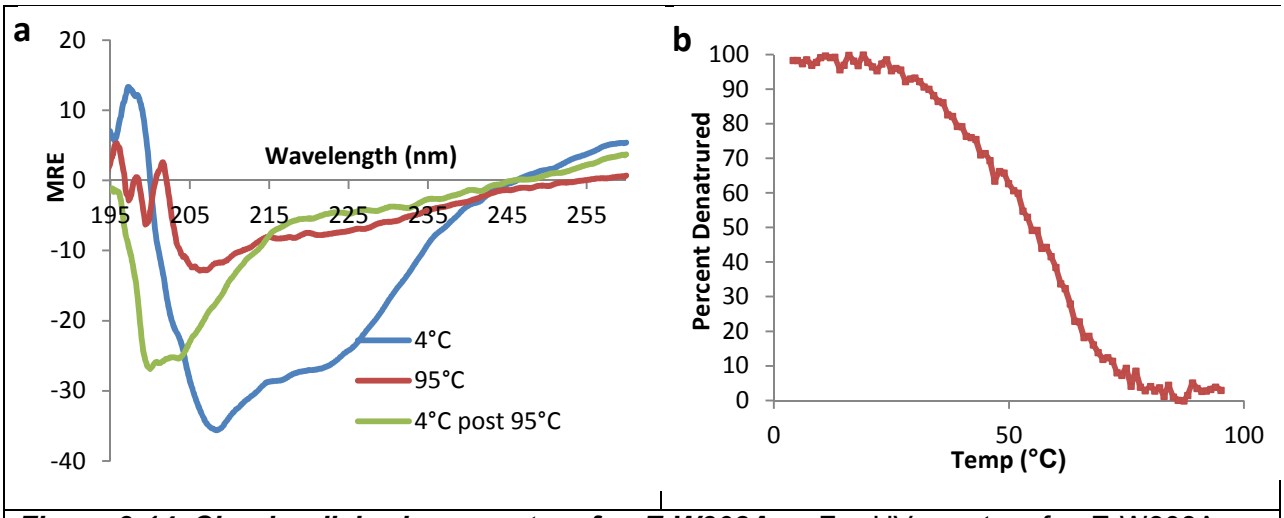

Figure 3-14. Circular dichroism spectra of gpE-W308A. **a.** Far-UV spectra of gpE-W308A recorded at 4°C (blue), Spectra recorded at 95°C (red), Spectra recorded after heating to 95°C and then cooling back to 4°C (green). **b.** Thermal denaturation curve of gpE-W308A monitored at 230 nm. Analysis of the data as described in Materials and Methods affords a melting temperature of 54.4 ± 0.5 ˚C.

Finally, I examined the stability of the mutant protein. Thermal denaturation of the protein, monitored by far-UV CD, revealed a modestly cooperative transition with a T_m = 54.4 ± 0.5˚C. Unfortunately, thermal unfolding is irreversible (Figure 3-14a), which precludes a rigorous thermodynamic analysis of the transition. As anticipated for a soluble monomeric protein, examination of the partially purified gpE W308A high speed supernatant by electron microscopy (EM) revealed no discernible higher order structures (data not shown).

GpE-W308A Assembles into Aberrant Structures. A small fraction of gpE-W308A is found in the pellet fraction of the high-speed centrifugation run (see Figure 3-12c) and I purified these assembled particles using my standard procapsid purification protocol (Materials and Methods). The purified particles were examined by EM, which revealed two unexpected features (Figure 3-15a). First, while a few assembled shells are observed, they are approximately half the diameter of a wild type gpE procapsid. These

smaller shells were incubated with urea at concentrations of 1 M, 2.5 M, 3 M, and 4 M, but no expansion was observed (data not shown). Due to the extremely low yield of the assembled shells, their small morphology, and their resistance to urea-triggered expansion, I did not investigate these particles further. A second and quite unexpected observation is the presence of apparent tetrameric structures in the micrographs of the assembled gpE-W308 protein. The nature of these aberrantly assembled structures is currently under investigation.

Characterization of Mutant gpE-D292A Procapsids. Unlike the gpE-W308A mutant protein described above, gpE-D292A purified in a similar fashion and with similar yield to wild type gpE procapsids. Procapsid containing fractions were analyzed by EM. As shown in Figure 3-15b, gpE-D292A assembles into not only native-like procapsids, but in addition a variety of malformed and aberrant structures. Unfortunately, the gpE-D292A particles have markedly decreased solubility compared to wild type procapsids and they are highly prone to aggregation upon concentration. This feature precludes the use of the mutant gpE-D292A shells in the biochemical studies described below and the particles were not investigated further.

WT gpE	10.05	mg protein/L of cell growth
gpE W308F	13.49	mg protein/L of cell growth
gpE W308A	3.11	mg protein/L of cell growth
gpE D292A	7.02	mg protein/L of cell growth

Table 3-3. Yields from protein purification of gpE procapsids. Concentrations were determined by UV and then validated by agarose gel when possible.

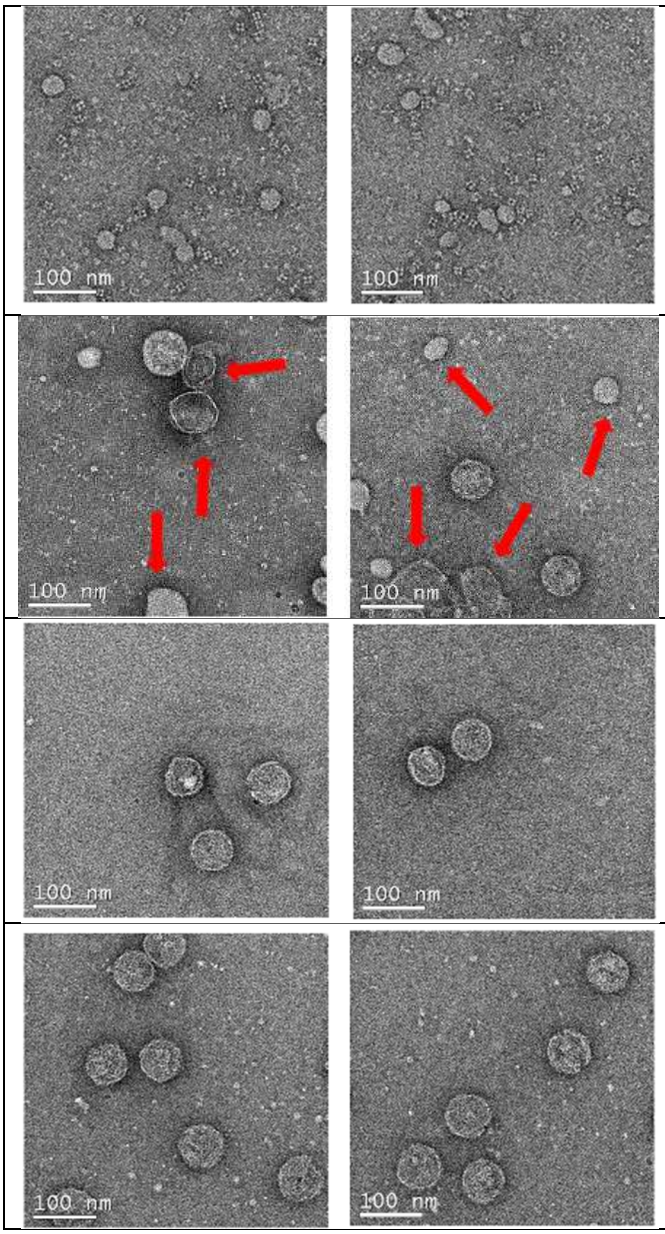

Figure 3-15. Electron micrographs of wild type and mutant procapsids.

a. Duplicate micrographs of gpE-W308A particles. Note the presence of small (~ 25 nm) shells and unusual tetrameric particles.

b. Duplicate micrographs of gpE-D292A particles. Note the presence of numerous aberrant structures and small procapsids indicated by arrows.

c. Duplicate micrographs of gpE-W308F procapsids. The particle morphology resembles wild type procapsids

d. Duplicate micrographs of wild type procapsids.

Characterization of Mutant gpE-W308F Procapsids. The gpE-W308F mutant protein assembles into large particles that were purified using my standard procapsid purification protocol (Materials and Methods). The yield of these particles was similar to that of gpE-WT (Table 3-3), indicating that the mutation did not have a major effect on particle assembly. Examination of the particles by EM shows a high resemblance to

wild-type procapsids, suggesting little to no disruption in procapsid assembly by the W308F mutation (Figure 3-15).

I next examined the effects of the mutation on procapsid structure and function. First, an expansion assay was performed to confirm that the procapsids could still be expanded *in vitro*. The data presented in Figure 3-16 indicates that while gpE-W308F procapsids can be expanded *in vitro,* significantly higher concentrations of urea are required compared to wild type procapsids. Further, unlike wild-type procapsids, there is less evidence of a cooperative expansion transition with the mutant. Control studies indicate that wild type procapsids are stable to up to 4.5M urea, suggesting that the results seen W308F procapsids reflect urea driven procapsid expansion and not global unfolding of the protein.

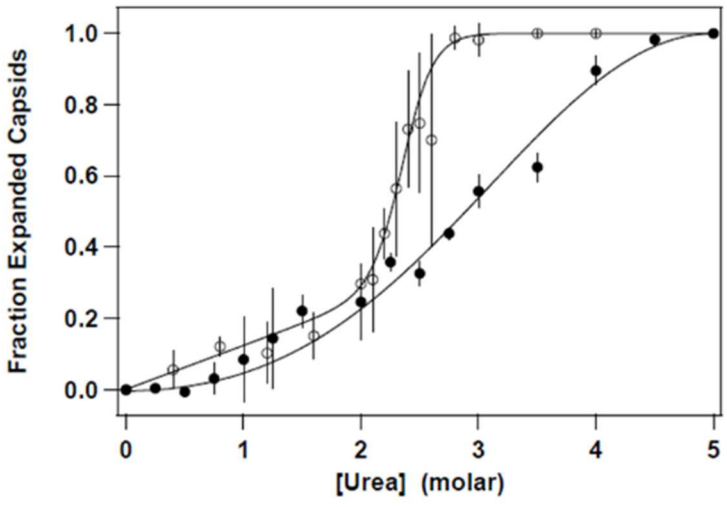

Figure 3-16. Urea-Triggered expansion of wild-type and gpE-W308F procapsids. The particles were incubated with urea and procapsid expansion quantified by agarose gel assay as described in Materials and Methods. Each data point represents n=3 independent experiments with standard deviation indicated with error bars. Open circles (○) curve represent wild type procapsids. Closed circles (●) represents gpE W308F procapsids. The data were analyzed according to Equation 2.1 (Materials and Methods) which affords $\Delta G(H_2O)$= 1.8 ± 0.4 kcal/mol and *m*= 0.46 ± 0.29kcal/mol*molar for the gpE-W308F procapsids, vs. $\Delta G(H_20)$= 10 ± 3.0 kcal/mol and *m*= 4.2 ± 1.3 kcal/mol*molar for WT gpE procapsid expansion

I next examined the capacity of the expanded gpE-W308F procapsids to add gpD, as required of a functional procapsid. Wild-type and gpE-W308F capsids (40 nM) were incubated in the presence of 16 μM gpD and decoration of the particles examined by agarose gel assay as described in Materials and Methods. As shown in Figure 3-17, the mutant particles bind wild type gpD in a 1:1 gpE to gpD stoichiometric ratio, similar to wild type procapsids. I next examined the capacity of the gpE-W308F procapsids to add the mutant gpD proteins described above. GpD-P17A and gpD-H19A decoration proteins were incubated with expanded gpE-W308F capsids. The data presented in Figure 3-17 demonstrates that binding of both mutant gpDs to gpE-W308F capsids appears to be similar to the wild type gpD protein.

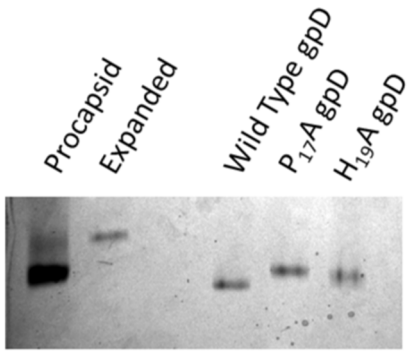

Figure 3-17. Agarose gel of gpD addition to gpE-W308F procapsids. W308F procapsid and expanded capsid standards are left. Addition of gpD-WT, gpD-P17A, and gpD-H19A to gpE-W308F are depicted in right three lanes. Further addition of either gpD did not result in additional shift in migration of the decorated shells.

Finally, I examined the capacity of gpE-W308F mutant procapsids to package a full-length lambda genome *in vitro*, the ultimate test of a functional procapsid particle. The packaging assay, as described above, is a DNase protection assay that reports on the amount of DNA packaged into the viral capsid. Wild type procapsids with wild type gpD were used as the positive control. The data presented in Figure 3-18 demonstrate that the gpE-W308F mutation strongly compromises the capacity of the procapsid to

package a full-length genome, with both wild-type and both mutant gpD decoration proteins.

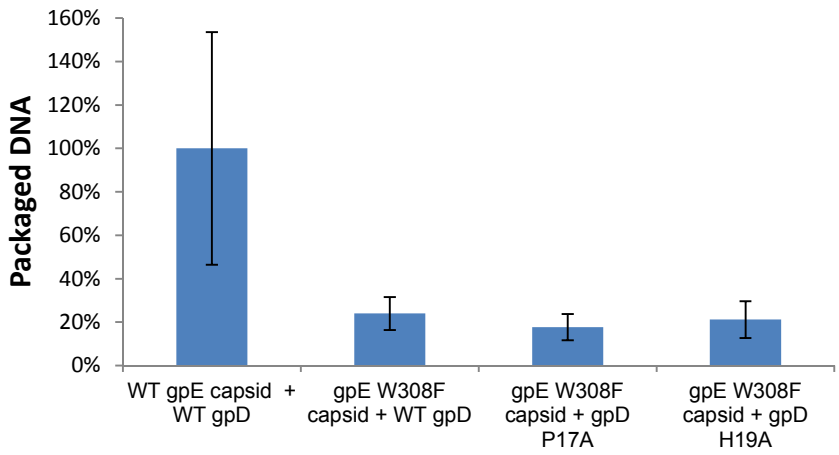

Figure 3-18. Packaging of a full length lambda genome. Graph depicting the packaged DNA as reported by DNase protection assay. Each bar represents results from three separate experiments and the error bars represent standard deviation. All values are normalized to WT procapsids decorated with WT gpD.

Discussion

The importance of shell expansion in the viral assembly pathway is made apparent by its prevalence in almost all complex dsDNA viral assembly pathways (Galisteo & King, 1993) (Heymann, Cheng, Newcomb, Trus, & Brown, 2003). In addition, the need for stabilization of the expanded shell from both the extreme internal force generated by the packaged DNA, and the external forces brought to bear by the environment, is just as vital. The method for stabilizing the expanded viral capsid varies depending on the virus: chemical crosslinking of the major capsid proteins, increased interaction between subunits in the expanded shell, and addition of a stabilizing decoration protein are a few examples (Fuller, et al., 2007b) (Tzlil, Kindt, Gelbart, & and Ben-Shaul, 2003). While the approaches differ, the end result is the same and a stable capsid is achieved.

In the case of bacteriophage lambda, addition of the gpD decoration protein is responsible for stabilization of the expanded capsid. This is evident from the requirement of gpD for the proper packaging of a lambda genome. Without gpD only small, sub genomic lengths of DNA can be packaged without the partial or complete loss of capsid structural stability (Yang, Maluf, & Catalano, 2008). The recent study by Hernando-Pérez, et al., which quantified the stability of lambda capsid shells by atomic force microscopy (AFM), reported that the expanded capsid is fragile relative to the procapsid, showing a decrease in yield force of 0.11 nN from procapsid to expanded capsid. Once decorated with gpD the expanded capsid is able to withstand up to 0.88±0.07 nN of external force (Hernando-Pérez, Lambert, Nakatani-Webster, Catalano, & Pablo, 2014).

Lambda packages its genome into preformed procapsids resulting in up to ~20 atmospheres of internal pressure (Fuller, et al., 2007b). This requires a robust capsid structure, which is provided by gpD. The proposed interactions that are responsible for the imparted stability by gpD to the capsid are numerous. For instance, published structural studies suggest that the N-terminus of gpD is important for binding to the capsid surface and for stabilizing the shell (Wendt & and Feiss, 2004). Based on my studies, I have proposed a number of additional interactions including hydrophobic interactions between the gpD trimer spike and the capsid surface, and in addition specific amino acid interactions between gpD and gpE in the binding and stabilization of the capsid surface by gpD.

Non-Covalent Interactions Between gpD and the Capsid Surface. In Chapter 2, I demonstrated that expansion of the procapsid exposes hydrophobic surface area in the

shell, which I have proposed provides a nucleation site for gpD trimer assembly. These hydrophobic surfaces are proposed to be buried in and to stabilize the procapsid state, but are exposed during expansion. In the present chapter, I have demonstrated that gpD binding to the expanded capsid shell does not occur at 10˚C but is very efficient at ≥ 25˚C. Hydrophobic interactions have been shown to play a larger role in burial of hydrophobic surface area at temperatures near 20°C, thus increasing the strength of the hydrophobic interaction in this temperature range (Baldwin, 1986). In sum, the temperature data is consistent with my hypothesis that gpD binding to the expanded shell relies on hydrophobic interactions, at least in part.

In addition, I have proposed specific interactions between residues in gpD and gpE in the shell, based on a pseudo-atomic model of the lambda capsid shell. The model suggested two important rings of residues, one of aspartic acids and one of tryptophans, that are important in the capsid surface interaction with gpD. Similar to the hydrophobic surfaces discussed above, these rings, formed at the three fold axes of the capsid by three gpE subunits, are proposed to be buried in the procapsid state and exposed during expansion (Nakatani-Webster, 2013). These residues were proposed to interact with His19 and Pro17, respectively, on the base of trimeric gpD as discussed above. It is important to note that the seemingly small nature of one or two amino acid interactions can in fact be very large, in relation to capsid binding and stabilization, due to the repetition on the capsid surface ~415 times. The importance of these interactions between gpE and gpD amino acid rings was investigated first by introducing mutations into gpD and then by the complementary mutation the gpE residues.

I directly tested my hypotheses using a mutagenesis approach, which demonstrates that while neither the P17A nor the H19A mutation grossly affect spike assembly at the capsid surface, both mutations strongly affect the capacity of the proteins to stabilize the shell sufficiently to allow the packaging of a full-length genome. I interpret this observation to indicate that the full complement of interactions are necessary for full stabilization of the capsid.

The gpD mutants serve to investigate one side of the proposed interactions between gpD and the expanded capsid during binding and stabilization of the shell. I therefore used complementary capsid mutations to define the resulting stabilization of the expanded capsid. An unexpected outcome was observed with the gpE-W308A mutation, which exhibits a significant shell-assembly defect. Moreover, the small amount of protein that did assemble formed small shells and apparent tetrameric assemblies. The nature of these novel tetramers is currently under investigation and the soluble, monomeric protein is being investigated as a candidate for crystallization of gpE which to date is still undocumented.

A different defect is observed with the gpE-D292A mutant, which assembles into heterogeneous, aberrant structures. Moreover, the shells are prone to aggregation and the data suggests that this mutation disrupts the regulation of procapsid formation and perhaps pre-maturely exposes hydrophobic surface area resulting in shell aggregation.

In contrast, gpE-W308F procapsids are structurally indistinguishable from wild type and interestingly, the purified preparation contains few pre-expanded capsids. A possible cause for the high degree of homogeneity came to light when gpE-W308F

procapsids were expanded with urea, which revealed that the gpE-W308F procapsids were more stable, exhibiting a greater $[urea]_{1/2}$ compared to wild type. It is important to note that there is no evidence of expansion intermediates, indicating that the mutant procapsids follow the same apparent two state expansion transition observed with wild type procapsids. I interpret these observations to indicate that the mutation of tryptophan to phenylalanine shifts the equilibrium in favor of the procapsid state. Thus, the gpE-W308F procapsids are more difficult to expand and there are less pre-expanded shells in the purified preparations.

Notwithstanding, the gpE-W308F shells, once expanded, bind gpD with similar affinity and stoichiometry as wild-type capsids. This suggests that there is no significant disruption of the geometry of gpD binding to the mutant capsid surface. These results correlate well with temperature studies suggesting that a major driving force in gpD binding to the expanded capsid surface is hydrophobic interactions. The hydrophobic interaction between gpD and the exposed surface of gpE-W308F capsids should not be significantly affected by the mutation (Matthews, 2001).

In contrast to the gpD *binding* data, deletion of a single gpD-gpE interaction has significant effects on the capacity of the shells to *package* a viral genome. This is observed regardless of whether the mutation is introduced into the decoration protein (i.e., gpD-P17A or gpD-H19A binding to WT capsids) or into the major capsid protein (i.e., gpE-W308F procapsids binding to either gpD-WT or gpD-P17A). Interestingly, introduction of a second binding defect (i.e., gpD-H19A binding to gpE-W308F procapsids) is not additive, and the dual mutations neither affect binding nor stabiliziation more than a single defect. This suggests that the decrease in expanded

capsid stability during DNA packaging due to the loss of one interaction between the proposed residues is as destabilizing as the loss of two interactions. Finally, I note that there is still packaging observed with gpE-W308A procapsids suggesting that not all stabilization of the expanded capsid is lost. These results correlate well with previous work showing there are important interactions between the N-terminus of gpD and the capsid surface, and that hydrophobic interactions continue to play a role in stabilizing the expanded capsid.

Conclusion. I have proposed that alternating rings of Trp and Asp provided by gpE on the expanded capsid surface interact with complementary rings of Pro and His on the base of trimerized gpD, to facilitate binding of gpD to the capsid surface and to stabilize the expanded capsid. Results presented here suggest that though not necessary for gpD binding to the capsid surface, these residues create a redundancy in *stabilizing* the capsid that is necessary but not ultimately critical as some capsid stabilization is still observed during DNA packaging. It is of interest that gpD-P17A and gpD-H19A both bind to the gpE-W308F capsids similarly to wild type. Importantly, gpD-H19A binds to the mutant capsids despite the fact that both of the putative gpD-gpE interactions have been modified, which suggests that a loss multiple interactions do not affect gpD *binding* to the capsid surface. I suggest that this is consistent with my hypothesis that binding of gpD to the expanded capsid relies on multiple, redundant interactions including ionic bonds, Pro-Trp interactions, hydrophobic interactions between the spike base and the capsid surface, and in addition multiple interactions between N-terminal residues of gpD and adjacent gpE subunits assembled into the capsid shell. This redundancy in capsid stabilization is not unexpected due to a stable

capsid being essential to withstand the internal and external pressures experienced by an infectious virus.

Chapter 4: Mechanism of gpD Self-Assembly at the Expanded Capsid Surface

Introduction

Bacteriophage lambda is a widely used model system to study the assembly pathways for complex dsDNA viruses (Fuller, et al., 2007b). A high degree of similarity is seen in all of these viruses with respect to DNA packaging, viral shell expansion and viral shell stabilization (Casjens S. R., 2011) (Galisteo & King, 1993) (Duda R. L., Hempel, Shabanowitz, Hunt, & Hendrix, 1995). Lambda has been extensively studied for many years, which has yielded a significant understanding of these important steps in virus assembly. Additionally these studies have provided a valuable model system for the design of protein based therapeutic nanoparticles (Chang, Song, Nakatani-Webster, Monkkonen, Ratner, & Catalano, 2014). A brief description of the lambda assembly pathway is provided here.

Procapsid Assembly. *In vivo* assembly of procapsids is described in detail in Chapter 1. Briefly, 12 copies of lambda protein gpB self-associate to form a dodecameric ring structure (Medina, Wieczorek, Medina, Yang, Feiss, & Catalano, 2010). This ring serves as a nucleation site for gpNu3 and gpE. gpNu3 is the lambda capsid scaffolding protein and gpE is the major capsid protein. Additionally the viral gpC protease is included in limited quantities (Medina, Andrews, Nakatani, & Catalano, 2011). Once gpNu3 and gpE have co-polymerized into the immature procapsid, gpNu3 is proteolyzed by gpC along with the N-terminal 20 residues of approximately six copies of gpB. GpC is also self-proteolytic and all of the proteolysis products exit the capsid

through holes in the immature shell (Figure 4-1) (Medina, Wieczorek, Medina, Yang, Feiss, & Catalano, 2010).

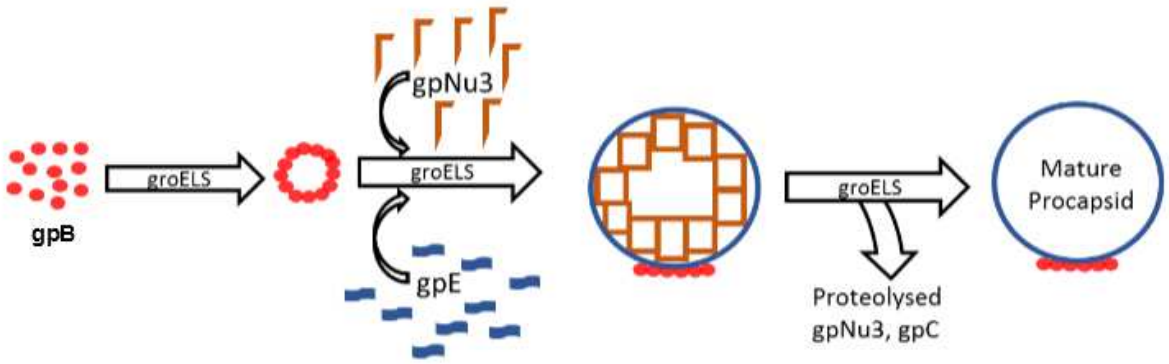

Figure 4-1. Scheme of lambda procapsid assembly in vivo. Twelve copies of gpB chaperoned by groELS form a dodecameric ring called the portal. The portal nucleates gpNu3 and gpE copolymerization, along with a limited number of gpC proteases, to form the immature procapsid. GpC is autoproteolytic and also degrades gpNu3 and the 20 N-terminal residues of ~ 6 copies of gpB in the portal. Proteolysis products leave through the portal of the mature procapsid.

In Vitro Particle Assembly. The assembly of viral shells *in vitro* has been reported for many viruses, including brome mosaic virus, cowpea chlorotic mottle virus, and human papillomavirus (HPV). These are referred to as virus like particles (VLP). Papillomavirus VLPs are currently used as a vaccine against HPV (Gardasil® marketed by Merck) (Villa, Perez, Kjaer, & al, 2007) (Aniagyei, DuFort, Kao C. C., & B., 2008) (Huang, et al., 2007). *In vitro* assembly systems have also aided in characterizing the pathways and the kinetic and thermodynamic features of capsid assembly, especially in the lambda, HK97, phage P22, and hepatitis B virus systems (Bourne, et al., 2008) (Parent, Doyle, Anderson, & Teschke, 2005) (Katen & Zlotnick, 2009). Bacteriophage lambda *in vitro* VLP assembly has been recently reported in our lab (Medina, Andrews, Nakatani, & Catalano, 2011). The particles are assembled using purified gpNu3 and

gpE, which co-assemble into icosahedral capsid shells. The *in vitro* assembled VLPs are morphologically similar to lambda procapsids assembled *in vivo*, except that they lack a portal structure.

Capsid Stabilization. *In vivo*, lambda procapsids undergo an expansion transition after packaging of ~15kb of the viral genome. This expansion step enlarges the diameter of the procapsid approximately 10 nm while increasing the volume of the shell 2-fold (Fuller, et al., 2007b) (Dokland & Murialdo, 1993). The stability of the capsid is decreased compared to the procapsid; however, stabilization of the expanded lambda capsid is achieved by addition of the decoration protein gpD to the expanded capsid surface (Hernando-Pérez, Lambert, Nakatani-Webster, Catalano, & Pablo, 2014) (Gaussier, Yang, & Catalano, 2006).

Previous studies examining the stability of procapsids in comparison to expanded capsids demonstrate that full stability of the capsid is not obtained until the decoration protein is bound to the surface of the capsid (Hernando-Pérez, Lambert, Nakatani-Webster, Catalano, & Pablo, 2014). Importantly, gpD has been used extensively in phage display and the lambda VLP system is well suited as a platform for *in vitro* assembly of display particles (Bratkovic, 2010). It has been shown in our lab that lambda VLPs expand in a manner similar to wild type procapsids and are subsequently able to add gpD in a similar ratio of 1:1 gpD to gpE as seen with wild type procapsids (Chang, Song, Nakatani-Webster, Monkkonen, Ratner, & Catalano, 2014). This ability of VLPs to expanded and bind gpD suggests they are a stable and valid candidate for nanoparticle development.

To gain further insight into the possible uses of lambda VLPs and their display capabilities decorated with gpD, a firm understanding of how gpD assembles at the capsid surface is necessary. An in depth description of gpD binding to the expanded capsid was presented in Chapter 3. Briefly, gpD is a monomer in solution but binds to the capsid surface as a trimer at the icosahedral three-fold axes. The resulting decorated capsid contains an approximate 1:1 ratio of gpE to gpD. Multiple binding interactions have been reported to mediate assembly of gpD at the expanded capsid surface (Yang, Maluf, & and Catalano, 2008) (Wendt & and Feiss, 2004). In addition these interactions are proposed to be responsible for the stabilization of the expanded capsid. While I have examined these interactions in detail in Chapter three of this thesis, these studies do not address mechanistic features of gpD trimerization at the expanded capsid surface.

Proposed Model for gpD Assembly. Previous studies have examined gpD assembly at the capsid surface, but have used DNA packaging as an indirect readout of binding. Yang and co-workers examined the gpD concentration dependence of the DNA packaging reaction *in vitro* (Yang, Maluf, & and Catalano, 2008). This study demonstrated a strong sigmoidal concentration dependence, which was interpreted as cooperative assembly of gpD trimers on the capsid; however, the concentration of gpD required to half-stimulate the reaction ($C_{1/2}$) increased with procapsid concentration, which led the authors to propose that there is an initial distributive phase in which gpD binds independently at the 140 three-fold axes. Thus, the higher the concentration of procapsids the more gpD must be added to “saturate” the distributed phase of binding. This is followed by a cooperative binding phase to afford the dimer and then trimer spike

at the nucleation site. In other words, there is a mix of distributive and cooperative binding for spike assembly. This model is presented in Figure 4-2.

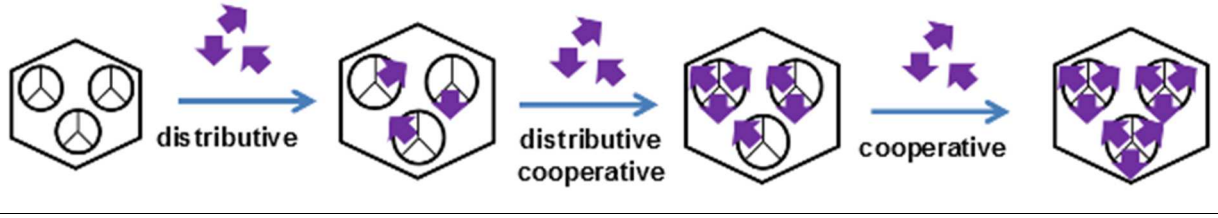

Figure 4-2. Proposed binding model for gpD addition to the capsid surface. Black hexagon and "peace signs" represent capsids and three-fold axes respectively. GpD, depicted as a purple arrow, first binds distributively over the three-fold axes until all are essentially saturated with protein. The second and then third gpD monomers then bind with increasing cooperativity to yield the trimer spike.

The work done by Yang, *et al*. utilized DNA packaging as an indirect readout for gpD addition and therefore did not directly examine gpD binding to the capsid (Yang, Maluf, & and Catalano, 2008). Further, no work, to date, has been done to dissect the relative placement of gpD monomers on the capsid surface during spike assembly. The exact placement of modified gpD proteins during spike assembly is an important question if gpD is to be used to assemble *defined* VLPs for theragnostic applications. In an effort to address these questions, I developed defined *in vitro* assays that directly measures gpD binding to the capsid surface. These materials and assays set the stage for future studies that will directly address the kinetic and thermodynamic features of gpD assembly at the capsid surface to directly test the model presented in Figure 4.2.

MATERIAL AND METHODS

Reference Chapter 5

RESULTS

The proposed model for gpD assembly at the capsid surface is a distributive binding event for the first gpD monomer, at each three-fold axis, followed by increasingly cooperative assembly of the subsequent two proteins to afford a trimeric spike (Figure 4-2). Here I describe studies designed to directly test this hypothesis.

Agarose gel Analysis of gpD Binding. I first developed an agarose gel assay to directly measure gpD binding to the expanded capsid shell. Procapsids were expanded in 2.5M urea and then exchanged into no magnesium buffer (50mM tris, pH 8 at 4°C) as described in Materials and Methods. The expanded capsids (130 nM) were incubated on the bench top for thirty minutes with the indicated concentrations of gpD. Samples were then loaded onto native agarose gels and the binding of gpD to the expanded capsid surface determined by the mobility shift in the capsid band. Figure 4-3 shows that the capsid migrates faster as gpD binds to the capsid surface. This is most likely due to the large negative charge imparted to the capsid when coated with 420 copies of gpD, which is negatively charged (Medina, Nakatani, Kruse, & Catalano, 2012).

In this study, a capsid concentration of 130 nM was used, which translates to a three-fold axis concentration of 18.2 μM (there are 140 three-folds per icosahedral shell). Initially, titration of gpD into the reaction mixture affords a small shift of the capsid band up to 33 uM gpD (two three-fold stoichiometric equivalents), resulting in a "smeared" band (Figure 4-3). As the concentration is further increased, the band cleanly shifts with no apparent intermediates, up to 57 uM gpD (three three-fold stoichiometric equivalents).

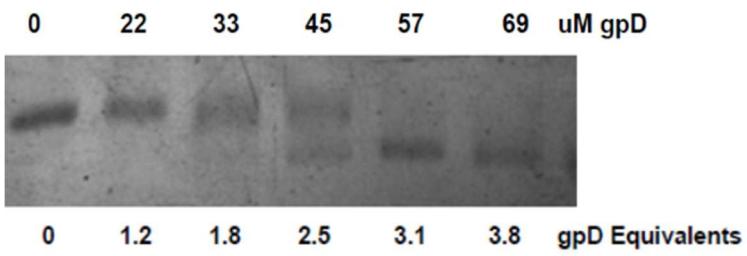

Figure 4-3. Gel of addition of gpD to expanded capsids. Lanes show band migration with gpD addition to capsids. The concentration of capsids was held constant at 130nM and gpD addition is presented in concentration units at top of the gel and in stoichiometric equivalents, relative to gpD binding sites, at the bottom of the gel.

In sum, while the agarose gel assay is useful as an initial screen for gpD binding to the capsid, rigorous quantitation of gpD binding as required for the present study requires a more sophisticated assay. My progress towards developing a useful assay is detailed below.

Labeling of gpD with Fluorescein. The need for a more sensitive binding assay led me to consider a fluorescence-based assay to examine gpD binding to the capsid surface. As a first step towards this goal, I utilized gpD-S42C, a single cysteine gpD mutant available in the lab (Chang, Song, Nakatani-Webster, Monkkonen, Ratner, & Catalano, 2014). This mutant protein projects the sole cysteine away from the capsid surface in the spike trimer (Figure 4-4). I hypothesized that labeling of gpD-S42C with fluorescein 5'-maleimide (Invitrogen) would afford me a fluorescent tag with which to monitor gpD assembly at the capsid surface.

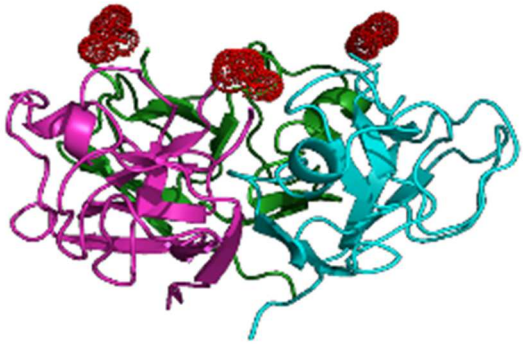

Figure 4-4. gpD S42C trimer. Side on view of gpD crystal structure (PDB# 1C5E) showing each gpD monomer in separate color. S42C is depicted in red mesh ball. The exposure of Cys 42 to solvent due to it lying on the apical side of the trimer suggests dye addition will not interfere with gpD binding to the trimer as well as allowing for high visibility of fluorophores bound to the Cys.

GpD-S42C was purified as previously described (Chang, Song, Nakatani-Webster, Monkkonen, Ratner, & Catalano, 2014) and then labeled with fluorescein 5'-maleimide (Invitrogen) as described in Materials and Methods (Chapter 5). Based on UV spectroscopy, ~80% of the free cysteines were modified with the fluorophore (data not shown). MALDI mass spectrometry of the labeled protein confirmed that fluorescein was bound to the full-length protein, based on the predicted molecular weight of gpD-S42C (11,441 Da from the gene sequence, minus the N-terminal methionine that is removed *in vivo*) and the molecular weight of a covalently-bound fluorescein 5'-maleimide (427 g/mol), which affords a labeled protein mass of 11,868 Da. The mass spectrum also suggests that a small amount of the protein (~ 5%) is labeled with two fluorescent tags (12,295 Da). The exact location of this second minor adduct was not further investigated. Integration of the peak areas suggests that the labeling efficiency is ~ 60%.

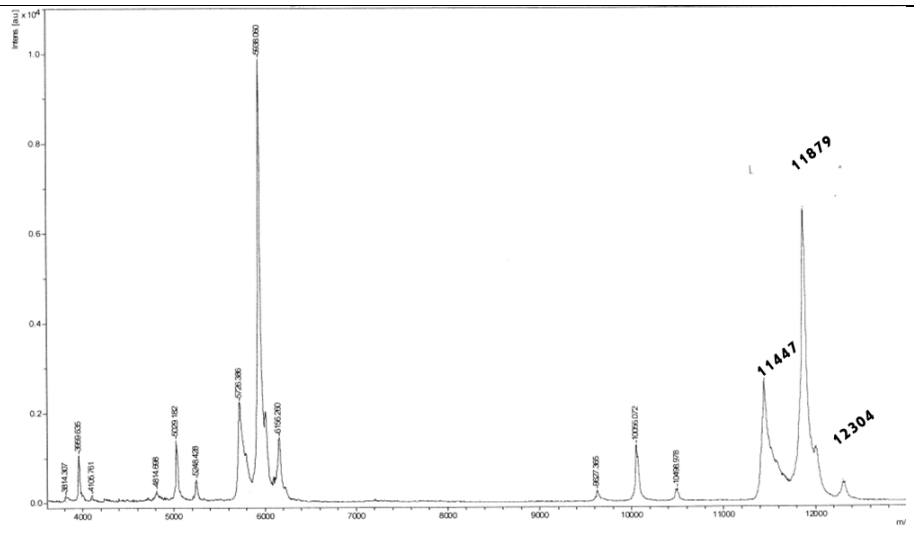

Figure 4-5. MALDI mass spectrometry analysis of gpD S42C labeled fluorescein. Peaks of gpD S42C and gpD-S42C labeled with fluorescein are present. The calculated molecular weight of gpD-S42C is 11,440 Da and the expected MW of fluorescein-labeled protein is 11,868 Da

Binding of gpD-S42C Fluorescein to Expanded Lambda Capsids. I next used the agarose gel assay to confirm that the fluorescein-labeled gpD-S42C protein was biologically active. The labeled gpD at the indicated concentration was incubated with the expanded capsids (119 nM) for 4 hours at room temperature and the samples were then run on a native agarose gel as described above. Figure 4-6 shows fluorescein labeled gpD bound to the capsid in a concentration-dependent manner and suggests a similar interaction as was observed with the unmodified wild-type gpD protein (compare with Figure 4-3).

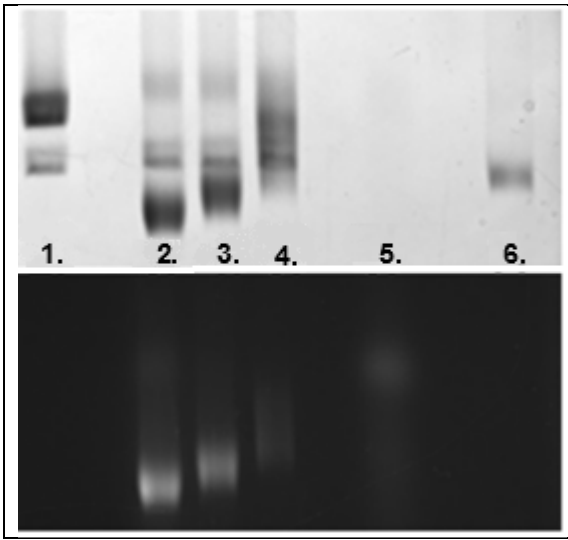

Figure 4-6. Gel showing fluorescein-labeled gpD S42C adds to expanded capsids *in vitro*. Top panel. Gel stained with Coomasie-blue. Bottom panel. Unstained image of fluorescence migrating in the gel. **Lane 1.** Expanded capsids (~119nM). **Lane 2.** Expanded capsids and ~50uM gpD-S42C fluorescein. **Lane 3.** Expanded capsids and ~30uM gpD-S42C fluorescein. **Lane 4.** Expanded capsids and ~10uM gpD-S42C fluorescein. **Lane 5.** 20uM gpD-S42C fluorescein. **Lane 6.** Expanded capsids and 20 μM wild type gpD.

Discussion

Scientists have studied and manipulated nanoparticles for considerably less time than the eons over which virus capsids have been evolutionarily optimized. Use of capsid proteins in the design of virus like particles allows us to capitalize on the wealth of robust self-assembling nanoparticles observed in virus biology. To be able to make full use of VLPs, however, a thorough understanding of shell structure and stabilization is necessary.

Data presented in Chapter 2 of this thesis shed light on the expansion and reversibility of urea-triggered capsid expansion. Additionally, the work presented in Chapter 3 detailed the interactions between gpD and the expanded capsid surface, focusing on the non-covalent interactions that are necessary for gpD binding and capsid stabilization. The insights gained from those studies can be applied to *in vitro* assembled VLPs, which have been shown to expand and add gpD in a similar manner as wild type procapsid. Despite this increased understanding of the driving forces

behind gpD binding to and stabilization of the expanded capsid, a detailed description of the mechanism for gpD trimer spike assembly at the capsid surface is still not clear.

Model of gpD addition. Published studies from our lab suggested a distributive binding event followed by a cooperative second and/or third binding event (Yang, Maluf, & and Catalano, 2008). The gel based assays described here are consistent with a multi-step assembly process, but do not provide sufficient resolution to convincingly test the hypothesis. Specifically, this assay lacks the required sensitivity and resolution to clearly distinguish between the addition of monomers, dimers and trimers. Therefore, I developed a fluorescence based assay for gpD addition. My data clearly demonstrates that gpD-S42C can be efficiently labeled with fluorescein and that the labeled protein adds to the expanded lambda capsid in a manner similar to that observed with the wild-type protein. Future studies in the lab will be directed at developing and optimizing a solution-based binding assay that can be monitored by fluorescence anisotropy.

Additionally, a FRET-based assay may be developed to probe for dimer and trimer interactions at the three-fold axes. The distance between adjacent Cys42 residues in a gpD trimer spike is 27.6 Å, which is ideally suited to probing for sequential addition of gpD monomers. Importantly, the distance between the three-fold axes on the shell surface is greater than 100Å, which ensures that FRET will only be observed between the gpDs at the same three fold axis. Unfortunately, I did not have time to pursue these studies further, but they remain an active area of study in the Catalano lab.

Chapter 5: Materials and Methods

Mature lambda DNA and molecular biology enzymes were purchased from New England Biolabs. Yeast extract, agar, and tryptone were purchased from DIFCO. Urea was purchased from Fisher Scientific and chromatography media was purchased from GE Healthcare. All other materials were of the highest quality available. Bacterial cultures were grown in shaker flasks and an Innova 4430 Incubator Shaker was used. GE Healthcare's Amersham Biosciences AKTApurifier core 10 System was used for all protein purifications. Sucrose density gradients were prepared using a Biocomp Model 107 gradient Master. High speed centrifugation including gradient centrifugation used a Beckman L-90K ultracentrifuge with a SW 28 rotor. Video Densitometry of SDS-PAGE and agarose gels utilized an EpiChemi3 darkroom system from UVP Bioimaging Systems, equipped with a Hamamatsu camera. Quantitation of the bands was performed using the Image Quant software package from Molecular Dynamics.

Circular Dichroism Spectroscopy. CD experiments were performed on a Jasco J-1500 CD spectrometer (kindly provided by the Department of Biochemistry, University of Washington). All spectra were acquired at 4°C with a 1 mm pathlength quartz cuvette in 50 mM Tris-HCl buffer, pH 8.0, containing 20 mM $MgCl_2$. The interval for data collection was 0.1nm with a bandwidth of 1nm.

Electron Microscopy. Each grid, 300 mesh carbon-coated copper (Ted Pella or EMS), was negatively glow-discharged using an Electron Microscopy Sciences Glow Discharger. The sample (2 ul) was applied to the grid and excess sample was blotted from the grid. The grids were then washed three times with water and stained either with Nano-W (Nanoprobes), which is a commercial preparation of methylamine

tungstate, or 2% uranyl acetate. Bright field electron microscopy was performed using University of Washington's NanoTech User Facility FEI Tecnai G2 F20 S-Twin TEM, equipped with Gatan CCD imaging systems.

Expression and Purification of Bacteriophage Lambda Procapsids Using Escherichia coli BL21(DE3)[pLysS][pT7Cap]. We previously described the construction of pT7Cap, a vector that expresses all of the lambda capsid genes from an IPTC inducible operon. (Yang & Catalano, 2003) The expressed proteins self-assemble into functional procapsids *in vivo*. Two liters of 2X-YT media, pH 7.2, containing 25 mM potassium phosphate, 5 mM glucose, and 50 ug/mL ampicillin was inoculated with a 20 mL overnight culture of *Escherichia coli* BL21(DE3)[pLysS][pT7Cap] cells derived from an isolated colony (Gaussier, Yang, & Catalano, 2006). The culture was maintained at 37°C until an OD_{650} of 0.6 - 0.7 was obtained at which point IPTG was added to a final concentration of 0.5 mM. The incubation was continued for additional 2 hours and the cells were harvested by centrifugation. Unless otherwise indicated, all subsequent steps were performed at 0°C – 4°C. The cell pellet was re-suspended in 50 mL ice-cold TMS buffer (50 mM Tris-HCl, pH 8.0, containing 20 mM $MgCl_2$ and 100 mM NaCl), the cells were lysed by French Press (680 psi), and the crude lysate was clarified by centrifugation (7,650 x g, 25 minutes). The procapsids were then harvested by centrifugation (87.2K x g, 3 hours) and the pellets were gently overlaid with 1 mL TMS buffer and left at 4˚C overnight. The overlay, which contained opaque, flocculent material, was carefully removed from each tube not disturbing the pellet. The combined overlays were loaded onto a 5 mL HiTrap Q Sepharose High Performance strong anion exchange column (GE Healthcare Life Sciences) equilibrated with TM buffer (50 mM

Tris-HCl, pH 8.0, containing 20 mM $MgCl_2$). The column was developed with a 0–250mM NaCl gradient and fractions were examined by SDS-PAGE for the presence of gpE. The procapsid-containing fractions were pooled, dialyzed against TM buffer, and concentrated using a 100 kDa MWCO centrifugal filter (Amicon). The sample was applied to a 10–40% sucrose gradient prepared in the same buffer and the gradients were centrifuged to equilibrium (87.2 x g, 3 hours). The procapsid band was visualized by light scattering in ambient light and the band was harvested by aspiration and dialyzed against TM buffer. The procapsids were then dialyzed against TM buffer and concentrated using a 100 kDa MWCO centrifugal filter and stored at 4°C until use.

Expression and Purification of Bacteriophage Lambda Procapsids from a Lambda Lysogen. The lambda lysogen NS428 (λ *A*am11 *b*2*red*3 *cI*ts857 *S*am7) contains an amber mutation in the terminase *A* gene but otherwise expresses all of the viral structural genes. Procapsids assemble normally but DNA cannot be packaged as a result of the terminase null phenotype. Lysogeny is maintained under the control of cI857, a temperature sensitive cI repressor.

Two liters of 2X-YT media, pH 7.2, containing 25 mM potassium phosphate, 5 mM glucose, and 50 ug/mL ampicillin was inoculated with a 20 mL overnight culture of *Eserichia coli* NS428 (λ *A*am11 *b*2*red*3 *cI*ts857 *S*am7) cells derived from an isolated colony. The culture was maintained at 32°C until an OD_{600} of 0.3 was obtained at which point the culture was shifted to 45 C for 15 minutes to induce the lysogen. Following induction cells were incubated at 38 ˚C for 60 minutes and the cells were harvested by centrifugation.

Unless otherwise indicated, all subsequent steps were performed at 0°C – 4°C. The cell pellet was re-suspended in 20 mL ice-cold TMS buffer (50 mM Tris-HCl, pH 8.0, containing 20 mM $MgCl_2$ and 100 mM NaCl), the cells were lysed by sonication and the crude lysate was clarified by centrifugation (7,650 x g , 25 minutes). The procapsids were then harvested by centrifugation (87.2K x g, 3 hours) and the pellets were gently overlaid with 1 mL TMS buffer and left at 4˚C overnight. The overlay, which contained opaque, flocculent material, was carefully removed from each tube not disturbing the pellet. The combined overlays were applied to a 10–40% sucrose gradient prepare in the same buffer. The gradients were then centrifuged to equilibrium (87.2 x g, 3 hours) and the procapsid band was visualized using Biocomp Piston Gradient Fractionator Model 152. The band was harvested by aspiration and dialyzed against TM buffer. The procapsids were then concentrated using a 100 kDa MWCO centrifugal filter and the sample was applied to a second 10–40% sucrose gradient and centrifuged to equilibrium (87.2 x g, 3 hours). The procapsid band was again visualized using Biocomp Piston Gradient Fractionator Model 152. The band was harvested by aspiration and dialyzed against TM buffer. The procapsids were then concentrated using a 100 kDa MWCO centrifugal filter and stored at 4°C until use.

Gel Electrophoresis. SDS-PAGE samples were mixed with 0.2 equivalents of 5x reducing SDS-PAGE loading buffer and boiled for no more than 2.5 minutes to minimize heat-induced degradation of the major capsid protein. Samples were loaded on to 15% polyacrylamide gels, run at 185 V, until the dye migrated to ~ 1 cm from the bottom of the gel. The gel was stained with Coomassie Brilliant Blue R-250 over-night with gentle

agitation. The gel was then destained with gentle agitation until the background was negligible (~ 18 hours).

Native agarose gel samples were mixed with 0.17 equivalents of 6x non-denaturing loading dye (2.5% Ficoll®-400, 11 mM EDTA, 3.3 mM Tris-HCL, 0.017% SDS, 0.015% bromophenol blue, pH 8.0 at 25°C) and 10-20 uL were loaded onto 0.4% or 1.2% agarose gel, as indicated in each individual experiment. Gels were run at 160 V for 90 min and then stained for 15 min in Coomassie Brilliant Blue R-250 with gentle agitation. The gel was then destained until the background was negligible (overnight). In each case, the protein bands were imaged and quantified by video densitometry as previously described. (Medina, Nakatani, Kruse, & Catalano, 2012)

Preparation of Expanded Capsid Shells. Expanded capsid shells were prepared as previously described (Medina, Nakatani, Kruse, & Catalano, 2012). Briefly and unless otherwise stated, purified procapsids (40 nM) were incubated in 50 mM Tris-HCl buffer, pH 8, containing 2.5 M urea and 3 mM $MgCl_2$ for 10 minutes on ice. Urea was then removed from the sample by buffer exchange using an 100kDa cutoff Amicon centrifugal filter unit to afford a preparation of expanded capsid shells in 50 mM Tris-HCl buffer, pH 8, containing less than 0.5 M urea and 0.5 mM $MgCl_2$.

Quantification of Procapsid Expansion. Procapsids were incubated as described above except that the concentration of $MgCl_2$ and urea were as indicated in each individual experiment. The mixture was incubated at 4°C degrees for 10 minutes and then loaded onto a 0.8 % agarose gel which was developed and stained as described above. The fractionated procapsid and expanded capsid bands were quantified by video densitometry and the fraction of expanded capsids was determined by,

$$F_E = \left(\frac{Intensity\ in\ Expanded\ Band}{Intensity\ in\ Procapsid\ Band + \ Intensity\ in\ Expanded\ Band}\right)$$

F_E was corrected for the small fraction of pre-expanded capsids in the procapsid preparation.

Thermodynamic Analysis of the Procapsid Expansion Data. Equation 2-1 (Chapter 2) was adapted from Santoro and Bolen (Santoro & Bolen, 1988) and used to analyze the procapsid expansion data quantified as described above. The entire urea expansion data set were fit to Equation 2 using non-linear least squares (NLLS) approaches using the Igor® data analysis package. The pre- and post-transition slopes and intercepts are floated in the fit to allow for increased accuracy in determining $\Delta G(H_2O)$ for the major transition. (Santoro & Bolen, 1988). This linear extrapolation method directly affords the $\Delta G(H_2O)$ and the denaturant *m* value for each data set.

In Vitro Decoration of Urea Expanded Lambda Capsid Shells To prepare gpD-decorated capsids, purified gpD (20 μM) was added to the expanded shells (40 nM capsids; 16.2 μM major capsid protein) and the mixture was incubated for 30 minutes at room temperature. The particles were then concentrated using a 100kDa cutoff centrifugal filter unit (Amicon) to remove any unreacted gpD (filtrate) and to afford gpD-decorated, expanded capsid shells (retentate).

The procapsids, the expanded capsids, and the gpD-decorated capsids all contain a portal complex but are devoid of scaffolding protein and the viral tail structure; importantly, all of the particles are catalytically active in the *in vitro* genome packaging reaction (Gaussier, Yang, & Catalano, 2006).

Site Specific Mutagenesis of gpD, the Lambda Decoration Protein. *Escherichia coli* BL21(DE3)[pD] cells that harbor a gpD expressing plasmid were a kind gift of Dr. J. Chang. The plasmid was isolated and used as a template for mutagenesis. Site specific mutations were introduced into this vector using the Stratagene QuickChange® Site Directed Mutagenesis kit according to the manufacturer's specifications and with the following primers.

pD-P17A forward primer: 5'-gggcaacagtgacgcggctcataccgc-3'

pD-P17A reverse primer: 5'-gcggtatgagccgcgtcactgttgccc -3',

pD-H19A forward primer: 5'-cagtgacccggctgctaccgcaaccgcg-3'

pD-H19A reverse primer: 5'-cgcggttgcggtagcagccgggtcactg-3'

The position of the mutation is underlined in each primer. The resulting plasmids were individually transformed into *Escherichia coli* DH5α cells and transformants selected by ampicillin resistance. Plasmids from these candidates were purified using QIAGEN Plasmid Mini Kits, and then sequenced to verify the mutations. Each plasmid was transfected into BL21(DE3)[pLysS] cells for protein expression. Expression from these vectors yield the gpD-P17A and gpD-H19A mutant proteins, respectively.

Purification of gpD Proteins Wild-type gpD, gpD-P17A, and gpD-H19A mutant proteins were expressed from BL21(DE3)[pLysS][pD], BL21(DE3)[pLysS][pD-P17A],

and BL21(DE3)[pLysS][pD-H19A] cells respectively, as previously described (Yang, Maluf, & and Catalano, 2008). Briefly, two liters of 2X-YT media, pH 7.2, containing 25 mM potassium phosphate, 5 mM glucose, and 50 ug/mL ampicillin were inoculated with a 20 mL overnight culture derived from an isolated colony. The culture was maintained at 37°C until an OD_{600} of 0.6 - 0.7 was obtained at which point IPTG was added to a final concentration of 0.5 mM. The incubation was continued for additional 2 hours and the cells were harvested by centrifugation. Unless otherwise indicated, all subsequent steps were performed at 0°C – 4°C. The cell pellet was re-suspended in 20mls of low salt buffer (20 mM Tris-HCl, pH 8.0, containing 20 mM NaCl, 0.1 mM EDTA, 7 mM β-ME), the cells were lysed by sonification using a Branson Sonifier 250 and the crude lysate was clarified by centrifugation (7,650 x g, 25 minutes). The supernatant was then heated to 50°C for 15 minutes followed by centrifugation at 10,000xg for 45 min at 4°C. The supernatant was then loaded onto a 5 mL HiTrap Q Sepharose High Performance strong anion exchange column (GE Healthcare Life Sciences) equilibrated with low salt buffer (20 mM Tris-HCl, pH 8.0, containing 20 mM NaCl, 0.1 mM EDTA, 7 mM β-ME). The column flow through, which contained gpD, was dialyzed against low salt buffer, concentrated using a 3 kDa MWCO centrifugal filter (Amicon), and stored at 4°C until further use.

Mutagenesis of gpE, the Lambda Major Capsid Protein. The plasmid pT7capDam7am43 was a generous gift of Dr. J. Chang. This vector is a derivative of pT7Cap (described above) in which an amber mutation has been introduced into the *D* gene. Protein expression from pT7capDam7am43 affords the gpE major capsid protein, the gpB portal protein, the gpNu3 scaffolding protein, and the gpC viral

protease, which self-assemble into functional procapsids *in vivo*. The plasmid was isolated and used as a template for mutagenesis. Site specific mutations were introduced into this vector using the Stratagene QuickChange® Site Directed Mutagenesis kit according to the manufacturer's specifications and with the following primers:

pE-W308A forward: 5'-ccgttacccgaaaaacgcggtgaccaccggcg-3'

pE- W308A reverse: 5'-cgccggtggtcaccgcgttttcgggtaacgg-3'

pE-W308F forward: 5'-cccgttacccgaaaaacttttgtgaccaccggcg-3'

pE- W308F reverse: 5'- cgccggtggtcacaaaagttttcgggtaacgg-3

pE-D292A forward: 5'-cattcaggatgcggccgcacagcgcgaag-3'

pE- D292A reverse: 5'-cttcgcgctgtgcggccgcatcctgaatg-3'

The position of the mutation is underlined in each primer. The resulting plasmids were individually transformed into *Escherichia coli* DH5α cells and transformants selected by ampicillin resistance. Plasmids from these candidates were purified using QIAGEN Plasmid Mini Kits, and then sequenced to verify the mutations. Each plasmid was transfected into BL21(DE3)[pLysS] cells for protein expression and procapsid isolation as described above.

Genome Packaging Assay Packaging was performed as described by published procedure (Yang, Maluf, & and Catalano, 2008) (Maluf, Gaussier, Bogner, Feiss, & and Catalano, 2006). In short, the 20 uL reaction consisted of 50 mM Tris-HCl buffer, pH 7.4, containing 9 mM NaCl, 10 mM MgCl2, 2 mM spermidine, 1.3 mM β-ME, 1 mM ATP, 150 nM IHF, 40 nM procapsids, 20uM gpD, and 2 nM full length lambda genome (48.5kb). The packaging reaction was initiated with the addition of the terminase holoenzyme at a final concentration of 100nM. The reaction was then incubated for 30 minutes at room temperature, at which point DNase was added to a final concentration of 10 μg/ml and allowed to incubate for 5 minutes. The reaction was stopped with the addition of 21uL phenol:chloroform. The aqueous layer (15 μl) was then removed and mixed with 5uL of 6x DNA loading dye (as described above). Samples were then loaded on to a 0.8% agarose gel, containing 0.5ug/mL of ethidium bromide, and run at 120 V for 1 hr. The DNase resistant, packaged DNA was visualized and quantified by video densitometry.

Fluorescein Labeling of gpD S42C. The lambda decoration protein gpD-S42C was expressed from *Escherichia coli* BL21(DE3)[pD-S42C] cells, a generous gift from Dr. J. Chang. Expression and purification of the protein was performed as described above.

GpD-S42C has a single cysteine residue that was site-specifically modified with fluorescein-5-maleimide (Invitrogen Molecular Probes) as follows. The probe was added to the protein (3.9ug) in a 5:1 molar basis ratio and the sample was incubated on the benchtop for 4 hours. The excess fluorescein was removed by buffer exchanging into

gpD low salt buffer (20 mM Tris-HCl, pH 8.0, containing 20 mM NaCl, 0.1 mM EDTA, 3 mM TECP) using 3 kDa MWCO centrifugal filter. The labeling efficiency was calculated by moles of dye divided by moles of protein based on UV, using A_{280} and A_{492} for the protein and the probe, respectively.

Mass Spectrometry. The purified gpD-S42C-fluorescein protein was also analyzed by MALDI mass spectrometry to characterize the products and to determine the labeling efficiency. MALDI data was kindly provided by Lucas Monkkonen using University of Washington Medicinal Chemistry Mass Spec lab Bruker Autoflex II MALDI instrument. The spectrum shows major peaks at 11,447, 11,879, and 12,304 Da, which are consistent with the molecular weight of the protein (11,440 Da) plus one and two molar equivalents of the fluorescein tag (427 Da), respectively. Integration of the peaks indicates that the labeling reaction was 60%.

Decoration of Expanded Lambda Capsids with gpD-S42C-Fluorescein. Expanded capsids (180 uM) were incubated with gpD-S42C-fluoresceine on the benchtop for 4 hours. The samples were then analyzed by agarose gel assay as described above. The capsid bands were visualized by Coomassie blue as described above and the decorated capsids were imaged by fluorescence using an EpiChemi3 darkroom system from UVP Bioimaging Systems, equipped with a Hamamatsu camera.

Chapter 6: Conclusion

The viral assembly pathway for complex dsDNA viruses contains four major steps as depicted in Figure 6-1. DNA packaging, shell expansion, shell stabilization, and full genome packaging are key steps in assembly of an infectious virus. Bacteriophage lambda serves as a model system to better understand many of these steps. The work laid out in this thesis provides insight into capsid expansion and stabilization of the expanded shell during viral assembly.

Figure 6-1. General virus assembly pathway for complex dsDNA viruses. The pathway is unidirectional *in vivo* and progresses though each step sequentially. DNA packaging, shell expansion, shell stabilization, and full genome packaging are the major step in the assembly pathway.

Assembly of a viral particle from concatemeric DNA and pre-formed procapsids is also observed in eukaryotic viruses, such as the herpesviruses, where packaging is also associated with a major change in the procapsid shell to yield a mature capsid. Indeed, capsid maturation steps are common in all the complex dsDNA viruses and the pathway is strongly conserved. The process is necessary for full-length genome packaging as it allows the viral shell to accommodate the full-length genome. This highly conserved step in viral assembly pathways has long been thought to be irreversible. The unidirectional nature would ensure that viral assembly continued in a one way fashion towards an infectious virus. Thus, it was surprising that expansion of

the lambda capsid *in vitro* is fully reversible. This feature allowed me to characterize this transition in detail.

Thermodynamic Characterization of Urea Driven Procapsid Expansion

Characterization of the expansion process *in vitro* revealed an possible two state reversible transition with urea and magnesium stabilizing the expanded and procapsid state, respectively. Due to the apparent two state nature of procapsid expansion, thermodynamic characterization was possible and revealed the free energy of expansion ($\Delta G(H_2O)$) was strongly affected by magnesium. Additionally, the denaturant "*m*" value of ~4 kcal/mol*M, obtained for the expansion of lambda procapsids, suggests a large exposure of hydrophobic surface area in the transition.

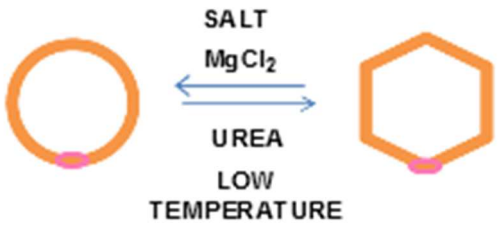

Figure 6-2. Equilibrium between lambda procapsid and expanded capsid. Urea and low temperature stabilize the expanded procapsid state while salt and $MgCl_2$ stabilize the expanded capsid state.

The novel thermodynamic characterization of lambda procapsid expansion using wild type procapsids described here allows for a greater understanding of the viral assembly process *in vivo*. Though specific values may not quantitatively apply to other viral systems, they offer a qualitative basis for comparison. An understanding of the energetics of expansion helps to better understand the stability of the procapsid and the

interactions that stabilize it in a general sense. Additionally the factors such as magnesium found to effect the equilibrium between procapsids and expanded capsids shed light on the complex interplay between procapsid stability and DNA packaging. The proposed interactions between magnesium and procapsid imparting stabilization, as well as possible stripping of magnesium from the procapsid interior to assist in DNA condensation and procapsid expansion, are suggestive of the complex yet delicate balance that mediate the process *in vivo* and that are likely recapitulated in all of the complex dsDNA viruses.

The proposed exposure of hydrophobic surface area on the capsid surface upon procapsid expansion was further supported by temperature experiments (Chapter 3). The understanding gained from these of studies and how the equilibrium between procapsids and expanded capsids is affected is depicted in Figure 6-2. The characterization of the expansion process also afforded insight into the subsequent assembly of the gpD decoration spike, and the non-covalent interactions that provide shell stability.

Vital Interactions for gpD Binding to and Stabilizing the Expanded Capsid

The expansion of the viral shell generally imparts instability along with the notable size increase. Stabilization of mature viral shells occurs in many different ways, depending on the virus. Bacteriphage HK97 crosslinks the major capsid protein, after proteolytic cleavage and the subsequent shell expansion, to stabilize the expanded shell. (Conway, Duda, Cheng, Hendrix, & Steven, 1995) In the case of phage P22, increased interaction between major capsid subunits directly stabilizes the expanded

shells. (Teschke, McGough, & Thuman-Commike, 2003). Finally, the addition of auxiliary “decoration” or “cementing” proteins is used to stabilize expanded viral shells. Indeed, the expanded capsid of bacteriophage lambda is unstable and requires addition of gpD, the lambda decoration protein, to the expanded capsid surface.

Multiple studies have looked at important interactions between gpD and the lambda expanded capsid surface. Further interactions proposed here resulted from expansion studies as well as the pseudo atomic model of gpE assembled into the capsid shell developed in our lab. The first interaction between gpD and the expanded capsid proposed to be important was hydrophobic interactions. This was proposed based on my thermodynamic interrogation of procapsid expansion that revealed a large and constant denaturant “*m*” value that is independent of magnesium concentration. Additionally structural studies indicate that the base of the gpD trimer spike is largely hydrophobic. My studies reported here support the hypothesis that hydrophobic surface areas on the expanded capsid play a role in binding of gpD to the mature shell. Since these regions are buried in the procapsid conformation, gpD does not interact with the unexpanded procapsid shell. It is hypothesized based on thermodynamic studies from Chapter 2 that the hydrophobic surface area exposed during expansion is concentrated at the icosahedral three-fold axes.

Further examination of the pseudo atomic model of gpE assembled into the capsid shell highlighted two residues at the capsid three-fold axes that form rings of Trp and Asp residues. These rings were of note due to complementary rings of His and Pro residues presented at the base of the gpD trimer spike, revealed by structural studies. The authors proposed that these residues might be important in binding of gpD to the

capsid. Support for this proposal came from the observation that residues are highly conserved in at least one other decoration protein, *shp,* known to bind and stabilize Phage 21 expanded capsids. Superposition of the gpD trimer structure onto gpE assembled at the three-fold axis reveals that the rings line up perfectly, aligning Pro-Trp and His-Asp for direct interaction.

The studies designed and reported in this work investigating the role of all four of these residues in gpD binding and stabilizing the expanded capsid suggest that while they are not necessary for gpD binding to the capsid, though are are essential for full capsid stabilization. Moreover the results suggest that loss of a single interaction did not completely abrogate capsid stabilization, based on the capacity to package a full-length genome. I suggest that while important, additional interactions, such as binding of the N-terminus of gpD with the capsid, also provides significant interactions critical for gpD stabilizing the capsid.

In sum, the addition of lambda decoration protein shows high redundancy in interactions that are important in both binding gpD to the expanded capsid as well as imparting stability. This underscores the importance of stabilization of the expanded lambda capsid and the conservation of the process in all of the complex dsDNA viruses suggests that similar features are present in other systems despite the variation in stabilization strategies.

It is tempting to speculate that the redundancy seen in stabilization of the expanded capsid upon gpD addition is necessary for viral stabilization and survival outside of the lab environment. Indeed, lambda is known to contain a number of “non-

essential” genes that are dispensable when the virus is grown under defined conditions in the lab, but that are required for existence when confronted with a less ideal natural environment. (Chauthaiwale, Therwath, & Deshpande, 1992) I suggest that the redundancy seen in lambda expanded capsid stabilization is a common feature present in all of the complex dsDNA viruses and the general features outlined here for lambda are generalizable.

Summary

It is hoped that the contributions of the research described here hasten growth in the field of physical virology and the use of virus like particles in the field of nanotechnology. Attempts to fully understand lambda procapsid expansion and subsequent stabilization with gpD suggest viral assembly is highly complex and redundant to ensure production of infectious progeny. Additionally the novel insight into the molecular interactions responsible for gpD assembly at the capsid surface and how these interactions stabilize the shell have implications on how modified decoration proteins can be used to decorate virus-like particles assembled *in vitro*. It is hoped that these principles may be used to develop lambda as a useful theragnostic nanoparticle.

Works Cited

Ackerman, H.-W. (2006). Classification of bacteriophages. 2nd ed. In E. R. Calendar, *The Bacteriophages* (pp. 8-16). New York, NY: Oxford University Press,.

Aniagyei, S. E., DuFort, C., Kao C. C., & B., D. (2008). Self-assembly approaches to nanomaterial encapsulation in viral protein cages. . *J Mater Chem, 18,* , 3763-3774.

Baldwin, R. L. (1986). Temperature dependence of the hydrophobic interaction in protein folding. . *Proc. Natl Acad. Sci. USA, 83*, 8069-8072.

Biedermannova, L., Riley, K. E., Berka, K., Hobza, P., & Vondrasek, J. (2008). Another role of proline: stabilization interactions in proteins and protein complexes concerning proline and tryptophane. *Phys. Chem. Chem. Phys., 2008, 10,*, 6350–6359.

Black, L. W. (1989). DNA packaging in dsDNA bacteriophages. *Annu Rev microbiol 43*, 267-292.

Bode, V. C., & Harrison, D. P. (1973). Distinct effects of diamines, polyamines, and magnesium ions on the stability of lambda phage heads. *Biochemistry, 12*, 3193-3196.

Bolen, D. W., & Santoro, M. M. (1988). Unfolding free energy changes determined by the linear extrapolation method. 2. Incorporation of ΔG° N-U values in a thermodynamic cycle. *Biochemistry 18*, 8069-8074.

Bourne, C., Lee, S., Venkataiah, B., Lee, A., Korba, B., Finn, M. G., et al. (2008). Small-molecule effectors of hepatitis B virus capsid assembly give insight into virus life cycle. *Journal of virology, 82(20),* , 10262-10270.

Brady, J. N. (1977). Dissociation of polyoma virus by the chelation of calcium ions found associated with purified virions. *J Virol 23(3),* , 717-24.

Bratkovic, T. (2010). Progress in phage display: evolution of the technique and its applications. *Cell. Mol. Life Sci. 67*, 749–767.

Brussow, H. (2013). Bacteriophage-host interaction: from splendid isolation into a messy reality. *Current Opinion in Microbiology, 16*, 500–506.

Calendar, R., & Abedon, S. T. (2006). *The Bacterio-phages.* New York, NY: Oxford University Press.

Casjens, S. (1974). Bacteriophage lambda FII gene protein: role in head assembly. *J Mol Biol 90(1)*, 1-20.

Casjens, S. R. (2005). Comparative genomics and evolution of the tailed-bacteriophages. *Current Opinion in Microbiology, 8*, 451–458.

Casjens, S. R. (2011). The DNA-packaging nanomotor of tailed bacteriophages. *Nature Reviews, Microbiology*, 647-656.

Casjens, S., & Hayden, M. (1988). Analysis in vivo of the bacteriophage P22 headful nuclease. *J Mol Biol 199(3)*, 467-474.

Casjens, S., & Hendrix, R. W. (1974). Localization and amounts of the major structural proteins in bacteriophage lambda. *J. Mol. Bio. 88*, 535-545.

Casjens, S., & King, J. (1975). Virus assembly. *Annu Rev Biochem 44*, 555-611.

Casjens, S., Hohn, T., & Kaiser, A. D. (1970). Morphological proteins of phage lambda: identification of the major head protein as the product of gene E. *Virology 42(2)*, 496-507.

Catalano, C. E. (2000). The terminase enzyme from bacteriophage lambda: a DNA-packaging machine. *Cell Mol Life Sci 57(1)*, 128-148.

Catalano, C. E. (2005). Viral genome packaging machines: an overview. In C. E. Catalano, *Viral Genome Packaging Machines: Genetics, and Mechanism* (pp. 1-4). New York, NY: Kluwer Academic Plenum Publishers.

Catalano, C. E., Cue, D., & Feiss, M. (1995). Virus DNA packaging: the strategy used by phage λ. *Molecular microbiology, 16(6)*, 1075-1086.

Ceres, P., Stray, S. J., & & Zlotnick, A. (2004). Hepatitis B virus capsid assembly is enhanced by naturally occurring mutation F97L. *Journal of virology, 78(17),*, 9538-9543.

Chang, J. R., Song, E., Nakatani-Webster, E., Monkkonen, L., Ratner, D. M., & Catalano, C. E. (2014). Phage Lambda Capsids as Tunable Display Nanoparticles. *Biomacromolecules 15,*, 4410−4419.

Chauthaiwale, V. M., Therwath, A., & Deshpande, V. V. (1992). Bacteriophage lambda as a cloning vector. *Microbiol Rev. 56(4)*, 577-591.

Conway, J. F., Cheng, N., Ross, P. D., Hendrix, R. W., Duda, R. L., & Steven, A. C. (2007). A thermally induced phase transition in a viral capsid transforms the hexamers, leaving the pentamers unchanged. *J. Struct. Biol. 158*, 224-232.

Conway, J. F., Duda, R. L., Cheng, N., Hendrix, R. W., & Steven, A. C. (1995). Proteolytic and conformational control of virus capsid maturation: the bacteriophage HK97 system. *J. Mol. Biol. 253*, 86-99.

Daniels, D., Schroeder, J., & Al, E. (1983). Complete Annotated Lambda Sequence. In (R. W. Hendrix, J. W. Roberts, F. W. Stahl, & R. A. Weisberg, *Lambda II* (pp. 522-523.). Cold Spring Harbor, NY.: Cold Spring Harbor Laboratory, .

Dodd, I. B., Shearwin, K. E., & Egan, J. B. (2005). Revisited gene regulation in bacteriophage lambda. *Curr Opin Genet Dev 15(2),*, 145-152.

Dokland, T., & Murialdo, H. (1993). Structural transitions during maturation of bacteriophage lambda capsids. *J Mol Biol 233(4)*, 682-694.

Duda, R. L., Hempel, J., Michel, H., Shabanowitz, J., Hunt, D., & Hendrix, R. W. (1995). Structural transitions during bacteriophage HK97 head assembly. *J Mol Biol 247*, 618-635.

Feldmann, H., Klenk, H. D., & Sanchez, A. (1993). Molecular biology and evolution of filoviruses. *Arch Virol Suppl. 7*, 81-100.

Fuller, D. N., Raymer, D. M., Kottadiel, V. I., Rao, V. B., & Smith, D. E. (2007). Single phage T4 DNA packaging motors exhibit large force generation, high velocity, and dynamic variability. *Proc. Natl Acad. Sci. USA, 104*, 16868-16873.

Fuller, D. N., Raymer, D. M., Rickgauer, J. P., Robertson, R. M., Catalano, C. E., Anderson, D. L., et al. (2007b). Measurements of single DNA molecule packaging dynamics in bacteriophage lambda reveal high forces, high motor processivity, and capsid transformations. *J Mol Biol 373(5)*, 1113-22.

Furth, M. E., & Wickner, S. H. (1983). Lambda DNA Replication. In J. W. R. W. Hendrix, *Lambda II* (pp. 145-155). Cold Spring Harbor, NY: Cold Spring Harbor Laboratory.

Galisteo, M. L., & King, J. (1993). Conformational transformations in the protein lattice of phage P22 procapsids. *Biophys J. 65*, 227-235.

Gaussier, H., Yang, Q., & Catalano, C. E. (2006). Building a virus from scratch: assembly of an infectious virus using purified components in a rigorously defined biochemical assay system. *defined biochemical assay system*, 1154-66.

Georgopoulos, C., Tilly, K., & Casjens, S. (1983). *Lambdoid phage head assembly. In Lambda II (Hendrix, R. W., Roberts, J. W., Stahl, F. W. &Weisberg, R. A., eds).* Cold Spring Harbor, NY: Cold Spring Harbor Laboratory.

Gertsman, I. G., Guttman, M., Lee, K., Speir, J. A., Duda, R. L., & Johnson, J. E. (2009). An unexpected twist in viral capsid maturation. *Nature,458(7238),*, 646-650.

Gradinaru, C. C., Marushchak, D. O., Samim, M., & Krull, U. J. (2010). Fluorescence anisotropy: from single molecules to live cells. *Analyst, 135, (3)*, 452-459.

Grünewald, K., & Cyrklaff, M. (2006). Structure of complex viruses and virus-infected cells by electron cryo tomography. *Current Opinion in Microbiology, vol. 9, issue 4*, 437-442.

Hang, J. Q., Tack, B. F., & Feiss, M. (2000). ATPase center of bacteriophage lambda terminase involved in post-cleavage stages of DNA packaging: identification of ATP-interactive amino acids. *J Mol Biol 302(4)*, 777-95.

Hendrix, R. W., & Casjens, S. (2006). Bacteriophage lambda and its genetic neighborhood. In R. &. Calendar, *The Bacteriophages 2nd edit.* (pp. 409–447). New: Oxford University Press.

Hernando-Pérez, M., Lambert, S., Nakatani-Webster, E., Catalano, C. E., & Pablo, P. J. (2014). Cementing proteins provide extra mechanical stabilization to viral cages. *Nature Communications 5, (4520)*.

Hershey, A. D., & Chase, M. (1952). Independent Functions of Viral Protein and Nucleic Acid in Growth of Bacteriophage. *The Journal of General Physiology*, 39-56.

Heymann, J. B., Cheng, N., Newcomb, W. W., Trus, B. L., & Brown, J. C. (2003). Dynamics of herpes simplex virus capsid maturation visualized by time-lapse cryo-electron microscopy. *Nat Struct Biol 10(5)*, 334-341.

Hochschild, A., & Lewis, M. (2009). The bacteriophage lambda CI protein finds an asymmetric solution. . *Curr Opin Struct Biol 19(1),* , 79-86.

Hofmeister, F. (1888). *Arch. Exp. Pathol. Pharmakol. 1 XXV*, 1-30.

Hohn, T. W. (1976). Capsid transformation during packaging of bacteriophage lambda DNA. *Philos. Trans. R. Soc. London, 276*, 51-61.

Huang, X., Bronstein, L. M., Retrum, J., Dufort, C., Tsvetkova, I., Aniagyei, S., et al. (2007). Self-assembled virus-like particles with magnetic cores. . *Nano letters, 7(8),*, 2407-2416.

Hwang, Y., Hang, J. Q., Neagle, J., Duffy, C., & Feiss, M. (2000). Endonuclease and helicase activities of bacteriophage lambda terminase: changing nearby residue 515 restores activity to the gpA K497D mutant enzyme. . *Virology 277(1)*, 204-14.

Imber, R., Tsugita, A., Wurtz, M., & Hohn, T. (1980). Outer capsid protein of bacteriophage lambda. *J. Mol. Biol. 139*, 277-295.

Iwai, H., Forrer, P., Plückthun, A., & Güntert, P. (2005). NMR solution structure of the monomeric form of the bacteriophage λ capsid stabilizing protein gpD. *Journal of biomolecular NMR, 31(4),*, 351-356.

Jardine, P. J., & Coombs, D. H. (1998). Capsid expansion follows the initiation of DNA packaging in bacteriophage T4. *J. Mol. Biol. 284*, 661-672.

Jenner, E. (1798). *An inquiry into the causes and effects ofthe variolae vaccinae.* London: Sampson Low.

Jun Xu, R. H. (2014). Chaperone-protein interactions that mediate assembly of the bacteriophage lambda tail to the correct length. *Journal of Molecular Biology 426(5)*, 1004-1018.

Kaguni, J. M. (2006). DnaA: controlling the initiation of bacterial DNA replication and more. *Annu Rev Microbiol 60*, 351-75.

Katen, S., & Zlotnick, A. (2009). The thermodynamics of virus capsid assembly. *Methods in enzymology, 455,*, 395-417.

Keen, E. C. (2012). Phage therapy: concept to cure. *Frontiers in Microbiology, 3 (238)*, 1-2.

Kochan, J., & Murialdo, H. (1983). Early intermediates in bacteriophage lambda prohead assembly. II. Identification of biologically active intermediates. *Virology 131(1)*, 100-115.

Kourilsky, P. (1973). Lysogenization by bacteriophage lambda. I. Multiple infection and the lysogenic response. *Mol Gen Genet 122(2),* , 183-195.

Kourilsky, P., & Knapp, A. (1974). Lysogenization by bacteriophage lambda. III. Multiplicity dependent phenomena occuring upon infection by lambda. *Biochimie 56(11-12),* , 1517-1523.

Kunzler, P., & Hohn, T. (1978). Stages of bacteriophage lambda head morphogenesis: physical analysis of particles in solution. *J Mol Biol, 122*, 191-211.

Lander, G. C., Evilevitch, A., Jeembaeva, M., Potter, C. S., Carragher, B., & Johnson, J. E. (2008). Bacteriophage lambda stabilization by auxiliary protein gpD: timing, location, and mechanism of attachment determined by cryo-EM. *Structure, 16*, 1399-1406.

Lansing Prescott, J. H. (1998). *Micorbiology 4th ed.* William C. Brown; 4th Edition edition .

Lederberg, E. M., & Lederberg, J. (1953). Genetic studies of lysogenicity in Escherichia coli. *Genetics 38(1)*, 51.

Lederberg, J. L. (1951). Recombination analysis of bacterial heredity. *Cold Spring Harb Symp Quant Biol 16*, 413-43.

Lee, K. K., Gan, L., Tsurata, H., Hendrix, R. W., Duda, R. L., & Johnson, J. E. (2004). Evidence that a Local Refolding Event Triggers Maturation of HK97 Bacteriophage Capsid. *J. Mol. Bio. 340*, 419-433.

Lee, K. K., Tsuruta, H., Hendrix, R. W., Duda, R. L., & Johnson, J. E. (2005). Cooperative reorganization of a 420 subunit virus capsid. . *J. Mol. Biol. 352*, 723-735.

Legendrea, M., Bartolia, J., Shmakovab, L., Jeudya, S., Labadiec, K., Adraitd, A., et al. (2014). Thirty-thousand-year-old distant relative of giant icosahedral DNA viruses with a pandoravirus morphology. *PNAS USA vol.111 (11)*, 4274–4279.

Louis-Jeune, C., Andrade-Navarro, M. A., & Perez-Iratxeta, C. (2012). Prediction of protein secondary structure from circular dichroism using theoretically derived spectra. . *Proteins. Structure, Function, and Bioinformatics. Volume 80, Issue 2,*.

Makhatadze, G. I., & Privalov, P. L. (1992). Protein interactions with urea and guanidinium chloride: a calorimetric study. *J. Mol. Biol. 226*, 491-505.

Maluf, N. K., Gaussier, H., Bogner, E., Feiss, M., & and Catalano, C. E. (2006). Assembly of bacteriophage lambda terminase into a viral DNA maturation and packaging machine. *Biochemistry 45(51)*, 15259-68.

Markovic-Housley, Z., Stolz, B., Lanz, R., & Erni, B. (1999). Effects of tryptophan to phenylalanine substitutions on the structure, stability, and enzyme activity of the IIABMan subunit of the mannose transporter of Escherichia coli. *Protein Science (8),7*, 1530-1535.

Matthews, B. W. (2001). Hydrophobic Interactions in Proteins. *ENCYCLOPEDIA OF LIFE SCIENCES, Nature Publishing Group*, 1-6.

Maxwell, K. L., Davidson, A. R., Murialdo, H., & Gold, M. (2000). Thermodynamic and functional characterization of protein W from bacteriophage lambda. The three C-terminal residues are critical for activity. . *J Biol Chem 275(25)*, 18879-86.

Medina, E. (2010). *Growing Pains of Bacteriophage Lambda: Examination of the Maturation of Procapsidsinto Capsids.* Seattle, WA: Universtiy of Washington.

Medina, E. M., Andrews, B. T., Nakatani, E., & Catalano, C. E. (2011). The bacteriophage lambda gpNu3 scaffolding protein is an intrinsically disordered and biologically functional procapsid assembly catalyst. *J Mol Biol, 412,*, 723-736.

Medina, E., Nakatani, E., Kruse, S., & Catalano, C. E. (2012). Thermodynamic Characterization of Viral Procapsid Expansion into a Functional Capsid Shell. *J Mol Biol 418*, 167-180.

Medina, E., Wieczorek, D., Medina, E. M., Yang, Q., Feiss, M., & Catalano, C. E. (2010). Assembly and maturation of the bacteriophage lambda procapsid: gpC is the viral protease. *J Mol Biol, 401,* , 813-830.

Mikawa, Y. G., Maruyama, I. N., & and Brenner, S. (1996). Surface display of proteins on bacteriophage lambda heads. *J Mol Biol 262(1)*, 21-30.

Murialdo, H. (1991). Bacteriophage lambda DNA maturation and packaging. *Ann Rev Biochem. 60*, 125–153.

Murialdo, H., & Becker, A. (1978). A genetic analysis of bacteriophage lambda prohead assembly in vitro. *J Mol Biol 125(1)*, 57-74.

Nakatani-Webster, E. (2013). *Controlled Assembly of Viral Surface Proteins into Biological Nanoparticles.* Seattle, WA: University of Washington.

Narajczyk, M., Baranska, S., Wegrzyn, A., & and Wegrzyn, G. (2007). Switch from theta to sigma replication of bacteriophage lambda DNA: factors involved in the process and a model for its regulation. *Mol Genet Genomics 278(1)*, 65-74.

Newcomb, W. W., Homa, F. L., Thomsen, D. R., Booy, F. P., Trus, B. L., Steven, A. C., et al. (1996). Assembly of the herpes simplex virus capsid: characterization of intermediates observed during cell-free capsid formation. *J. Mol. Biol. 263*, 432-446.

Oppenheim, A. B., Kobiler, O. S., Court, D. L., & Adhya, S. (2005). Switches in bacteriophage lambda development. *Annu. Rev. Genet*, 39, 409-429.

Ortega, M., & Catalano, C. .. (2006). Bacteriophage lambda gpNu1 and Escherichia coli IHF proteins cooperatively bind and bend viral DNA: implications for the assembly of a genome-packaging motor. . *Biochemistry 45,* , 5180-9.

Pace, C. N., & Shaw, K. L. (2000). Linear extrapolation method of analyzing solvent denaturation curves. *Proteins 4*, 1-7.

Parent, K. N., Doyle, S. M., Anderson, E., & Teschke, C. M. (2005). Electrostatic interactions govern both nucleation and elongation during phage P22 procapsid assembly. *Virology, 340(1)*, 33-35.

Pennazio, S., & Roggero, P. (2000). The discovery of the chemical nature of tobacco mosaic virus. *Riv Biol. 93(2)*, 253-81.

Randall-Hazelbauer, L., & Schwartz, M. (1973). Isolation of the bacteriophage lambda receptor from Escherichia coli. *J Bacteriol 116(3)*, 1436-46.

Rao, V. B. (2008). The bacteriophage DNA packaging motor. *Annual review of genetics*, 42, 647-681.

Rayaprolu, V., Kruse, S., Kant, R., Venkatakrishnan, B., Movahed, N., et al. (2013). Comparative Analysis of Adeno-Associated Virus Capsid Stability and. *J Virol.;87(24)*, 13150-60.

Rice, P., Yang, S.-W., Mizuuchi, K., & Nash, H. (1996). Crystal Structure of an IHF-DNA Complex: A Protein-Induced DNA U-Turn. *Cell 87,*, 1295-1306.

Roizman, B., & Palese, P. (1996). Multiplication of viruses: an overview. In B. N. Fields, *Fields Virology* (pp. 101-111). New York, NY: Lippincott-Raven.

Rossmann, M. G., Arnold, E., Erickson, J. W., Frankenberger, E. A., Griffith, J. P., Hecht, H.-J., et al. (1985). Structure of a human common cold virus and functional relationship to other picornaviruses. *Nature, Volume 317, Issue 6033,*, 145-153 .

Rubinchik, S., Parris, W., & Gold, M. (1994). The in vitro endonuclease activity of gene product A, the large subunit of the bacteriophage lambda terminase, and its relationship to the endonuclease activity of the holoenzyme. *J Biol Chem 269(18)*, 13575-85.

Salunke, D. M., Caspar, D. L., & Garceat, R. L. (1989). Polymorphism in the assembly of polyomavirus capsid protein VP1. *Biophys. J. Biophysical Society(56)*, 887-900.

Sanger, F., Air, G. M., Barrell, B. G., Brown, N. L., Coulson, A. R., Fiddes, J. C., et al. (1977). Nucleotide sequence of bacteriophage ΦX174 DNA. *Nature 265 (5596)*, 687–695.

Santoro, M. M., & Bolen, D. W. (1988). Unfolding free energy changes determined by the linear extrapolation method. 1. Unfolding of phenylmethanesulfonyl alpha-chymotrypsin using different denaturants. *Biochemistry 18*, 8063-8068.

Santoro, M. M., & Bolen, D. W. (1992). A test of the linear extrapolation of unfolding free energy changes over an extended denaturant concentration range. *Biochemistry, 31*, 4901-4907.

Sanyal, S., Yang, T.-C., & Catalano, C. (2014). Integration Host Factor Assembly at the Cohesive End Site of the Bacteriophage Lambda Genome: Implications for Viral DNA Packaging and Bacterial Gene Regulation. *Biochemistry 53,*, 7459-7470.

Singh, P., Nakatani, E., Goodlett, D. R., & Catalano, C. E. (2013). A Pseudo-Atomic Model forthe Capsid Shell of Bacteriophage Lambda Using Chemical Cross-Linking/Mass Spectrometry and Molecular Modeling. *Journal of molecular biology, 425(18)*, 3378-3388.

Sternberg, N., & Hoess, R. H. (1995). Display of peptides and proteins on the surface of bacteriophage lambda. *lambda. Proc. Natl Acad. Sci. USA, 92, 1609–1613.*, 1609–1613.

Sternberg, N., & Weisberg, R. (1977). Packaging of coliphage lambda DNA: II. The role of the gene D protein. *J. Mol. Biol. 117*, 733–759.

Sulakvelidze, A., Alavidze, Z., & Morris, J. G. (2001). Bacteriophage therapy. *Antimicrobial agents and chemotherapy, (45)3*, 649-659.

Teschke, C. M., McGough, A., & Thuman-Commike, P. A. (2003). Penton Release from P22 Heat-Expanded Capsids Suggests Importance of Stabilizing Penton-Hexon Interactions during Capsid Maturation. *Biophysical Journal Volume 84*, 2585–2592.

Thirion, J. P., & and Hofnung, M. (1972). On some genetic aspects of phage lambda resistance in E. coli K12. *Genetics 71(2)*, 207-16.

Tomizawa, J., & Ogawa, T. (1968). Replication of phage lambda DNA. *Cold Spring Harb Symp Quant Biol 33*, 533-51.

Tomka, M. A., & Catalano, C. (1993). Physical and Kinetic Characterization of the DNA Packaging Enzyme from Bacteriophage Lambda. *The Journal of Biological Chemistry (268) 5*, 3056-3065.

Trus, B. L., Booy, F. P., Newcomb, W. W., Brown, J. C., Homa, F. L., Thomsen, D. R., et al. (1996). The herpes simplex virus procapsid: structure, conformational changes upon maturation, and roles of the triplex proteins VP19c and VP23 in assembly. *J Mol Biol 263(3)*, 447-462.

Tsay, J. M., Sippy, J., Feiss, M., & Smith, D. E. (2009). The Q motif of a viral packaging motor governs its force generation and communicates ATP recognition to DNA interaction. *Proc. Natl Acad. Sci. USA, 106*, 14355-14360.

Tzlil, S., Kindt, J. T., Gelbart, W. M., & and Ben-Shaul, A. (2003). Forces and pressures in DNA packaging and release from viral capsids. *Biophys J 84(3)*, 1616-27.

Villa, L. L., Perez, G., Kjaer, S. K., & al, e. (2007). Quadrivalent vaccine against human papillomavirus to prevent high-grade cervical lesions. *The New England journal of medicine, 356(19)*, 1915-1927.

Wendt, J. L., & and Feiss, M. (2004). A fragile lattice: replacing bacteriophage lambda's head stability gene D with the shp gene of phage 21 generates the Mg2+-dependent virus, lambda shp. *Virology 326(1)*, 41-46.

Wurtz, M., Kistler, J., & Hohn, T. (1976). Surface structure of in vitro assembled bacteriophage lambda polyheads. *J. Mol. Biol. 101*, 39-56.

Yanagi, K. a. (1989). Destabilization of herpes simplex virus type 1 virions by local anesthetics, alkaline pH, and calcium depletion. *Arch Virol 108(1-2),*, 151-9.

Yang, F., Forrer, P., Dauter, Z., Conway, J. F., Cheng, N., Cerritelli, M. E., et al. (2000). Novel fold and capsid-binding properties of the lambda-phage display platform protein gpD. *Nat Struct Biol 7 (3)*, 230-237.

Yang, Q., & Catalano, C. E. (2003). Biochemical Characterization of Bacteriophage Lambda Genome Packaging in Vitro. *Virology 305,* , 276–287 .

Yang, Q., Maluf, N. K., & Catalano, C. E. (2008). Packaging of a unit-length viral genome: the role of nucleotides and the gpD decoration protein in stable nucleocapsid assembly in bacteriophage lambda. *J Mol Biol 383(5)*, 1037-1048.